Dissertation

Dissecting the role of endothelium in COVID-19 and progressive pulmonary fibrosis

Submitted by

Elisabeth Fließer, MSc.

For the Academic Degree of

Doctor of Philosophy (PhD)

At the Medical University of Graz,

Ludwig Boltzmann Institute for lung vascular research

Under the Supervision of

Grazyna Kwapiszewska-Marsh, PhD

2024

Statutory Declaration and Disclosures

I hereby declare that this thesis is my own original work and that I have fully acknowledged by name all of those individuals and organizations that have contributed to the research for this thesis. Full acknowledgement has been made in the text to all other material used. Throughout this thesis and in all related publications I followed the "Guidelines of the Medical University of Graz on Good Scientific Practice".

Parts of this dissertation are published in the following peer-reviewed original research articles, as well parts of the published work are being reproduced in this dissertation:

Birnhuber A [1, 2], Fließer E [1, 2], Gorkiewicz G [3], Zacharias M [3], Seeliger B [4], David S [5], Welte T [4], Schmidt J [6], Olschewski H [7], Wygrecka M [8, 2], Kwapiszewska G [1, 9, 2]. **Between inflammation and thrombosis: endothelial cells in COVID-19**. Eur Respir J. 2021 Sep 9;58(3):2100377. doi: 10.1183/13993003.00377-2021. PMID: 33958433; PMCID: PMC8112008.

[1] Ludwig Boltzmann Institute for Lung Vascular Research, Graz, Austria.

[2] Authors contributed equally.

[3] Diagnostic and Research Institute of Pathology, Medical University Graz, Graz, Austria.

[4] Dept of Respiratory Medicine, Hannover Medical School, Hannover, Germany.

[5] Institute of Intensive Care, University Hospital Zurich, Zurich, Switzerland.

[6] Dept of Nephrology and Hypertension, Hannover Medical School, Hannover, Germany.

[7] Division of Pulmonology, Medical University of Graz, Graz, Austria.

[8] Center for Infection and Genomics of the Lung, Universities of Giessen and Marburg Lung Center, Member of the German Center for Lung Research, Giessen, Germany.

[9] Otto Loewi Research Center, Medical University of Graz, Graz, Austria.

Citation:	Between inflammation and thrombosis: endothelial cells in COVID-19 Anna Birnhuber, Elisabeth Fließer, Gregor Gorkiewicz, Martin Zacharias, Benjamin Seeliger, Sascha David, Tobias Welte, Julius Schmidt, Horst Olschewski, Malgorzata Wygrecka, Grazyna Kwapiszewska European Respiratory Journal Sep 2021, 58 (3) 2100377; DOI: 10.1183/13993003.00377-2021
Material:	Figure 1

Acknowledgement Wording:	Reproduced with permission of the ERS 2024: European Respiratory Journal Sep 2021, 58 (3) 2100377; DOI: 10.1183/13993003.00377-2021

Fließer E [1#], Birnhuber A [1#], Marsh LM [1], Gschwandtner E [2], Klepetko W [2], Olschewski H [3], Kwapiszewska G [1, 4]. **Dysbalance of ACE2 levels - a possible cause for severe COVID-19 outcome in COPD**. J Pathol Clin Res. 2021 Sep;7(5):446-458. doi: 10.1002/cjp2.224. Epub 2021 May 12. PMID: 33978304; PMCID: PMC8239572.

[1] Ludwig Boltzmann Institute for Lung Vascular Research, Graz, Austria.

[2] Division of Thoracic Surgery, Department of Surgery, Medical University of Vienna, Vienna, Austria.

[3] Division of Pulmonology, Medical University of Graz, Graz, Austria.

[4] Otto Loewi Research Center, Medical University of Graz, Graz, Austria.

[#] Contributed equally

All Co-authors have explicitly agreed to the use of their data in this dissertation.

Date: 28.02.2024

Acknowledgements

This work was conducted at the Ludwig Boltzmann Institute for Lung Vascular Research. The PhD student Elisabeth Fließer received funding from the Austrian Research Promotion Agency (FFG, project number: 34926649) and from the Medical University of Graz through the PhD program “Molecular Medicine” (MolMed).

I want to thank my supervisor Dr. Grazyna Kwapiszewska and the members of my Dissertation committee Anna Birnhuber, PhD, Univ.Prof. Erwin F. Wagner, PhD and Valentina Biasin, PhD for their guidance and support. In advance I want to additionally thank my defense committee consisting of Research Prof. Priv.-Doz. Dr.med.univ. Dr.rer.nat. Luka Brcic, Edda Spiekerkoetter, M.D. and Duncan J. Stewart, M.D. for thoroughly reviewing my thesis and for their constructive input and support during my defense.

The isolation of polymorphnuclear leucocytes was done by the group of Univ.-Prof. Dr.med.univ. Akos Heinemann, Division of Pharmacology, Otto Loewi Research Center, Medical University of Graz, Graz, Austria.Transmission electron microscopy was performed in cooperation with the Core Facility Ultrastructural Analysis, Medical University of Graz, Graz, Austria. Parts of the figures have been created using www.BioRender.com or www.smart.servier.com.

Table of contents

Statutory Declaration and Disclosures 2
Acknowledgements 4
Table of contents 5
List of abbreviations 8
List of Figures 10
List of Tables 11
Abstract (German) 12
Abstract (English) 13
Introduction (State of the art and hypothesis) 14
Chronic lung diseases (CLDs) 14
Progressive pulmonary fibrosis 14
Immune system in lung fibrosis 16
Endothelial cells (ECs) and pulmonary vasculature in lung fibrosis 17
Angiogenesis in PF 21
Vascular permeability in PF 22
Endothelial activation and inflammation in PF 23
Coronavirus disease 2019 (COVID-19) and PF 23
Treatment of PPF 28
Endothelial-directed therapy options 29
Rationale of the study 30
Detailed materials and methods 32
Human tissue and plasma 32
Bleomycin mouse model 34
Quantitative real-time PCR (qRT-PCR) 35
Public microarray dataset 37
Immunofluorescence staining 37
Immunohistochemistry staining 37
Human lung tissue sections 37
Murine lung tissue sections 38
Visiopharm 38
Analysis of human lung tissue 38
Analysis of murine lung tissue 38
ELISA and multiplex assay 39
Human plasma 39
Murine plasma 39

Transmission electron microscopy (TEM) 39
In-vitro analyses 39
Cell isolation 39
Endothelial barrier monitoring 40
Immunofluorescence staining of HPAECs 41
Adhesion assay 41
Transmigration assay 41
Statistics: Correlation analysis 42
Results 43
Results 1: Chronic lung diseases and COVID-19 43
Gene expression analysis of COVID-19 relevant entrance and priming proteins 43
Results 2: Endothelial cells in severe COVID-19 44
Gene expression analysis of vascular identity, barrier and injury markers in severe COVID-19 44
Vascular injury in severe COVID-19 45
Circulatory levels of vascular and inflammatory factors in COVID-19 46
Results 3: Endothelial cells in pulmonary fibrosis 48
Ultrastructural properties of the pulmonary endothelium 48
Endothelial integrity and activation in pulmonary fibrosis 49
The relationship between endothelial activation, tissue fibrosis and lung inflammation 50
Alterations of activation and integrity markers in whole lung tissue 52
Loss of vascular endothelial barrier function in pulmonary fibrosis 53
Endothelial response to a pro-inflammatory/anti-fibrotic environment 54
Adhesion of immune cells to endothelial monolayers 55
Translocation of immune cells through endothelial monolayers 56
Endothelial-related molecules can be measured in the systemic circulation 57
Endothelial alterations during disease onset and progression 58
Discussion 61
COVID-19 and chronic lung diseases 61
COVID-19, endotheliopathy and development of COVID-19-PF 63
Endothelial cells in PPF 65
Dysregulation of endothelial activation in PF 66
Dysregulation of endothelial barrier integrity in PF 67
Biomarker research 68
Alterations of the vascular compartment during lung fibrosis onset and progression 69
Limitations of the study 70
Conclusion 70

References.. 72

List of abbreviations

aCAP	Alveolar capillaries (aeorcytes)
ACE2	Angiotensin-converting-enzyme 2
ADAM	A Disintegrin and Metalloprotease
Ang	Angiotensin
ARDS	Acute respiratory distress syndrome
AT1R	Angiotensin II receptor type 1
AT2R	Angiotensin II receptor type 2
BMI	Body mass index
BSA	Bovin serum albumin
BSG	Basigin
CD	Cluster of differentiation
CEC	Circulating endothelial cell
CLD	Chronic lung disease
COPD	Chronic obstructive pulmonary disease
COVID-19	Coronavirus disease 2019
CRP	C-reactive protein
CTRL	Control
DAD	Diffuse alveolar damage
ECIS	Electrical cell-substrate impedance sensing
ECM	Extracellular matrix
EDTA	Ethylenediaminetetraacetic acid
eNOS	Endothelial nitric oxide synthase
FCS	Fetal calf serum
FEV1	Forced expiratory volume in 1 second
FGF	Fibroblast growth factor
FVC	Forced vital capacity
gCAP	General capillary endothelial cells
GM-CSF	Granulocyte-macrophage colony-stimulating factor
GWAS	Genome-wide association studies
HEPES	4-(2-hydroxyethyl)-1-piperazineethanesulfonic acid
HIF	Hypoxia inducible factor
HP	Hypersensitivity pneumonitis
HPAEC	Human pulmonary artery endothelial cell
HUVEC	Human umbilical vein endothelial cell
ICAM	Intercellular adhesion molecule
ICU	Intensive care unit
IFN	Interferon
IL	Interleukin
IP-10	Interferon gamma-induced protein 10
IPAH	Idiopathic pulmonary arterial hypertension
LH	Lung homogenate
LTX	Lung transplantation
MACS	Magnetic activated cell sorting
MCP-1	Monocyte chemoattractant protein 1
M-CSF	Macrophage colony-stimulating factor
MIP-2	Macrophage inflammatory protein
MMP	Matrix metalloproteinase
mPAP	Mean pulmonary arterial pressure
MUC5B	Mucin 5B
NO	Nitric oxide

NSIP	Non-specific interstitial pneumonia
PBMC	Peripheral blood mononuclear cell
PBS	Phosphate-buffered saline
PCT	Procalcitonin
PDGF	Platelet-derived growth factor
PEDF	Pigment epithelium-derived factor
PF	Pulmonary fibrosis
PFA	Paraformaldehyde
PH	Pulmonary hypertension
PMNL	Polymorphnuclear leucocyte
pO_2	Partial pressure of O_2
PPF	Progressive pulmonary fibrosis
PTT	Partial thromboplastin time
PVR	Pulmonary vascular resistance
qRT-PCR	Quantitative real time polymerase chain reaction
RAS	Renin-angiotensin-system
ROS	Reactive oxygen species
S1P	Sphingosine-1-phosphate
SARS-CoV2	Severe acute respiratory syndrome coronavirus 2
scRNA-seq	Single cell RNA sequencing
SOFA score	Sepsis-related organ failure assessment score
TAZ	Transcriptional coactivator with PDZ-binding motif
TEM	Transmission electron microscopy
TF	Tissue factor
TFPI	Tissue factor pathway inhibitor
TGF	Transforming growth factor
Thbd	Thrombomodulin
Tie2	TEK tyrosine kinase
TLC	Total lung capacity
TMPRSS2	Transmembrane protease, serine 2
TNF	Tumor necrosis factor
UIP	Usual interstitial pneumonia
VCAM	Vascular cell adhesion molecule
VEGF	Vascular endothelial growth factor
vWF	von Willebrand factor
WPB	Weibel Palade Body
YAP	Yes-associated protein

List of Figures

Figure 1: Lung fibrosis patho-mechanism.

Figure 2: Overview of the renin-angiotensin-system (RAS).

Figure 3: Intussusceptive angiogenesis.

Figure 4: Proposed hypothesis of the dissertation.

Figure 5: COVID-19 relevant mediators in different chronic lung diseases.

Figure 6: Correlation between pulmonary ACE2 gene expression and forced vital capacity (FVC %).

Figure 7: Gene expression of endothelial cell markers are upregulated in lungs of severely ill COVID-19 patients.

Figure 8: Severe COVID-19 is associated with increased immune cell infiltration and diffuse vWF distribution.

Figure 9: Soluble endothelial markers are increased in COVID-19 plasma.

Figure 10: Soluble markers of inflammation are increased in COVID-19 plasma.

Figure 11: COVID-19 is associated with strong correlations between soluble markers of coagulation.

Figure 12: The endothelial ultrastructure is changed in pulmonary fibrosis.

Figure 13: Endothelial cells are structurally distinct compared to donor endothelium.

Figure 14: Remodeled and inflamed regions correlate with endothelial alterations.

Figure 15: Integrity and activation marker gene expression in donor and fibrosis transplant lungs.

Figure 16: Impairment of endothelial barrier in lung fibrosis.

Figure 17: Endothelial cell behavior in a pro-inflammatory milieu.

Figure 18: Adhesion of immune cells to endothelial cells.

Figure 19: Transmigration of immune cells through endothelial cells.

Figure 20: Endothelial cell markers in the systemic blood circulation.

Figure 21: Schematic overview of the experimental strategy for the performance of the bleomycin-induced time course mouse model.

Figure 22: Changes of endothelial marker gene expression over time.

Figure 23: Endothelial activation over time in the lungs of bleomycin-treated mice.

Figure 24: Changes of circulating endothelial cell markers over time in bleomycin-treated mice.

Figure 25: Markers of endothelial dysfunction in COVID-19.

List of Tables

Table 1: Clinical characteristics of COVID-19 patients and CONTROLS used for gene expression analysis.

Table 2: Clinical characteristics of COPD, IPAH and PF patients and CONTROLS used for gene expression analysis.

Table 3: Clinical characteristics of endstage disease patients and donors used for gene expression and plasma analysis.

Table 4: Clinical characteristics of COVID-19 patients and CONTROLS used for plasma analysis.

Table 5: Clinical characteristics of COPD, IPAH and PF patients and CONTROLS used for ACE2 plasma analysis.

Table 6: Antibodies used for immunohistochemistry and immunofluorescence stainings.

Abstract (German)

Endothelzellen, die innerste Schicht aller Blutgefäße, können im Verlauf einer SARS-CoV2 Infektion stark beeinträchtigt werden. Anhaltende endotheliale Fehlfunktion, ein charakteristisches Merkmal von Long-COVID, wurde mit der Entwicklung von progressiver Lungenfibrose in Verbindung gebracht. Etwa 25% der schweren COVID-19-Fälle sind davon betroffen. Progressive Lungenfibrose ist ebenso eine zentrale Komponente zahlreicher anderer chronischer Lungenerkrankungen, wie z.B. idiopathische Lungenfibrose, systemische Sklerose oder allergische Alveolitis. Alle diese fibrotisierenden interstitiellen Lungenerkrankungen teilen endotheliale Fehlfunktionen, die sich zum Beispiel als Gefäßumbau und daraus resultierender pulmonaler Hypertonie, Koagulopathie, Integritätsverlust, Hyperaktivierung und Entzündung sowie erhöhte Angiogenese oder dem Absterben von Gefäßen manifestieren können. Bisher konzentrierte sich die Forschung hauptsächlich auf die Rolle von Epithelzellen und Fibroblasten in der Pathogenese der progressiven Lungenfibrose, während Endothelzellen wenig erforschtes zelluläres Kompartiment darstellen. Basierend auf den Beobachtungen in COVID-19, vermuten wir, dass das vaskuläre Endothel eine zentrale Rolle in der Pathogenese von progressiver Lungenfibrose spielt. Durch die Untersuchung von Lungengewebe, sowie Plasmaproben von schwer erkrankten COVID-19-Patienten bestätigten wir, dass das Endothel signifikant von SARS-CoV-2 beeinträchtigt ist. Dies äußerte sich in einer starken Hochregulierung mehrerer endothelbezogener Integritäts- und Aktivierungsmarker (z.B. ICAM-1, vWF, VEGFR-2, VCAM-1, E-Selektin, CD31 IL-6 oder MCP-1) in den Lungen von COVID-19 Patienten sowie im Plasma infizierter Personen. Unsere anschließende Analyse des Endothels in mit interstitieller Lungenerkrankung-assoziierter Fibrose zeigte ähnliche Ergebnisse. Zusammenfassend zeigen wir basierend auf Lungentransplantat-Proben, Patientenplasma, isolierten pulmonalen Arterienendothelzellen und einem öffentlich zugänglichen Microarray Dataset, dass die Struktur und Funktion von Endothelzellen in fibrotischen Lungen signifikant verändert sind. Auf struktureller Ebene beobachteten wir geschwollene, unregelmäßig geformte Endothelzellen, die den Eindruck einer Hyperaktivierung vermittelten. Die Hyperaktivierung wurde durch unsere *in-vitro*-Analyse weiter bestätigt. Hier beobachteten wir eine erhöhte Sensitivität gegenüber pro-inflammatorischer Stimulantien und eine erhöhte Adhäsion von Immunzellen an Endothelzellen aus fibrotischen Lungen. Dies ging mit einer ausgeprägten Beeinträchtigung der Integrität einher, die sich in einer reduzierten Barrierefunktion sowie einem Verlust der typischen Endothelzell-Anordnung *in-vitro* ausdrückte. Darüber hinaus zeigten wir in einem *in-vivo* Mausmodell, dass diese Veränderungen bereits zu Beginn der Krankheit erkennbar sind. Unsere Ergebnisse bestätigen die Beeinträchtigung der Endothelzellen in der PF-Pathogenese und legen nahe, dass die Wiederherstellung der vaskulären Homöostase eine neuartige Therapiestrategie darstellen könnte.

Abstract (English)

Endothelial cells, the inner lining of all blood vessels, are heavily affected in COVID-19. The ongoing endothelial dysfunction, a hallmark of long-COVID, has been linked to the progression to pulmonary fibrosis, affecting approximately 25% of severe COVID-19 cases.

Progressive pulmonary fibrosis (PPF) is also associated with numerous other chronic lung diseases, such as idiopathic pulmonary fibrosis, systemic sclerosis or hypersensitivity pneumonitis. All of these fibrosing interstitial lung diseases (ILDs) share endothelial maladaptations, which can manifest for example as vascular remodeling and pulmonary hypertension, coagulopathy, integrity loss, hyper-activation and inflammation and/or elevated angiogenesis or vessel loss. So far, research in the field has focused mainly on the role of epithelial cells and fibroblast to myofibroblast differentiation in the pathogenesis of progressive pulmonary fibrosis. The vascular endothelium however remains an under-investigated cellular compartment in the disease. Based on the compelling evidence from COVID-19, which suggests endothelial cells as crucial drivers of fibrogenesis, we hypothesized that the vascular endothelium is also involved in the pathogenesis of PPF.

Through examination of lung tissue as well as plasma samples from severely ill COVID-19 patients, we confirmed that the endothelium is significantly impacted by SARS-CoV-2. This was manifested as strong upregulation of several endothelium-related integrity and activation markers (e.g. ICAM-1, vWF, VEGFR-2, VCAM-1, E-selectin, CD31 IL-6 or MCP-1) in COVID-19 lungs as well as plasma of infected individuals. Our subsequent analysis of the endothelium in PPF showed similar results. Collectively, through the utilization of human lung transplant samples, patients' plasma, isolated pulmonary artery endothelial cells, and a publicly available transcriptomic dataset of PPF, we demonstrate that endothelial cells (ECs) are significantly altered in structure and function in PPF. On the structural level, we observed swollen, misshaped ECs, which gave the impression of hyper-activation. The endothelial hyper-activation was further corroborated by our *in-vitro* analysis, which uncovered increased sensitivity to a pro-inflammatory milieu and simultaneous elevated immune cell adhesion to fibrotic ECs. This was associated with a pronounced dysfunction of endothelial integrity, which was represented in a reduced barrier strength as well as loss of the typical endothelial cobblestone structure *in-vitro*. Furthermore, the incorporation of the bleomycin mouse model of lung fibrosis revealed that these changes are already evident at the onset of the disease.

Our findings corroborate a vascular component in PF pathogenesis and suggest that the re-establishment of vascular homeostasis might become a novel therapy strategy.

Introduction (State of the art and hypothesis)

Chronic lung diseases (CLDs)

CLDs, such as chronic obstructive pulmonary disease (COPD), pulmonary hypertension (PH) or interstitial lung disease (ILD), including pulmonary fibrosis (PF) encompass conditions affecting the airways and other lung structures. Despite the varied underlying patho-mechanisms, severity levels, and progression patterns, CLDs contribute to approximately 3 million deaths annually.

COPD manifests itself as chronic inflammatory disease leading to emphysematous destruction of the airways and limitation of expiratory airflow (1, 2). Besides cigarette smoke, air pollution, dust, fume or viral/bacterial infections are major triggers of the disease. In addition, autoimmunity and cell senescence are crucial contributors to the structural deterioration and hyper-inflammation in COPD patients. The loss of lung function is driven by the occurrence of acute exacerbations in COPD patients, which are periods of exaggerated pulmonary obstruction and inflammatory processes (1, 2). As underlying disease mechanisms are still understood poorly, there are only limited therapeutic options available. Thus, COPD is the third leading cause of death worldwide (1, 2).

Idiopathic pulmonary hypertension (IPAH) is another chronic inflammatory lung disease, marked by intimal hyper-proliferation, medial hypertrophy and adventitial cell proliferation (3). The hyper-proliferative phenotype leads to increased pulmonary vascular resistance and elevated mean pulmonary arterial pressure at rest (mPAP, ≥20 mmHg). As the disease advances, endothelial function loss is increasing and intimal fibrosis together with thrombosis lead to the development of so-called plexiform lesions (3). To differentiate between IPAH and PH due to other causes, such as pulmonary vascular disease or left heart disease, it is important to also include the values of the pulmonary vascular resistance (PVR) and pulmonary arterial wedge pressure (PAWP) in the diagnosis (4). Based on these hemodynamic measurements together with clinical presentation (e.g. connective tissue disease, infections, heart failure, chronic lung diseases, systemic disorders, metabolic disorders) and therapeutic management, PH is generally divided into 5 subgroups, including the following:

Group 1 Pulmonary arterial hypertension (PAH)

Group 2 PH associated with left heart disease

Group 3 PH associated with lung diseases and/or hypoxia

Group 4 PH associated with pulmonary artery obstructions

Group 5 PH with unclear and/or multifactorial mechanisms.

Prevalence and therapeutic strategies differ depending on the subgroup (4).

Progressive pulmonary fibrosis

Progressive pulmonary fibrosis (PPF) refers to the non-resolving, fibrosing phenotype observed across various subtypes of ILDs (5, 6). Broadly, ILDs are divided into 5 sub-categories, including ILDs related to distinct primary diseases (e.g. sarcoidosis or eosinophilic pneumonia), ILDs related to environmental

triggers (e.g. hypersensitivity pneumonitis), drug-induced ILDs, ILDs associated with autoimmune diseases (e.g. Systemic Sclerosis, Rheumatoid Arthritis or Sjögren's Syndrome) and ILDs of unknown cause (idiopathic pulmonary fibrosis, IPF) (7). Patients with PPF experience ongoing and advancing lung fibrosis, despite receiving the maximum conventional therapy (6).

The progressive fibrosing phenotype is characterized by a severe decline in lung function, increasing distortion of the normal lung architecture due to excessive extracellular matrix (ECM) deposition and a mortality rate of 69% beyond 5 years in untreated patients (8). The occurrence of an acute exacerbations decreases the 3 months survival rate even to approximately 40% (9). Acute exacerbation is marked by a severe worsening of parenchymal remodeling, coupled with a sudden respiratory decline and is linked to heavy inflammation and endothelial injury (9). Usually PPF follows a usual interstitial pneumonia (UIP) pattern (5, 10). UIP characterizes itself by spatial and temporal heterogeneity of fibrotic changes and the presence of ground glass opacities (areas of increased attenuation due to decreasing amounts of air), septal thickening, traction bronchiectasis (airway dilation) and honeycombing (enlarged airspaces) (10). In rare cases, the non-specific interstitial pneumonia (NSIP) pattern is observed in PPF, however, patients with NSIP typically respond well to treatment (6, 10). PPF is recognized as a multi-factorial condition, triggered by a combination of genetic and epigenetic pre-disposition as well as environmental risk factors. Environmental factors include for example antigens, bacterial and viral infections, cigarette smoke, silica or metal dust (5, 10, 11). Together with advanced age and diet, these factors trigger epigenetic shifts, which are marked by changes in DNA methylation patterns, modifications of histones and the presence of micro-RNAs, further resulting in mRNA degradation and the inhibition of proper protein translation (10, 11). Mutations are specifically associated with genes related to telomeres and their premature and accelerated shortening and to the promoter of Mucin 5B (MUC5B), a mucin important for epithelial clearance and host defense (5).

A continuous exposure to the above-mentioned triggers and environmental factors in genetically predisposed individuals leads to a repeated injury of the alveolar epithelium and subsequent destruction of the alveolar-endothelial barrier. The lacking ability to properly reestablish the barrier induces immune cell recruitment, heavy inflammation and the establishment of a pro-fibrotic environment, composed of platelet-derived growth factor (PDGF)-AA and PDGF-BB, fibroblast growth factor (FGF)-2, vascular endothelial growth factor (VEGF) and macrophage colony-stimulating factor (M-CSF) amongst others (5). Following this, fibroblasts become activated and undergo differentiation into apoptosis-resistant myofibroblasts, which then produce exuberant amounts of ECM (5, 7). See scheme Figure 1.

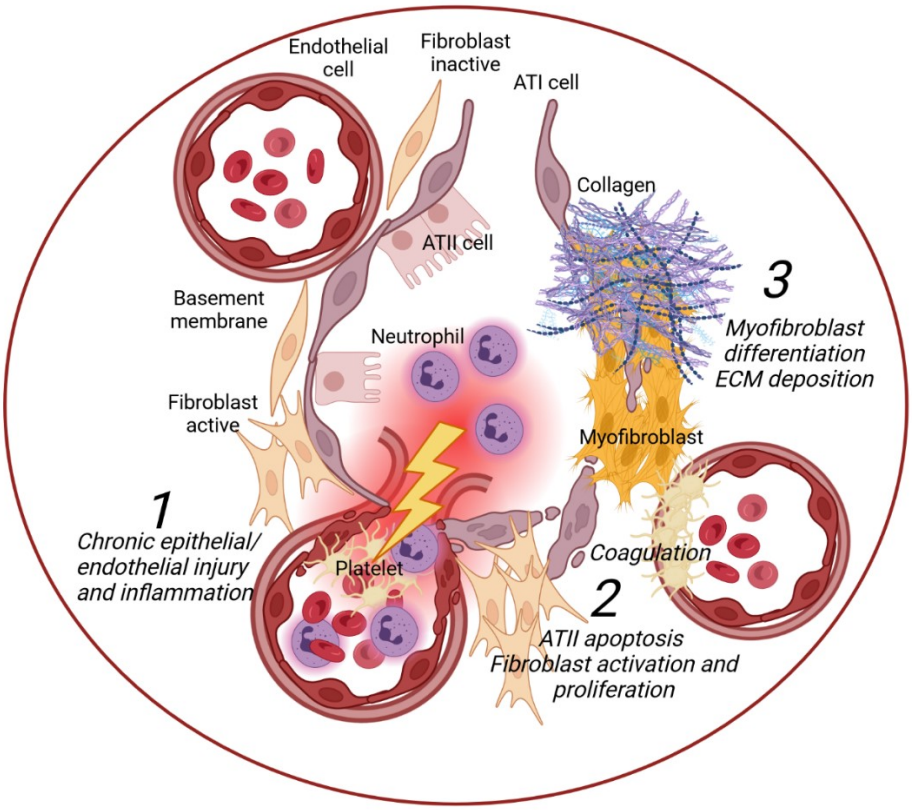

Figure 1: Lung fibrosis patho-mechanism. Environmental factors, such as viruses, bacteria, dust or smoke trigger a chronic epithelial injury, which leads to the destruction of airway epithelium, basement membrane and endothelial barrier in genetically predisposed individuals (1). Plasma leakage, cell apoptosis and inflammation induce a repair reaction (2), which is characterized by migration, activation and proliferation of fibroblasts. Their differentiation causes the accumulation of apoptosis-resident myofibroblasts, which produce excessive amount of extracellular matrix and thus trigger the irreversible scarring of the lung (3). Created with BioRender.com (Agreement number: JD26HLA04B).

Immune system in lung fibrosis

The chronic injury and non-resolving parenchymal remodeling in PPF is accompanied by the presence of persistent inflammation. The persistent inflammation is characterized by elevated inflammatory infiltration, upregulation of pro-inflammatory signaling and increased levels of pro-inflammatory mediators in the lungs and circulation of lung fibrosis patients (12). Increased presence of inflammatory cells and mediators is moreover associated with accelerated progression of the disease. In addition, autoantibodies against heat shock protein 70 and periplakin, a cytoskeleton component, have been detected in the circulation and bronchoalveolar lavage of patients suffering from idiopathic PF. The presence of autoantibodies is associated with more severe disease and thus suggests that autoimmunity is another component contributing to fibrosis pathogenesis (12-14).

In genome-wide association studies (GWAS), genetic variants linked to increased risk for and severity of lung fibrosis are involved in inflammatory processes, host defense and immune response (12-14). Single nucleotide polymorphism affected genes include for example toll interacting protein (*TOLLIP)*, an inhibitor of toll-like receptor signaling, toll like receptor 3 (*TLR3)*, a component of anti-viral signaling

or human leucocyte antigen (*HLA)* regions, which are important for the induction of adaptive immune responses (14).

Endothelial cells (ECs) and pulmonary vasculature in lung fibrosis

The pulmonary vasculature encompasses a vast surface area within the lungs to ensure proper gas exchange and nutrient supply. In addition to that, it holds significant functional importance in maintaining a silent, anti-coagulative state in the lung (15). This is mainly achieved through the production of the two mediator nitric oxide (NO) and prostaglandin-1 (=prostacyclin), which inhibit platelet activation, adhesion and aggregation. NO furthermore serves as a crucial vasorelaxant, thereby inhibiting inappropriate vasoconstriction (15). The pulmonary vasculature consists of arteries, veins and capillaries, which are sub-classified based on structural features, such as the degree of elasticity and muscularity (16). ECs form the thin layer in the innermost part, the so-called intima, which has a large number of adherens and tight junctions. Those junctions are important to maintain the barrier integrity, which limits the transfer of fluids, proteins and other blood constituents to the pulmonary interstitium (15, 16). Moreover, ECs can be sub-divided by their functional specialization. Only recently, capillary ECs have been subdivided into two distinct populations, the general capillary cells (gCap), as well as the alveolar capillary cells or aerocytes (aCap) (17). aCaps are important for immune cell translocation and gas exchange and play a significant role in alveologenesis and thus maturation of the lung. On the contrary, gCap cells are responsible for endothelial homeostasis and regeneration and act as endothelial stem cells (17-19).

PF is characterized by several vascular abnormalities, which manifest as vessel narrowing and occlusion, plexiform lesions, intima proliferation and thickening of the smooth muscle cell layer (20-22). Moreover, PH is a common comorbidity/complication in PF, leading to worse disease outcome in patients. PH is defined by an increase of PVR above 3 and elevated mPAP (> 20 mmHg) (3). The prevalence of PH is about 25% in patients with different forms of PPF, who are referred to lung transplantation (23). The prevalence can significantly increase depending on the specific fibrosis subtype. For example, in HP patients, the prevalence of PH ranges from 30 to 50%, while in IPF the prevalence ranges from 40 to even 85% (23). Furthermore, alterations in the distribution and structure of the pulmonary vasculature have been noted in fibrotic lungs. This manifested as diffuse vascularization as well as atypical anastomoses between the systemic and pulmonary vasculature (24). To uphold the functions and minimize dysfunction, ECs possess specialized receptors and mediators:

VWF

Von-Willebrand-Factor (vWF) is a glycoprotein, which is only synthesized in ECs and to a lesser extent in platelets and megakaryocytes, the progenitors of platelets (25). vWF is stored in special organelles, the Weibel Palade bodies (WPB), together with cytokines and mediators important for vascular

homeostasis, angiogenesis and inflammation . Loss of vWF leads to a disturbed distribution of WPB across the endothelium and thus dysregulation in angiogenesis and inflammatory responses. vWF is secreted upon endothelial injury (26, 27). In the circulation vWF exerts two main functions. First, it is an important carrier for the blood-clotting protein Factor VIII and inhibits its' degradation. Second, it is a sensor for vessel damage and induces platelet adhesion and aggregation (26, 27). The activity of vWF is dependent on its size. vWF exists as multimer in the circulation. Greater size in the multimer corresponds on increased activity of vWF (26, 27). Therefore, cleavage via the metalloprotease Adam-13 is important for vascular homeostasis. Less is known about the role of inflammation. However, as vWF provides binding sites for leucocytes, an implication in immune cell rolling, adhesion and extravasation is assumable (26, 27).

Elevated levels of plasma vWF can be measured in various conditions, including for example systemic sclerosis, diabetes mellitus or acute lung injury and is associated with thromboembolic events (28, 29). Increased pulmonary levels of vWF have been measured in a rat model of radiation-induced lung fibrosis. Whether this is due to increased biosynthesis or stronger retention of vWF in the endothelium is not clear until now (29).

Thrombomodulin

Thrombomodulin (Thbd) is an integral membrane glycoprotein, which is constitutively expressed on the surface of ECs (30). Thbd maintains endothelial thrombo-resistance via binding of thrombin and subsequent activation of protein C (30). Mouse models with Thbd mutations or endothelial-specific Thbd deletion have been shown to be unable to generate protein C and are thus in a hyper-thrombotic/hyper-coagulable state (30). Reduced Thbd expression and/or increased soluble Thbd levels have therefore been associated with endothelial injury and vascular dysfunction (30). Moreover, loss of endothelial Thbd led to increased inflammatory signaling and endothelial activation *in-vitro(30)*. Treatment of PF patients with human soluble Thbd demonstrated favorable efficacy, as evidenced by improved 3-month survival and enhanced respiratory function (31-33).

CD31

The platelet endothelial adhesion molecule cluster of differentiation (CD)-31 is a glycoprotein, which is constitutively expressed on the endothelial surface (34). CD31 has efficient signaling ability and is involved in various cellular events, including immune cell transmigration and regulation of endothelial permeability, motility and phenotype (34). Underlying mechanisms are mostly unknown, however impaired immune cell translocation as well as enhanced vascular permeability was confirmed in both rat and mouse models via administration of anti-CD31 antibodies or specific knockout of CD31 (34). CD31 has been implicated in various inflammatory and vascular conditions, including atherosclerosis,

rheumatoid arthritis, multiple sclerosis or sepsis. The functional diversity complicates the utilization of CD31 as a therapeutic target, as targeting it is frequently associated with vascular dysfunction and loss of a functional vascular barrier integrity (34).

VE-Cadherin

VE-Cadherin is an endothelial restricted cell adhesion molecule, which is required for the formation of vascular adherens junction and thus the establishment and maintenance of a proper, functional endothelial barrier (35, 36). The junction marker consists of five extracellular cadherin domains, a transmembrane domain and a cytoplasmic tail. VE-Cadherin form homophilic and multimeric complexes at the adhesion junctions (35, 36). VE-Cadherin is indispensable for the formation of a functional vasculature. This was validated in mice lacking VE-Cadherin, resulting in their inability to survive (35, 36). Functional blocking of VE-Cadherin, leucocyte docking to ECs or the presence of soluble tumor necrosis factor (TNF)-α, VEGF, thrombin or histamine, amongst other factors, induces cell-cell contact disruption, vascular permeability and increased immune cell transmigration (35, 36).

Intercellular adhesion molecule (ICAM)-2

ICAM-2 is a transmembrane glycoprotein of the immunoglobulin superfamily, which is expressed constitutively at the site of endothelial junctions, but also on the vascular surface. ICAM-2 was shown to have important roles in both endothelial barrier formation and maintenance and immune cell trafficking (34, 35, 37). *In-vitro* knock-out of ICAM-2 led to increased gap formation in human umbilical vein ECs (HUVECs), although VE-Cadherin levels have not been changed and *in-vivo*, mice deficient of ICAM-2 exhibited a significantly increased thrombin-induced vascular permeability (35). On the other hand, ICAM-2 knock-out mice or mice treated with anti-ICAM-2 antibody had a significantly reduced neutrophil accumulation (34). Thus, it is assumed that ICAM-2 together with ICAM-1 is important for neutrophil/immune cell adhesion and translocation.

ICAM-1

ICAM-1 is a transmembrane glycoprotein of the immunoglobulin superfamily, which is expressed on the surface of ECs in response to a pro-inflammatory milieu. ICAM-1 consists of five extracellular domains, a transmembrane domain and a short cytoplasmic domain (38). Post-transcriptional alternative splicing results in different ICAM-1 variants, which can influence disease-specific outcomes, due to altered ligand-receptor structure and functional adaptations. This was for example shown in experimental autoimmune and inflammation models (39). ICAM-1 is a main conductor of immune cell adhesion, rolling and translocation (37, 38). Moreover, ICAM-1 downstream kinase signaling, ICAM-1 induced cytokine production and ICAM-1 mediated regulation of the actin cytoskeleton is influencing barrier strength and integrity (38).

Vascular cell adhesion molecule (VCAM)-1

VCAM-1 is a glycoprotein of the immunoglobulin superfamily, which is expressed on the surface of the endothelium in response to pro-inflammatory stimuli (40). It consists of either six or seven extracellular domains, a transmembrane domain and a small cytoplasmic tail (40). VCAM-1 is important for immune cell adhesion and rolling and facilitates their transmigration as it induces endothelial gap formation via generation of reactive oxygen species (ROS), activation of matrix metalloproteinases (MMPs) and the formation of stress fibers (41). Its neutralization or knock-down was shown to significantly reduce immune cell recruitment and translocation both *in-vitro* and *in-vivo* (42). VCAM-1 is implicated in different immunological disorders, as rheumatoid arthritis, asthma bronchiale and organ transplant rejection (40). In IPF patients, elevated pulmonary gene expression levels of VCAM-1 correlated with a reduced lung function (40).

Vascular endothelial growth factor receptor (VEGFR)-2

VEGFR-2 is a transmembrane protein of ECs, which gets activated upon homo- or heterodimerization (43). Binding of its ligands VEGF-A, VEGF-C or VEGF-D induces endothelial proliferation, invasion, migration, survival and finally vascularization. VEGFR-2 VEGF-A signaling is central for vasculogenesis (= de-novo formation of blood vessels from endothelial precursors) and angiogenesis (= growth, sprouting and splitting of existing vasculature) and VEGFR-2 deficient mice are not viable due to impaired endothelial development (43). In addition, VEGFR-2 is an important conductor of vascular permeability via endothelial nitric oxide synthase (eNOS) activation and subsequent nitric oxide (NO) generation (43). Blocking of VEGFR-2 signaling with the tyrosine kinase inhibitor SU5416 was shown to attenuate bleomycin-induced lung fibrosis in mice (44).

Interleukin (IL)-8

Generally, interleukins participate in the innate and adaptive immune response and facilitate the proliferation, differentiation and recruitment of inflammatory/immune cells (45). In PF, increased levels of interleukins have been measured in the lung, bronchoalveolar fluid as well as the blood circulation of patients. The levels are not only differing between healthy individuals and patients, but are also varying depending on the stage of the disease (45). IL-8 is secreted from immune cells, but also fibroblasts and ECs. It belongs to the CXC-subfamily of chemokines (chemoattractant for neutrophils) and exists in two different forms, depending on its length (monocyte-derived IL-8 versus endothelial/fibroblast-derived IL-8) (46). The main functions include immune cell attraction, activation and migration. Additionally, IL-8 acts as chemoattractant on fibroblasts during the process of wound healing and induces their migration and deposition of collagen and fibronectin (46). IL-8 is implicated in various inflammatory conditions/diseases, including for example COPD, ARDS or asthma bronchiale

(46). In PF, serum levels of IL-8 have been correlated with worsened lung function and increased mortality (45).

P-selectin

P-selectin is a type I membrane protein, which is constitutively expressed and stored in either α-granules of platelets or WBP of ECs (47). Upon activation of platelets and ECs due to a pro-inflammatory, injurious trigger, P-selectin is transferred to the cell surface and also being shed and secreted to the circulation (47). P-selectin has two main functions, which are recruitment of leucocytes to the site of inflammation and facilitation of platelet-platelet interaction. The main ligand for leucocyte recruitment is P-selectin glycoprotein ligand 1. Moreover, increased levels of P-selectin induce the synthesis and secretion of tissue factor (TF) by monocytes. Therefore, P-selectin is a central conductor in coagulation and thrombus formation (47, 48). In PF patients, a significant increase of both platelet activity and soluble P-selectin levels have been measured (48). The genetic ablation or antibody-mediated neutralization of P-selectin have been shown to attenuate the extent of parenchymal remodeling in the mouse models of bleomycin-induced PF and in the GATA-1$^{(low)}$ mouse model of myelofibrosis (49).

Angiogenesis in PF

Research indicates the presence of altered angiogenesis, which is defined as the formation of new blood vessels from existing vasculature, in PF. A notable increase in CD34-positive ECs has been observed in non-fibrotic regions of fibrotic lung biopsies, while fibrotic foci lacked CD34-positive and Thbd-positive capillaries, as well as vWF-positive vessels (50-52). This was further confirmed in a rat model of bleomycin-induced PF as well as in a lung fibrosis model of adenovector-mediated transforming growth factor (TGF)-β transfer in rats (53, 54). The capillary regression was associated with advanced age in a mouse model of bleomycin-induced PF (55). The reduced ability for proper angiogenesis and vascular remodeling was associated with an impaired chromatin accessibility due to dysfunctional transcriptional signaling as assessed by an integrative epigenetic and transcriptional analysis (18).

In human lungs affected by fibrosis, imbalances of pro- and antiangiogenic factors have been measured. Proangiogenic IL-8 was elevated in PF lungs, while antiangiogenic interferon-gamma-inducible protein (IP)-10 was reduced as compared to donor specimen (56). Moreover, fibrotic foci showed increased levels of antiangiogenic pigment epithelium-derived factor (PEDF), while proangiogenic VEGF was diminished in these areas (57, 58). Lungs of bleomycin-treated mice exhibited elevated proangiogenic macrophage inflammatory protein (MIP)-2 and neutralization of MIP-2 or administration of antiangiogenic mediator IP-10 significantly improved the fibrotic phenotype (59, 60).

Mice deficient of IP-10 showed worsened fibrotic remodeling (61). However inhibition of angiogenesis via CXC motif chemokine receptor (CXCR)-2 antagonist DF2162 was reported to ameliorate PF in the bleomycin model (62). In line, scRNA-seq revealed that an endothelial subpopulation enriched in proangiogenic genes was significantly larger in bleomycin-treated rats as compared to controls (63). On the contrary, the deficiency of endothelial ETS-related gene (ERG), a mediator of chromatin remodeling, was associated with the repression of angiogenesis-associated genes (e.g. Mmp14, Semag3 and Tek) and a worse fibrotic phenotype in young mice treated with bleomycin as compared to the non-deficient littermates (18).

Vascular permeability in PF

The endothelial barrier integrity is maintained by specific molecules, such as VE-Cadherin, occludin or claudin-5, which form tight and adherens junctions (64). In fibrotic lungs, signs of endothelial integrity disruption are evident. This phenomenon was assessed through the administration of various contrast agents, which exhibited significantly faster clearance from fibrotic lungs compared to healthy ones (65, 66). An accelerated clearing rate was correlated with a more pronounced decline in lung function (65, 66). Moreover, leaky vessels were suggested to serve as a trigger for fibrinogen extravasation and fibrin deposition in the interstitium and cross-linked fibrin complexes can subsequently induce their replacement by exuberant amounts of granulation tissue and maturation of the granulation tissue to connective tissue (67).

Different signaling pathways and mediators of vascular permeability have been reported to be dysregulated in both the human disease and animal models of PF, including the sphingosine-1-phosphate (S1P) – S1P-receptor signaling axis, the angiopoietin-1 (Ang-1)/angiopoietin-2 (Ang-2)—tunica internal endothelial cell kinase-2 (Tie-2) receptor axis and the VEGFR-2-VEGF-A axis. S1P deficiency enhanced the vascular permeability and worsened the fibrotic phenotype in the bleomycin mouse model (68). On the contrary, another study showed that S1P-kinase inhibition led to an improvement in the disease progression and S1P-kinase levels have been associated with an accelerated lung function decline and mortality in PF patients (69, 70). The knockdown of S1P-kinase in mice and therefore absence of S1P reduced fibrotic remodeling in mice (70). Studies on the VEGFR-2-VEGF-A axis led to controversial findings as well. On one hand, inhibition of VEGF-signaling via gene therapy or specific inhibitors effectively reduced lung fibrosis in mice treated with bleomycin, while VEGF-overexpression worsened fibrogenesis (44, 54, 71, 72). On the other hand, another findings, indicated an improvement in lung fibrosis when vascular endothelial growth factor (VEGF) is overexpressed (73, 74).

Furthermore, the permeability enhancer Ang-2 is elevated in the serum and bronchoalveolar lavage fluid of PF patients and correlates with acute exacerbation (75-77).

Endothelial activation and inflammation in PF

ECs actively participate in and serve as crucial regulators of immune and inflammatory responses. This primarily relies on the expression of specific adhesion molecules (e.g. VCAM-1, ICAM-1) and selectins (E-selectin, P-selectin, L-selectin) on the vascular surface (15).

Single cell RNA sequencing (scRNA-seq) uncovered an immune-cell like EC population in murine lungs, which was enriched in genes related to functions such as immune cell adhesion, activation, migration and their functionality (78). In parallel, two novel capillary subpopulations have been identified in murine and human lungs by scRNA-seq, referred to as “general capillary ECs” (gCap) and “aerocytes” (aCap) (17, 79). Both have been enriched in genes related to immune responses, including “immune cell trafficking” or “antigen presentation”. gCap have additionally been enriched in genes important for vascular homeostasis and repair and were diminished in lung tissue samples from PF patients (79). In the presence of a pro-inflammatory milieu (lipopolysaccharide-stimulation) pulmonary ECs reacted more sensitive, as measured by a significant downregulation of canonical vascular markers (78).

EC adhesion molecules can exist as both, as transmembrane as well as a soluble form (80). The process of adhesion molecule cleavage from the cell surface is called ectodomain cleavage and is facilitated by different proteases, including MMPs, disintegrin metalloproteinases (ADAMs), neutrophil elastase, cathepsins and proteinase-3 (81). *In-vitro* the levels of soluble adhesion molecules were increased after ECs were cultured in a pro-inflammatory milieu (TNF-α) (82). Shedding has been postulated as an important regulatory mechanism of inflammation, as increased adhesion molecule shedding is characteristic for many inflammation-driven diseases, like sepsis, vasculitis, atherosclerosis, cancer and also PF (81, 83-85). Soluble VCAM-1, ICAM-1, and IL-8 have been proposed as predictors for poor transplant-free survival, poor progression-free survival, and overall poor survival in the patients and sVCAM-1, sICAM-1 and sP-selectin have been associated with reduced lung function and worse disease outcome (86-88).

Coronavirus disease 2019 (COVID-19) and PF

Over the last years, pulmonary fibrosis has also been recognized as a potential consequence of severe acute respiratory syndrome coronavirus 2 (SARS-CoV-2) infection (89-93). SARS-CoV-2 was initially observed in Wuhan, China, in late 2019 causing pneumonia-like infections with unusual characteristics. Soon after, the COVID-19 pandemic was declared by the world health organization on March 11th 2020, with approximately 7 million deaths until now. The manifestation of COVID-19 varies, ranging from asymptomatic course of infection to cases with few symptoms and severe disease, including pneumonia, acute respiratory distress syndrome (ARDS) and the need for admission to the intensive care unit (ICU) (94). SARS-CoV-2 is a single stranded positive-sense RNA virus and belongs to the beta-

coronavirus group (95). The virus is composed of a spike (S) protein, a membrane (M) protein, an envelope (E) protein and a nucleocapsid (N) protein (90). Binding and fusion between the virus and host cell membrane depends on the interaction between the surface S protein and the angiotensin-converting enzyme 2 (ACE2), the main vehicle for viral entrance into pulmonary epithelial cells (90, 96). The S protein is a homotrimer, which is cleaved by the host cell convertase furin to generate the subunits S1 and S2. S1 is needed for binding between the virus and host cell, while S2 is important for firm anchoring (97). The conformational change induced by furin-cleavage triggers an additional cleavage step in the S2 subunit. Cleavage by the target cell transmembrane serine protease 2 (TMPRSS2) or lysosomal protease cathepsin L results in a fusion pore, which allows the viral genome to enter the target cell (97) .

ACE2 is a zinc metallopeptidase and an important component of the renin-angiotensin-system (RAS) (98). While ACE generates angiotensin (ANG) II from ANG I, ACE2 generates angiotensin (1-9) from ANG I and Ang (1-7) from ANG II (98). ANG I is originating from renin-mediated Angiotensinogen cleavage. ANG II induces vasoconstriction, inflammation and oxidative stress by binding to its receptor ANG II type 1 receptor (AT1R). Ang (1-7) and Ang (1-9) lead to vasodilation by binding to the receptors AT2R or Mas (98). The balance between vasoconstriction and vasodilation, and consequently vascular homeostasis, stems from the central influence of the renin-angiotensin system on NO metabolism (Figure 2) (99). NO is a central mediator for the maintenance of a quiescent endothelium and is produced by the eNOS (100). eNOS is active in the presence of ACE2, but deactivated in the presence of increasing ANG II levels (99). In COVID-19 patients, ANG II levels are significantly upregulated and correlate with the viral load and degree of lung injury (101).

Besides ACE2, basigin (BSG, CD147) is another transmembrane protein on epithelial cells facilitating the entrance of SARS-CoV2. Suppression of BSG via silencing or antibodies resulted in a reduction of viral infection, however the exact interaction mechanisms between SARS-CoV2 and BSG remain unknown (102).

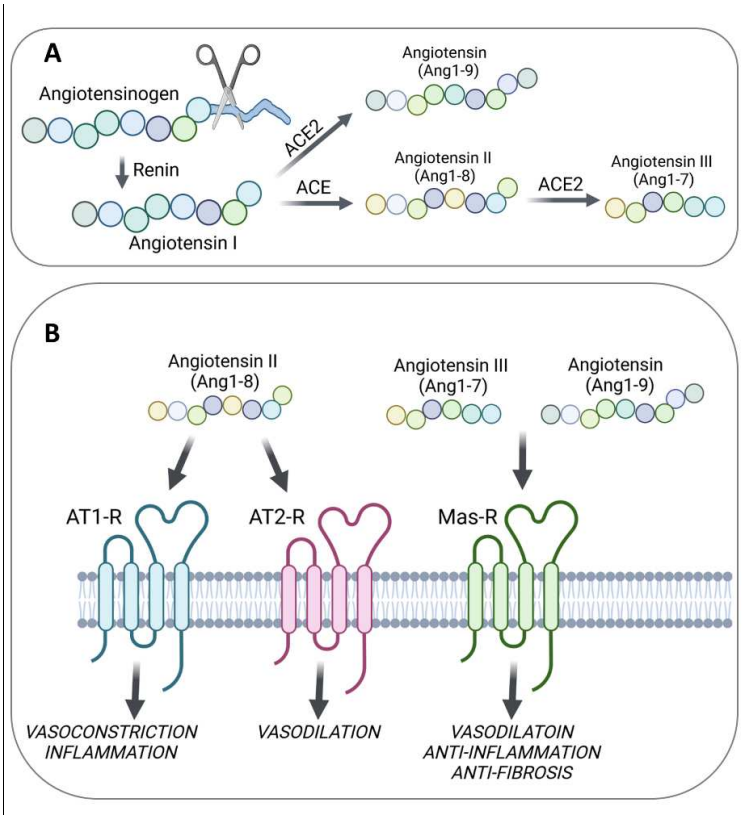

Figure 2: Overview of the renin-angiotensin-system (RAS). (A) Cleavage enzymes and products of angiotensinogen. (B) Receptors AT1-R, AT2-R and Mas-R and their corresponding ligands as well as resulting functional alterations upon binding. Created with BioRender.com (Agreement number: XO26H9TUC5 and OQ26H9TX80).

COVID-19 is associated with marked morphological and molecular vascular alterations. Key features like alveolar-capillary damage, edema, micro-thrombosis, angiogenesis and increased platelet activation pointed towards a substantial vascular involvement right from the early stages of the pandemic (96). Depending on the severity of the infection, extensive alveolar-capillary damage can cause “diffuse alveolar damage” (DAD), which is characterized by barrier disruption, edema and hyper-inflammation (103). DAD is the histological hallmark of ARDS (103). ARDS is presented by severely impaired gas exchange and hypoxemia due to excessive destruction of the alveolar-capillary barrier and is coming along with loss of endothelial function, obliteration of the microvasculature and heavy vascular inflammation (103, 104). The exuberant inflammatory response observed in severe COVID-19 is commonly referred to as “cytokine storm” (96). The cytokine storm, consisting of crucial inflammatory cytokines such as IL-1, IL-2, IL-6, TNF-α, interferon (IFN)-γ, IP-10, granulocyte-macrophage colony-stimulating factor (GM-CSF), monocyte chemoattractant protein-1 (MCP-1), and IL-10 triggers the disruption of vascular adherens and tight junctions as well as shedding of glycocalix components (100, 105). This is followed by further endothelial activation, characterized by increased expression of surface adhesion molecules (e.g. ICAM-1, VCAM-1, E-selectin), release of pro-inflammatory cytokines as well as vWF and mitochondrial/oxidative stress (100, 106). The hyper-

inflammatory state is accompanied by a strong pro-coagulative environment in severely ill individuals, which together is widely recognized as “immuno-thrombosis”. Immuno-thrombosis refers to the maladapted interplay between the hyper-activated endothelium, the immune system and the coagulation cascade (100, 107). The lack of homeostasis mediator NO and simultaneous inflammation-induced overexpression of TF trigger the recruitment and adhesion of immune cells as well as the secretion and aggregation of platelets (99, 100, 108). Platelets from severely ill patients demonstrate heightened activation and aggregation capability, attributed to an increased surface expression of P-selectin (107). Neutrophils are recruited increasingly from the early stages of infection onward. They release proteolytic enzymes, chemokines, cytokines and ROS on the one hand and undergo programmed cell death, called NETosis, which leads to the formation of extracellular web-like structures (NETs) containing DNA, histones, proteins, enzymes, coagulants and other factors. Both mechanisms promote inflammation and coagulation (107). TF induces thrombin generation, which in further consequence propagates fibrin deposition (108). This interaction among neutrophils, NETs, fibrin and hyperactive platelets leads to the formation of intra- and extravascular fibrin clots, which cannot be degraded, as the pro-inflammatory environment disrupts anti-coagulative and pro-fibrinolytic pathways (108). A notable increase in the shedding of fibrinolytic thrombomodulin from the endothelial surface is commonly observed in COVID-19 (99). Additional vascular abnormalities frequently observed in critically ill COVID-19 patients include intussusceptive, non-sprouting angiogenesis and endothelial senescence (100). Intussusceptive angiogenesis is accompanied by increased circulatory levels of angiogenesis mediators, such as VEGF, VEGFR-1, PDGF, MMP-2 or hypoxia inducible factor (HIF)-1α and is further promoting permeability, vascular leakage and infiltration of immune cells (Figure 3) (99). Endothelial senescence serves as a primary stress response and is accompanied by further inflammation (109). Dysbalances of various endothelial dysfunction-related markers can be measured in critically ill COVID-19 patients, including D-dimer (coagulation), vWF (coagulation, inflammation), factor VIII (coagulation), plasminogen activator inhibitor (PAI)-1 (endothelial damage and senescence), Thbd (fibrinolysis), P-selectin (coagulation), Ang-2 (angiogenesis), E-selectin, ICAM-1, VCAM-1, IL-6, IL-8 and MCP-1 (activation and inflammation) or syndecan-1 (glycocalix damage) (100, 106).

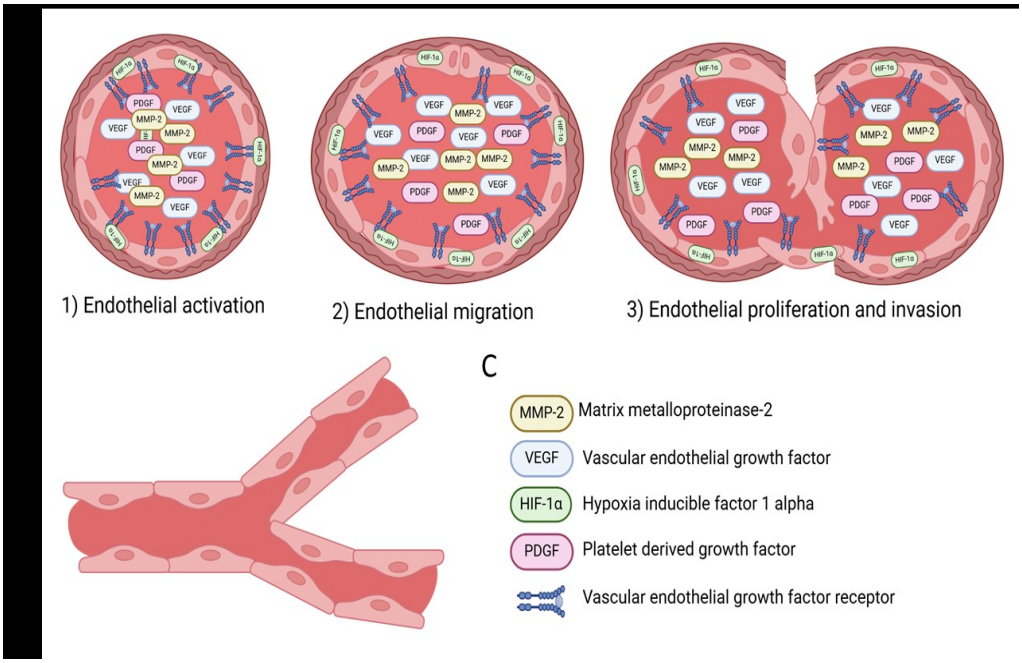

Figure 3: Intussusceptive angiogenesis. (A) Schematic overview of intussusceptive, branching angiogenesis in the presence of pro-angiogenic mediators Matrix Metalloproteinase (MMP)-2, vascular endothelial growth factor (VEGF), hypoxia inducible factor (HIF)-1α and platelet derived growth factor (PDGF) as well as vascular endothelial growth factor receptor (VEGF-R). The process is divided into endothelial activation (1), migration (2) and proliferation and invasion into the lumen of the existing vessel (3). (B) Newly formed, branched vessel after intussusceptive angiogenesis. (C) Mediators participating in intussusceptive angiogenesis. Created with BioRender.com (Agreement number: WG26H9TN7C).

After resolution of the acute phase of ARDS, some patients exhibit persistent presence of fatigue, shortness of breath, cognitive abnormalities and limited capabilities to perform daily activities. These symptoms can persist for months or even years and are commonly referred to as "long COVID" (110, 111). In this context, the potential development of progressive pulmonary fibrosis represents a significant concern associated with long COVID. The prevalence of COVID-associated fibrosis remains undefined. Estimates indicate that around one-third of individuals who have recovered from the virus may experience fibrotic manifestations in the lungs (112). The prevalence is also dependent on the duration of the initial infection (112). SARS-CoV-2 is thought to provoke the development of PPF based on 2 mechanisms: 1) through continuous and excessive viral invasion of the pulmonary epithelium, activating abnormal wound healing and 2) through the persisting accumulation of immune cells, which are propagating a pro-fibrotic milieu (90). Mediators and pathways, which are important and well-characterized in ILD-associated PPF, have also been shown to be upregulated in COVID-19 associated PF. Upon those, TGF-β, a highly pro-fibrotic molecule, is continuously elevated in severe COVID-19 (113). Moreover, WNT signaling is crucial in the regulation of cell proliferation and migration in both, pulmonary inflammation and fibrosis. In COVID-19, Wnt5a and Wnt11 have been proposed as biomarkers indicating the disease severity (114). Another signaling axis implicated in the pathophysiology of fibrotic lung diseases is the Hippo - Yes-Associated Proteins (YAP) and

Transcriptional co-activator with PDZ-binding motif (TAZ) pathway (115). Aberrant activation of the Hippo – YAP/TAZ signaling pathway causes disturbed lung alveolar regeneration and exuberant fibroblast activation, thus leading to increased fibrotic remodeling (115). The pathway is also exuberantly activated during COVID-19 disease, as it acts antiviral as well (116). In addition COVID-19 associated PF follows a UIP pattern, similar to most ILD-PPFs (112). Parenchymal abnormalities, including ground glass opacities, septal thickening, and traction bronchiectasis or honeycombing have been identified in nearly 25% of severely ill COVID-19 patients at the one year follow-up examination (112). Several studies indicate that the risk factors for the development of lung fibrosis due to COVID-19 are comparable to those of ILD-PPF and include advanced age (> 40 years), male sex, smoking or comorbidities (e.g. diabetes, hypertension, cardiovascular disease). In the case of COVID-19 prolonged hospitalization, the need for intensive care unit (ICU, > 16 days) and mechanical ventilation depict additional risk factors (89, 112).

The main predictor for the progression to lung fibrosis following a severe COVID-19 infection is the occurrence/presence of ARDS. As mentioned above, ARDS is characterized by the disruption of the alveolar-capillary barrier, causing endothelial dysfunction, microvascular destruction and heavy vascular inflammation (103, 104). The initial injury phase is followed by a repair phase and finally a fibro-proliferative response. The extent of the fibro-proliferative response is closely associated with poor prognosis in ARDS (103, 104). The underlying mechanisms causing persistent, non-resolving fibro-proliferation in a subset of COVID-19 - ARDS patients are poorly understood so far (89). However, the risk of progressing to the unregulated fibro-proliferative phenotype cannot be overlooked, as ARDS has an overall prevalence of 3.6% amongst COVID-19 patients (117). Long-term data must be awaited, which will resolve whether long-COVID associated fibro-proliferation results either in a self-resolving or progressive and irreversible phenotype.

Treatment of PPF

Despite extensive research efforts, PPF is still regarded a non-curable disease (118). The availability of anti-fibrotic and disease-modifying treatment options is limited, with Pirfenidone and Nintedanib being the only approved drugs for IPF to date (118). Due to rapid loss of proper lung function and architecture, lung transplantation remains inevitable in PPF patients (6).

Pirfenidone is a pharmacological compound with anti-inflammatory and anti-fibrotic properties (119). Although the exact underlying mechanisms of action remain unknown, Pirfenidone attenuates fibroblast proliferation, inhibits myofibroblast differentiation and reduces collagen and ECM as well as pro-inflammatory cytokine synthesis (119). The drug, which got approved in 2008 for the treatment of IPF, was shown to significantly lower mortality, forced vital capacity decline, hospitalization rate and

increases exercise capacity. Adverse effects are generally mild and can be circumvented by adjusting the dose (119).

Nintedanib is a small-molecule tyrosine kinase inhibitor, which got approved for the treatment of IPF in 2014 (120). The drug interferes with PDGF-receptor, FGF-receptor and VEGF-receptor signaling, thereby inhibiting fibroblast proliferation and differentiation (120). Moreover, Nintedanib inhibits the growth of various other cells, including endothelial cells, smooth muscle cells and pericytes. Thus it also limits vascular remodeling as well as the extent of inflammation, by reducing the release of pro-inflammatory cytokines (120).

Various studies have been conducted or are currently ongoing to proof whether the two anti-fibrotic drugs are also effective in other fibrosing ILDs. In 2019, the INBUILD study was published, reporting that Nintedanib is effective for the treatment of 5 major ILD entities, including Hypersensitivity Pneumonitis (HP), autoimmune ILDs, idiopathic NSIP unclassifiable idiopathic interstitial pneumonia and other ILDs (121). Whether Pirfenidone is also feasible to be applied in various fibrosing ILDs remains unknown, as the RELIEF study had to be terminated early due to too low numbers of recruited patients (6, 122) .

Currently, individuals with HP or NSIP commonly undergo anti-inflammatory/immunomodulatory treatment, whereas connective tissue disease related ILDs are treated with immunosuppressive therapy options. As anti-inflammatory treatment was shown to have harmful effects in IPF patients (122), leading to elevated mortality, a thorough and precise diagnosis of the exact ILD entity holds paramount significance.

Endothelial-directed therapy options

While the precise mechanism of action of the two approved anti-fibrotic drugs, Pirfenidone and Nintedanib, are not fully understood, they both, in part, operate through the endothelial VEGFR-2 VEGFA signaling axis. Besides, other endothelial-directed therapies have been investigated in various clinical trials (120, 123).

Sildenafil, a vasodilating phosphodiesterase-5 inhibitor for the treatment of PH, has been shown in the 2016 INSTAGE trial to further decrease the decline of FVC in a combination therapy with Nintedanib (124).

More recently, the INCREASE trial tested inhaled Treprostinil, a vasodilating and anti-coagulative prostacyclin analog, in ILD-PH patients (125). Administering Treprostinil over a period of 16 weeks led to a significant improvement in the 6 minute walk distance (6MWD), a reduction of N-terminal pro-B-type natriuretic peptide (NT-proBNP) levels and a slowed progression of the disease (126). Currently, a prospective study of inhaled Treprostinil is underway, with initial results being awaited soon.

Rationale of the study

Despite distinct clinical, radiological, and pathological features, ILDs and COVID-19 share a common progressive fibrotic phenotype. This phenotype is characterized by epithelial injury, accumulation of fibroblasts and myofibroblasts, as well as excessive ECM production.

So far, research in the field of PPF has mainly focused on the interplay of an initial epithelial injury and the subsequent aberrant fibroblast activation and differentiation into myofibroblasts (127, 128). However, as the epithelium is separated from the endothelium only by a thin basement membrane, the initial injury must affect the capillaries as well. Particularly in COVID-19, it becomes evident that alveolar destruction is closely linked to a significant impairment of the endothelial compartment. As demonstrated by our research and that of others, this phenomenon is characterized by a hyper-activated, hyper-inflamed, and hyper-coagulable endothelium (129). It is accompanied by metabolic maladaptation, loss of vascular integrity, and increased shedding of endothelial surface and glycocalix components (129).

Similar observations have recently also been reported in PPF associated with ILD. Reports highlighting pronounced vascular remodeling and inflammation, abnormal alveolar-capillary permeability, and aberrant coagulation and vessel density are becoming more prevalent (129). Furthermore, endothelium-targeting therapy options are now being considered, as they demonstrate significant improvements in the disease for the first time (125, 126, 130, 131).

Based on the reported findings and observations, **we hypothesized that the endothelium is dysfunctional in COVID-19 and PPF and plays a central and active role, rather than acting as a passive bystander, in the disease pathogenesis** (Figure 4).

The overarching aim of the project was to comprehensively evaluate alterations of the endothelium in PPF, with regard to spatial and temporal changes of its activation and integrity. For this purpose, we performed a detailed analysis of ECs on a structural, functional, transcriptional and protein level both locally in the lungs as well as systemically in the blood circulation of PPF patients and controls. As a complementary approach, we utilized the bleomycin-induced mouse model of PF-PH to investigate time-dependent alterations over the course of the disease.

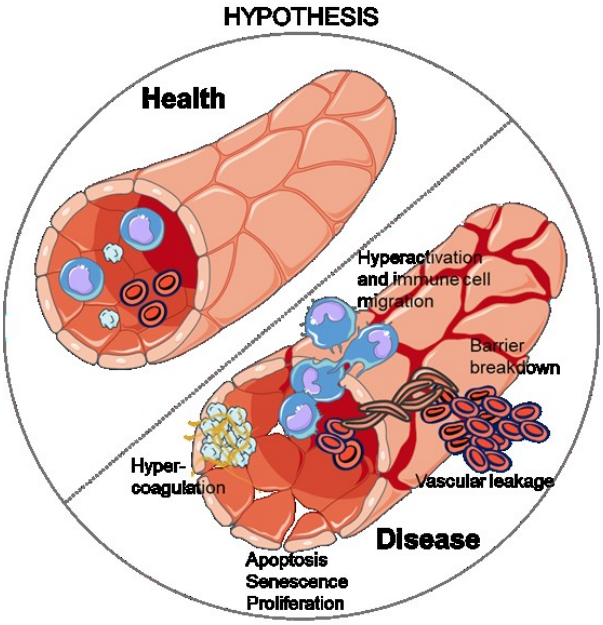

Figure 4: Proposed hypothesis of the dissertation. The endothelium is dysfunctional in COVID 19 and PPF and actively participates in the disease pathogenesis. Created with Smart Servier Medical Art.

Detailed materials and methods

Human tissue and plasma

Lung tissue samples were collected post mortem from 19 critically ill COVID-19 patients and 11 age and sex-matched autopsy controls without any lung pathology at the Medical University of Graz (ethic number: 32-362 ex 19/20) (Table 1), from patients with COPD (n = 28), IPAH (n = 10) and PF (n = 10) (Table 2) and from 16 PF patients and 19 donors (Table 3) during lung transplantation at the Department of Surgery, Division of Thoracic Surgery at the Medical University of Vienna (ethic number: 976/2010).

Ethylenediaminetetraacetic acid (EDTA) plasma samples were collected from 21 critically ill COVID-19 patients and 22 age and sex-matched healthy controls (Table 4) at the Hannover Medical School, Hannover, Germany and from the Department of Clinical Immunology and Transfusion Medicine at the Justus-Liebig University of Giessen, Germany (ethic numbers: SEPSIS/ARDS Registry 8146_BO_K_2018 and 05/00). EDTA plasma samples from 19 PF patients were collected during lung transplantation at the Department of Surgery, Division of Thoracic Surgery at the Medical University of Vienna (ethic number: 976/2010). 28 healthy control plasma samples were collected by the Biobank at the Medical University of Graz (ethic number: 23-408 ex 10/11) (Table 3). Plasma samples from 25 COPD, 15 IPAH and 10 PF patients were collected either prospectively from an IPAH cohort of patients undergoing right heart characterization at the Medical University of Graz (ethic number: 23-408 ex 10/11) or during lung transplantation at the Medical University of Vienna (ethic number: 976/2010). Control plasma (n = 35) was collected prospectively at the Biobank of the Medical University of Graz (ethic number: 23-408 ex 10/11) (Table 5). Plasma samples were stored at -80°C until further analysis.

Written informed consent was obtained from all patients/participants.

Table 1: Clinical characteristics of COVID-19 patients and CONTROLS used for gene expression analysis. CRP = C-reactive protein.

Autopsy lung tissue samples		
	COVID-19	**CONTROL**
Subjects (n)	19	11
Age (years)	78.4 ± 9.5	72.9 ± 8.2
Sex (male:female)	13:6	6:5
CRP (mg/l)	114.1 ± 86.6	54.9 ± 109.9
D-dimer (mg/l)	3.0 ± 2.9	NA
Fibrinogen (mg/ml)	4.9 ± 0.9	3.1 ± 1.6
Thrombocytes (n/l)	201.0 ± 78.0	214.0 ± 63.8

Table 2: Clinical characteristics of COPD, IPAH and PF patients and CONTROLS used for gene expression analysis. LTX = lung transplantation. BMI = body mass index. FEV1 = forced expiratory volume in 1 second. FVC = forced vital capacity. pO_2 = partial pressure of O_2.

	Donor	COPD	IPAH	PF
Subjects (N)	10	28	10	9
Sex (male:female)	4:6	13:16	3:7	6:3
Age at LTX (years)	41 (± 18.7)	57 (± 5.6)	31 (± 12.2)	56 (± 9.2)
BMI (kg/m²)	25 (± 4.3)	22 (± 2.5)	20 (± 3.1)	25 (± 4.2)
Smoking status (never/former/active/unknown)	NA	1/23/0/5	NA	NA
FEV1 (% predicted)	NA	23 (± 11.2)	73 (± 7.0)	43.3 (± 10.7)
FVC (% predicted)	NA	48 (± 18.1)	80 (± 9.2)	43 (± 10.1)
mPAP (mmHg)	NA	32 (± 10.8)	68 (± 26.9)	41 (± 6.8)
pO_2 (mmHg)	NA	70 (± 12.1)	70 (± 13.8)	60 (± 20.4)

Table 3: Clinical characteristics of endstage disease patients and donors used for gene expression and plasma analysis. TLC = total lung capacity.

	Transplant lung tissue		Plasma samples	
	Donor	PF	Control	PF
Subjects (n)	19	16	28	19
Classification	NA	1 IPF, 15 other fibrosing ILDs (1 familial PF, 14 HP)	NA	7 IPF, 12 other fibrosing ILDs (1 familial PF, 8 HP, 1 NSIP, 2 unclassifyable)
Age at lung transplantation (years)	48.5 ± 14.5	57.2 ± 6.8	56.3 ± 7.7	61.5 ± 7.4
Sex (female/male)	10/9	5/11	19/9	6/13
BMI (kg/m²)	24.8 ± 4.0	25.3 ± 3.7	27.0 ± 8.2	26.4 ± 3.8
FEV1 (% predicted)	-	46.6 ± 17.3	-	54.6 ± 21.6
FVC (% predicted)	-	38.0. ± 14.6	-	50.3 ± 24.1
mPAP (mmHg)	-	31.9 ± 8.5	-	39.7 ± 11.2
TLC (% predicted)	-	50.8 ± 16.5	-	64.7 ± 21.3
CRP (mg/l)	-	1.7 ± 2.2	-	1.4 ± 2.0
PH (yes/no)	-	13/3	-	16/3

Table 4: Clinical characteristics of COVID-19 patients and CONTROLS used for plasma analysis. PCT = Procalcitonin. PTT = Partial Thromboplastin Time. SOFA score = Sepsis Related Organ Failure Assessment Score.

Plasma samples		
	COVID-19	**CONTROL**
Subjects (n)	21	22
Age (years)	59 (19-82)	61 (19-78)
Males (%)	90	89
BMI (kg/m²)	29 (15-62)	NA
CRP (mg/l)	151 (68-292)	NA
PCT (µg/l)	1 (0.1-6.6)	NA
D-dimer (mg/l)	4 (1-35)	NA
Fibrinogen (mg/ml)	7 (4-9)	NA
PTT (s)	36 (26-55)	NA
SOFA score	13 (9-17)	NA
Thrombocytes (n/l)	247 (99-581)	NA
Mechanical ventilation (%)	100	NA
Received vasopressors (%)	100	NA

Table 5: Clinical characteristics of COPD, IPAH and PF patients and CONTROLS used for ACE2 plasma analysis.

PLASMA				
	Donor	**COPD**	**IPAH**	**PF**
Subjects (N)	35	24	15	10
Sex (male:female)	NA	8:16	4:11	7:3
BMI (kg/m2)	NA	22.4 (± 3.2)	23.7 (± 2.8)	26.7 (± 3.7)
Smoking status (never/former/active/unknown)	NA	2/22/1/0	NA	NA
FEV1 (% predicted)	NA	23.7 (± 9.8)	76.8 (± 10.1)	45.9 (± 11.3)
FVC (% predicted)	NA	50.3 (± 16.4)	81.2 (± 12.9)	38.4 (± 8.8)
mPAP (mmHg)	NA	30.3 (± 9.7)	56.2 (± 24.5)	41.2 (± 9.3)
pO2 (mmHg)	NA	66.3 (± 11.7)	46.2 (± 16.8)	54.5 (± 16.2)

Bleomycin mouse model

Mice (C57BL6 background) were kept at the Biomedical Research facility of the Medical University of Graz in isolated and ventilated cages with 12-hour light/dark cycles. Water and chow were supplied ad libitum. Experienced Personnel took care of the mice daily. The well-being of the animals was further

assured through nesting material and tunnels. To minimize the animals' stress level, it was avoided to keep single mice alone in cages and mice were transferred to the experimental facility at least 3 days prior to the experiment. All animal experiments were approved by the local authorities (Austrian Ministry of Education, Science and Culture) and performed in accordance with the EU directive 2010/63/EU.

Bleomycin (1.5 U/kg body weight, Sigma Aldrich) or saline was applied intratracheally with a MicroSprayer Aerosolizer (Penn-Century, Pennsylvania, US) under light (~2%) isoflurane anesthesia. Either 3 days, 14 days or 21 days after bleomycin administration, lung function measurements (FlexiVent, Meyers GmbH, Germany) were conducted prior to opening the thorax and exsanguinating the mice by collecting the maximum volume of blood from the right ventricle. The blood was collected in tubes containing 30 µl 3.6% sodium citrate for plasma collection. 1 ml phosphate-buffered saline (PBS) supplemented with 2mM EDTA and protease inhibitors (Sigma Aldrich, Missouri, US) was used to lavage the lungs. The bronchoalveolar lavage was kept on ice until centrifugation for 5 minutes at 500 g at 4°C for cell collection. Cells were fixed in 1% paraformaldehyde (PFA) in PBS for 20 minutes, washed with magnetic activated cell sorting (MACS) buffer and used for flow cytometry analysis. After lung lavage, an incision was made in the left atrium to flush the lungs with PBS rough the right ventricle until the lungs appeared in white color. A suture was applied below the right lung lobes to tie them off. The middle right lobe was collected in medium for flow cytometry analysis. The remaining right lobes were shock frozen in liquid nitrogen for further RNA and protein analysis. The left lobe was filled with formalin, taken out of the murine thorax and fixed in formalin for 24 hours before embedding in paraffin.

Quantitative real-time PCR (qRT-PCR)

Human and murine lung tissue samples were collected and cryopreserved in liquid nitrogen. Human pulmonary endothelial cells were lysed in buffer RLT (Qiagen, Hilden, Germany) and stored at -80°C. Prior to RNA isolation, tissue was homogenized in a Magnalyser (Roche Diagnostics, Rotkreuz, Switzerland). RNA was isolated from homogenized tissue or lysed cells using either the peqGOLD Total RNA Kit (Peqlab, Erlangen, Germany) or the the innuPREP RNA Mini Kit (IST Innuscree, Berlin, Germany) according to the manufacturer's instructions. cDNA synthesis was done using the qScript™ cDNA Synthesis Kit (Quantabio, Massachusetts, US) according to the manufacturer's instructions. qPCR was run on a LightCycler® 480 System (Roche Applied Science, Penzberg, Germany) using the QuantiFast® SYBR® Green PCR kit (Qiagen). qPCRs were performed according to the following protocol: 5 minutes at 95 °C (5 seconds at 95 °C, 5 seconds at 60 °C, and 10 seconds at 72 °C) × 45. Primer specificity was confirmed with melting curve analysis and gel electrophoresis. Primer sequences are shown in Table

4. Hydroxymethylbilane synthase (HMBS/PBGD) and beta-2-microglobulin (B2M) were used as the reference genes.

The ΔCt values were calculated using the following formula:

$$\Delta Ct = Ct\ (reference\ gene) - Ct\ (gene\ of\ interest)$$

ΔCt values of donors and patients or saline and bleomycin treated mice were normalized to the mean gene expression of donors/saline treated mice (ΔΔCt):

$$\Delta\Delta Ct = \Delta Ct\ diseased - mean\ \Delta Ct\ of\ all\ controls$$

Table 1. List of applied human (Hs) and murine (Mm) primers.

Gene name	**Primer sequence forward 5´ - 3´**	**Primer sequence reverse 5´ - 3´**
Hs_PECAM1	TCCGTTGCGAATCGATCAGT	ACGTCTTCAGTGGGGTTGTC
Hs_THBD	ACATCCTGGACGACGGTTTC	CGCAGATGCACTCGAAGGTA
Hs_CDH5	GCCCATGAAGCCCTCGGATTA	GTATCGGAGGTCGATGGTGG
Hs_ICAM2	CGGATGAGAAGGTATTCGAGGT	CACCCACTTCAGGCTGGTTAC
Hs_ICAM1	AGCTTCGTGTCCTGTATGGC	TTTTCTGGCCACGTCCAGTT
Hs_VCAM1	TGTTTGCAGCTTCTCAAGCTTTT	GATGTGGTCCCCTCATTCGT
Hs_VWF	GGAGCATGTACAGCTTTGCG	CCCAAGATACACGGAGAGGC
Hs_SELP	GATGGGAAATGCCCCTTGAA	ACAGGCTGGTCCAGAGCTAAT
Hs_IL8	ATAAAGACATACTCCAAACCTTTCCAC	AAGCTTTACAATAATTTCTGTGTTGGC
Hs_ACE2	CGAGTGGCTAATTTGAAACCAAGAA	ATTGATACGGCTCCGGGACA
Hs_TMPRSS2	CACGGACTGGATTTATCGACAA	CGTCAAGGACGAAGACCATGT
Hs_BSG	CTGTTCGTGCTGCTGGGATT	GGAGCCAAGGTCTTCTACGG
Hs_FURIN	GCAAAGCGACGGACTAAACG	TGCCATCGTCCAGAATGGAGA
Hs_B2M	CCTGGAGGCTATCCAGCGTACTCC	TGTCGGATGGATGAAACCCAGACA
Hs_HMBS	ACCCTAGAAACCCTGCCAGAGAA	GCCGGGTGTTGAGGTTTCCCC
Mm_Pecam1	ACGCTGGTGCTCTATGCAAG	TCAGTTGCTGCCCATTCATCA
Mm_Kdr	GCCTCTGTGACTTCTTTGCG	GGGGGATGGAGAAAATCGCC
Mm_Thbd	TAGGGCCCTGGATCGGTTTA	CTGGTGTGGTTATCGCCAGT
Mm_Icam1	TCCGCTACCATCACCGTGTA	CAGGGTGAGGTCCTTGCCTA
Mm_Vcam1	CTGGGAAGCTGGAACGAAGT	GCCAAACACTTGACCGTGAC
Mm_Vwf	GGAGCATGTACAGCTTTGCG	CCCAAGATACACGGAGAGGC
Mm_Selp	TCTGGACCGGAAAGACTGGA	ACACCAAACTCTCCGTGGAC
Mm_Cxcl1	CCTTGACCCTGAAGCTCCCT	CGGTGCCATCAGAGCAGTCT

Mm_B2m	CGGCCTGTATGCTATCCAGAAAACC	TGTGAGGCGGGTGGAACTGTG
Mm_Hmbs	TCCGGAGGCGGGTGTTGAGG	GCCAGAGAAAAGTGCCGTGGG

Public microarray dataset

The microarray dataset GSE47460 (132), containing PF lung transplant and donor samples, was downloaded from GEO DataSets and expression values for the genes *PECAM1*, *THBD*, *KDR*, *ICAM1*, *ICAM3*, *VCAM1, SELP*, *VWF* and *CXCL8* were extracted from the platforms GPL14550 and GPL6480. After a batch effect was excluded, pooling of all samples resulted in a total number of 254 PF and 108 control samples.

Immunofluorescence staining

Immunofluorescence staining was performed on formalin fixed paraffin embedded lung tissue samples from COVID-19 patients and autopsy controls. 2.5 µm thick tissue sections were deparaffinized in ROTICLEAR® (Carl Roth, Karlsruhe, Germany) and decreasing concentrations of ethanol. Antigen retrieval was done in citrate buffer (pH 6) for 20 minutes in a 95°C hot water bath. After cooling down, sections were incubated with 3% H2O2 in Methanol for 10 min and blocked in 5% donkey serum and 3% bovine serum albumin (BSA) in PBS for 30 minutes each. The primary antibodies CD45 (1:250, #10558, Abcam, Cambridge, UK) and vWF (1:1000, #M0616, California, US) were applied overnight at 4°C and antibody detection was done with Alexa Fluor 488 and 555 secondary antibody (1:500, ThermoFisher Scientific, Massachusetts, US). DAPI (1:1000, #62248, ThermoFisher Scientific) was used for nuclei staining and slides were preserved in Fluorescence Mounting Medium (#S302380-2, DAKO Agilent). Imaging was done on an A1 confocal laser microscope (Nikon, Tokyo, Japan) at 60X magnification. A summary of antibody details can be found in Table 6.

Immunohistochemistry staining

Human lung tissue sections

Formalin-fixed and paraffin-embedded lung tissue samples were cut into 2.5 µm thick sections for histological analysis. Deparaffinization was done in ROTICLEAR® (Carl Roth), followed by decreasing concentrations of ethanol. Antigen retrieval was performed using citrate buffer (pH 6) in a 95°C hot water bath for 20 minutes. Sections were treated with 3% H2O2 in Methanol for 10 minutes, blocked in 2.5% normal horse serum (Vector Laboratories) for 30 min and incubated with the primary antibodies against CD45 (1:250, #10558, Abcam), VE-Cadherin (1:500, #TA804746, eubio, Vienna, Austria) / vWF (1:1000, #M0616, DAKO Agilent) / CD31 (1:250, #NB600-562, Novus Biologicals, Colorado, US) and Collagen 1 antibody (1:500, #1310-01, Southern Biotech, Alabama, US) overnight at 4°C. The primary antibodies were detected using the Blue/AP Substrate Kit (#LS-J1089, Vector Laboratories, California, US), the DAB/HRP Substrate Kit (#SK-4105, Vector Laboratories), the

StayYellow/HRP Substrate Kit (#ab169561, Abcam) or the ImmPACT Vector Red/AP Substrate Kit (#SK-5105, Vector Laboratories).

Detection was done according to the manufacturer's instructions. When using StayYellow, slides were air dried and permanently mounted in aqueous mounting medium. Otherwise, slides were dehydrated in increasing concentrations of ethanol and ROTICLEAR and permanently mounted in ROTI®Mount (#HP68.1, Carl Roth). Images were obtained using an Olympus VS120 slide-scanning microscope (Olympus) at 40X magnification. A summary of antibody details can be found in Table 6.

Murine lung tissue sections

2.5 µm formalin-fixed, paraffin-embedded murine lung tissue sections were deparaffinised and rehydrated in ethanol. Sections were treated with sodium citrate buffer (pH6) and Bloxall Blocking Solution (#VECSP-6000, Vector Laboratories) and blocked with 2.5% normal horse serum ((#S-2012-50, Vector Laboratories). Thereafter, sections were incubated with the primary antibody against vWF (1:100, #A0082, DAKO Agilent) overnight at 4°C. Antibody detection was done using the ImmPACT Vector Red/AP Substrate Kit (#SK-5105, Vector Laboratories) according to the manufacturer's instructions. Counterstaining was done using FastGreen (0.1% w/v in 1% acetic acid, #F7258-25G, Sigma Aldrich). Slides were dehydrated in ROTICLEAR® solution (#A538, Carl Roth) and permanently mounted in ROTI®Mount (#HP68.1, Carl Roth). Images were obtained using an Olympus VS200 slide-scanning microscope (Olympus) at 40X magnification. A summary of antibody details can be found in Table 6.

Visiopharm

Analysis of human lung tissue

The vascularization was quantified in donor and fibrosis lung tissue slides stained against vWF, Collagen type I and CD45, as described above. The quantification was done using the Visiopharm image analysis software (VIS 2020.08, Visiopharm, Hoersholm, Denmark). Twenty regions of interest were selected randomly per slide. The area of vWF, collagen type I and CD45 has been determined in each region and subsequently normalized to the entire area of each selected region. A Collagen type I portion of 15% or more has been defined as "fibrotic region". Regions with less than 15% Collagen type I have been defined as "non-fibrotic region".

Analysis of murine lung tissue

The vascularization was quantified in lung tissue slides from mice treated either with saline or bleomycin (3 days, 14 days, 21 days), which have been stained against vWF as described above. The quantification was done using the Visiopharm image analysis software (VIS 2020.08). Twenty regions of interest were selected randomly per slide. The area of vWF and Fastgreen-positive areas (= tissue) have been determined in each region and subsequently normalized to the entire area of each selected region.

ELISA and multiplex assay

Human plasma

A customized magnetic bead-based Human Luminex Discovery Assay (#LXSAHM, R&D Systems, Minnesota, US) was used to quantitatively determine protein levels of CD31, Thrombomodulin, VEGFR-2, ICAM-1, VCAM-1, P-selectin, vWF and IL-8 in plasma samples of PF patients and corresponding controls. The assay was conducted based on the manufacturer's instructions and fluorescence emission levels were determined on a BioPlex-200 (Bio-Rad). Protein levels of human ACE2 (#SEB886Hu; Dianova GmbH, Hamburg, Germany), VE-Cadherin (#DCADV0, R&D Systems) and ICAM-2 (#ab46080, Abcam) were measured using a sandwich high-sensitivity ELISA according to the manufacturer's instructions. Absorption values were determined on a ClarioStar microplate reader (BMG Labtech, Ortenberg, Germany). Plasma levels of E-selectin, P-selectin, ICAM-1, VCAM-1 and CD31 were determined in COVID-19 plasma samples and corresponding controls using a customized, bead-based LEGENDplex assay. The quantification was done by flow cytometry. Plasma levels of vWF (#EHVWF, ThermoFisher Scientific), IL-6 (#430507), IL-8 (#431507), TNF-α (#430207) and MCP-1 (#438807, all Biolegend, California, US) were measured based on sandwich high-sensitivity ELISA on a ClarioStar microplate reader.

Murine plasma

Murine plasma levels of VE-Cadherin (#ab206980, Abcam), Thrombomodulin (#MTHBD0, R&D Systems), ICAM-1 (#EMICAM1ALPHA, Thermofisher Scientific), VCAM-1 (#EMVCAM1, Thermofisher Scientific), vWF (#ab208980, Abcam) and P-selectin (#EMSELP, Thermofisher Scientific) were determined using sandwich high-sensitivity ELISA. The assays were performed according to the manufacturer's instructions and absorption values were measured on a ClarioStar microplate reader.

Transmission electron microscopy (TEM)

Fresh human fibrosis and donor lung transplant tissue samples were fixed with 2% (m/v) PFA and 2.5% (m/v) glutaraldehyde in 0.1M cacodylate buffer, pH 7.2, and post-fixed in osmium tetroxide. Consequently, samples were dehydrated, embedded in epoxy resin and cut into 70 nm ultrathin sections (UC 7Ultramicrotome, Leica Microsystems, Wetzlar, Germany). Following to uranyl acetate staining, images were taken using a transmission electron microscope (EM 900 or EM109, Zeiss, Jena, Germany).

In-vitro analyses

Cell isolation

For the isolation of human donor and fibrosis pulmonary artery endothelial cells (HPAECs), pulmonary arteries (< 2 mm in diameter) were collected from transplant lung tissue. After removing the adventitia, pulmonary arteries were cut and minced and digested in an enzymatic digestion solution containing PBS, 5 mg/ml DNase (#04716728001, Sigma Aldrich) and 35 mg/ml Collagenase A (#11088793001,

Sigma Aldrich). The digestion was done for 40 min at 37°C on an orbital shaker (50 rpm). Subsequently, the cell suspension was passed through a 100 µm cell strainer and centrifuged at 350g for 7 minutes to collect the cell pellet. Cells were resuspended in RPMI complete medium (#31870-074, ThermoFisher Scientific) containing 10% fetal calf serum (FCS), 1% penicillin and streptomycin and 1% L-Glutamin. Thereafter, cells were MACS-sorted using the human CD31 MicroBead Kit (#130-091-935, Miltenyi) according to the manufacturer's instructions. Cells were applied on a LS column (#130-042-401, Miltenyi, Gladbach, Germany) and separation was done on a MidiMACS Separator. After three consecutive washing steps with basal EGM-2 Endothelial Medium (#CC-3156, Szabo Scandic, Vienna, Austria), the CD31+ cell fraction was collected in EGM-2 Endothelial Medium with EC supplementary kit (#CC-3156 and #CC-4176, Szabo Scandic) and culture in gelatin-coated T25/T75 flasks at 37°C and 5% CO_2. The MACS separation was repeated at least up to passage 3.

Additionally, cryopreserved donor HPAECs were purchased from Lonza (#CC-2530, Basel, Switzerland). Cells up to passage 7 were used for experiments.

For the isolation of human peripheral blood granulocytes, ca. 5 ml of 3.8% sodium citrate were filled up to ca. 40 ml with freshly drawn healthy donor blood (17-291 ex 05/06) and centrifuged for 20 minutes at 400g without brake. After removal of the platelet-rich plasma (top), 6 ml of 6% dextran was added and the tube filled up to 50 ml of 0.9% saline. After 30 minutes incubation at room temperature, the upper phase was put onto 15 ml of peripheral blood mononuclear cells (PBMC) spin medium (#60-00092, pluriSelect, Leipzig, Germany) and centrifuged for 20 minutes at 400g without brake. Thereafter, PBMCs, the saline phase and PBMC spin medium was removed and polymorphnuclear cells (PMNL) were washed twice with 20 ml HBSS buffer. For haemolysis, the cell pellet was resuspended in 10 ml 0.2% saline, gently mixed and filled up to 20 ml with 1.6% saline. After addition of 10 ml HBSS, the suspension was centrifuged at 400g for 7 minutes and cells were re-suspended in 10 ml washing buffer (PBS pH 7.4 without Ca^{2+} and Mg^{2+} containing 0.1% BSA and 10 mM HEPES (4-(2-hydroxyethyl)-1-piperazineethanesulfonic acid) and 10 mM glucose) and counted.

Endothelial barrier monitoring

The endothelial barrier establishment and maintenance was measured using the electrical cell-substrate impedance sensing system (ECIS, Applied Biophysics, New York, US). Donor and fibrosis HPAECs were seeded on 8W10E+ PET Chips (#72040, Applied Biophysics) at a density of 70.000 cells/well in full EGM-2 Endothelial Medium. Chips were pre-activated with 10 mM L-cystein (Sigma Aldrich) and pre-coated with 1% gelatine. Chips were transferred to the ECIS machine to monitor the establishment and maintenance of the endothelial barrier at 4,000 Hertz (Hz) over a period of approximately 48 hour every 60 seconds. Monitoring was done in full EGM-2 Endothelial Medium

throughout the whole experiment. Data are represented as absolute resistance values versus time and as the mean of the maximum resistance reached. The measurements were done in quadruplicates.

Immunofluorescence staining of HPAECs

Donor and fibrosis HPAECs were seeded on eight-well chamber slides (Falcon, Corning, New York, US) after pre-coating with 1% gelatine at a density of 20.000 cells/well in full EGM-2 Endothelial Medium and kept at 37°C and 5% CO_2. As the endothelial monolayer was fully established (approximately 48h after seeding), cells were fixed in 4% (m/v) paraformaldehyde in MACS buffer (PBS + 2mM EDTA + 0.5% (m/v) bovine serum albumin) for 25 min and blocked with 5% (m/v) donkey serum and 3% (m/v) BSA in PBS at room temperature. Cells were incubated overnight with the primary antibody against VE-Cadherin (1:100, #AF938, R&D Systems). The following day antibody detection was done using Alexa Fluor 555 secondary antibody (1:500, #A21432, ThermoFisher Scientific). DAPI (1:1000, #62248, ThermoFisher Scientific) was used to stain the nuclei and slides were preserved using Fluorescence Mounting Medium (#S302380-2, Agilent Dako). Imaging was done on an A1 confocal laser microscope (Nikon) at 60X magnification. A summary of antibody details can be found in Table 6.

Adhesion assay

Donor and fibrosis HPAECs were seeded on eight-well chamber slides (Falcon, Corning) after pre-coating with 1% gelatine at a density of 20.000 cells/well in full EGM-2 Endothelial Medium and kept at 37°C and 5% CO_2. As the endothelial monolayer was fully established, the medium was changed to basal EGM-2 Endothelial Medium containing 5% FCS and kept at 37°C and 5% CO_2 for another hour. Thereafter, cells were pre-stimulated with either vehicle, 10 ng/ml TNF-α (#11343015, Immunotools, Friesoythe, Germany), 10 ng/ml IFN-γ (#11343534, Immunotools) or 10 ng/ml IL-1β (#200-01B, Peprotech, Korea, Asia) for 1 hour at 37°C and 5% CO_2 in basal EGM-2 Endothelial Medium containing 5% FCS.

Isolated PMNLs were pre-stained with CellTracker™ Green CMFDA Dye (#C7025, ThermoFisher Scientific) according to the manufacturer's instructions and re-suspended in basal EGM-2 Endothelial Medium containing 5% FCS. 500.000 PMNL were added to the pre-stimulated HPAECs, after stimuli have been removed and allowed to adhere for 1.5 hour at 37°C and 5% CO_2. Subsequently, cells were fixed in 4% (m/v) paraformaldehyde in MACS buffer (PBS + 2mM EDTA + 0.5% (m/v) bovine serum albumin) for 25 minutes. The mean count of adhered PMNLs was determined by imaging of five random regions at 10X quantification.

Transmigration assay

Donor and fibrosis HPAECs were seeded on 96-well transwell inserts (3.0 µm Pore Polycarbonate Membrane, Corning) pre-coated with 1% gelatin at a density of 5000 cells/well in full EGM-2 Endothelial Medium at 37°C and 5% CO_2. After approximately 72-96 hours medium was changed to

basal EGM-2 Endothelial Medium containing 5% FCS. Cells were kept at 37°C and 5% CO_2 for another hour prior to pre-stimulation with either vehicle, 10 ng/ml TNF-α, 10 ng/ml IFN-γ or 10 ng/ml IL-1β for 1 hour. Thereafter, the medium was changed to basal RPMI medium containing either 5% or 0% FCS and 500.000 PMNLs in basal RPMI medium (0% FCS) were added to the upper compartment. PMNLs were allowed to migrate to the lower compartment containing RPMI with either 5% FCS or 0% FCS for 2.5 hour at 37°C. PMNLs were collected from the lower compartment, fixed in PBS containing 1% (m/v) paraformaldehyde and quantified on a Cytoflex S flow cytometer (Beckman Coulter, California, US).

Statistics: Correlation analysis

Data were analysed at least from 3 independent experiments per assay. Graphs and statistical analysis were performed in R (version number 4, www.r-project.org). Data are shown as single data points with lines indicating the mean or as boxplots with dot-plot overlay. Specific tests used for each experiment are indicated in the figure legends. Probability values of $p < 0.05$ were considered statistically significant.

Table 2: Antibodies used for immunohistochemistry and immunofluorescence stainings.

Antibody	Company	Order#	Species	Dilution
CD45	Abcam	#10558	rabbit	1:250
vWF	Dako Agilent	#M0616	mouse	1:1000
VE-Cadherin	Eubio	#TA804746	mouse	1:500
CD31	Novus Biologicals	#NB600-562	mouse	1:250
Collagen I	Southern Biotech	#1310-01	goat	1:500
vWF	DAKO Agilent	#A0082	rabbit	1:100
VE-Cadherin	R&D Systems	#AF938	goat	1:100

Results

Results 1: Chronic lung diseases and COVID-19

Gene expression analysis of COVID-19 relevant entrance and priming proteins

During the initial stages of the COVID-19 pandemic, there was uncertainty regarding whether patients with chronic lung diseases were at a heightened risk of infection. Additionally, it was unclear whether infected individuals with chronic lung diseases experienced more severe infections, leading to increased rates of hospitalization and mortality. To investigate this, we assessed the gene expression levels of various molecules that are crucial for the entry and modification of SARS-CoV-2 in the lung tissue derived from endstage COPD, IPAH and PF as well as in donor tissue. The analysis revealed that lungs affected by COPD exhibited the most pronounced dysregulations. While the gene expression of entrance receptor ACE2 and cleavage protease TMPRSS2 were significantly upregulated in COPD as compared to donors, host cell convertase FURIN and alternative entrance mediator BSG were significantly downregulated (Figure 5A). No significant changes were observed between donor, IPAH and PF groups (Figure 5A). ACE2 can also be cleaved from the surface of epithelial cells and it has been reported, that soluble ACE2 is significantly increased in infected individuals suffering from severe COVID-19. The exact mechanisms of sACE2-SARS-CoV2 interaction is not elucidated yet, however it has been proposed, that sACE2-SARS-CoV2 complex formation supports spreading of the virus throughout the body and leads to the entrance of increased number of viral particles (133). Interestingly, we measured significantly lowered levels of sACE2 in the plasma of both, uninfected endstage COPD and PF patients (Figure 5B). Increased gene expression levels of ACE2 correlated significantly with improved FVC (%) in COPD patients (Figure 6). No other correlations with clinical parameters or hemodynamics have been found for any disease group.

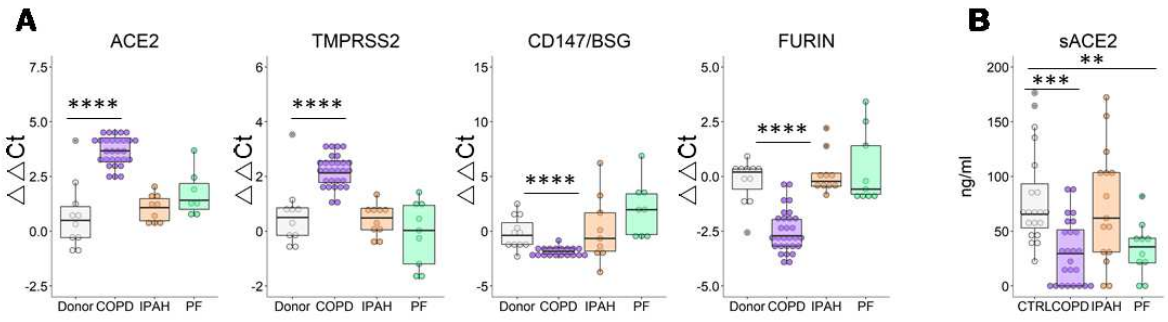

Figure 5: COVID-19 relevant mediators in different chronic lung diseases. (A) Gene expression of ACE2, TMPRSS2, CD147 (BSG) and FURIN in whole lung tissue from COPD, IPAH, PF patients and donors evaluated by RT-qPCR. (B) EDTA plasma levels of ACE2 in donor, COPD, IPAH and PF samples measured by ELISA. Kruskal-Wallis testing was performed. *: p<0.05; **: p<0.01; ***: p<0.001. . Reproduced with permission of JOHN WILEY AND SONS (license number: 5737500756530) (134).

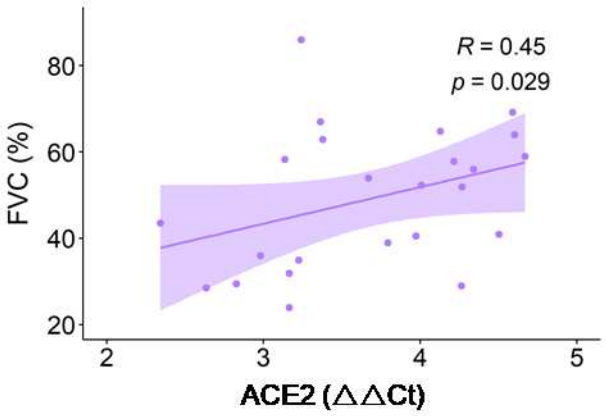

Figure 6: Correlation between pulmonary ACE2 gene expression and forced vital capacity (FVC %). Correlation analysis of ACE2 gene expression in the lung and forced vital capacity (FVC (%)) in COPD based on Spearman's rank calculation. Reproduced with permission of JOHN WILEY AND SONS (license number: 5737500756530) (134).

Results 2: Endothelial cells in severe COVID-19

Gene expression analysis of vascular identity, barrier and injury markers in severe COVID-19

Already at the very beginning of the COVID-19 pandemic, early studies have shown that endothelial-associated factors, such as VCAM-1 and IL-8 and inflammatory factors, such as MCP-1 are increased in COVID-19 lung tissue (135). In addition, endothelial dysfunction was associated with poor disease outcome early on (136). The exact mechanisms and affected endothelial functions that lead to vasculopathy were previously unknown. Here we analyzed the gene expression levels of a comprehensive set of vascular markers implicated in EC activation (E-selectin, ICAM-1, VCAM-1), barrier integrity and cell identity (CD31, VEGFR-2) and in injury/repair response (P-selectin, vWF) in lung tissue of severely affected COVID-19 patients (n = 19) and autopsy controls without pulmonary pathology (n = 11, provided by Assoz. Prof. Priv.-Doz. Dr.med.univ. Gregor Gorkiewicz, Diagnostic and Research Center for Molecular Biomedicine, Medical University of Graz).

Our analysis indeed revealed a striking upregulation of the gene expression levels of ICAM-1, vWF and VEGFR-2 (KDR) in COVID-19 lung tissue as compared to control tissue, indicating that different endothelial-related functions are affected in the course of a SARS-CoV-2 infection (Figure 7).

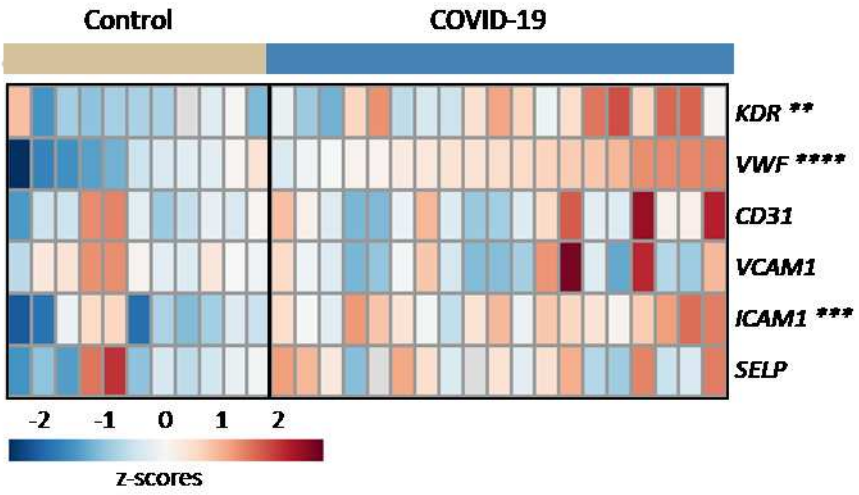

Figure 7: Gene expression of endothelial cell markers are upregulated in lungs of severely ill COVID-19 patients. qPCR analysis of endothelial vascular endothelial growth factor receptor (VEGFR)-2 (KDR), von Willebrand Factor (vWF), CD31, vascular cell adhesion molecule (VCAM)-1, intercellular adhesion molecule (ICAM)-1 and P-selectin (SELP) in lung tissue homogenate of severely ill COVID-19 patients (n = 19) and controls (n = 11). The heatmap represents relative expression by showing z-scores. Reproduced with permission of the ERS 2024: European Respiratory Journal Sep 2021, 58 (3) 2100377; DOI: 10.1183/13993003.00377-2021 (106).

Vascular injury in severe COVID-19

Pro-thrombotic vWF is released from ECs in case of vascular damage. To prove the increased presence of the endothelial injury marker on a protein level, we conducted immunofluorescence staining. The staining uncovered an intense, but patchy and diffuse vWF signal in COVID10 lung tissue as compared to control samples. This was coming along with an elevated extravasation of inflammatory cells (Figure 8). This supports the notion, that the endothelium is highly activated and damaged in COVID-19.

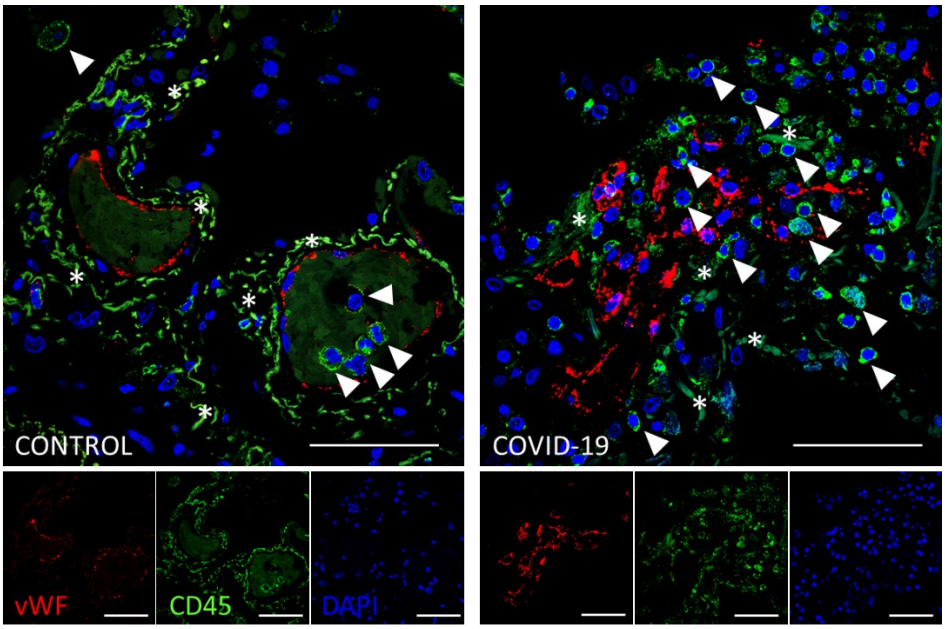

Figure 8: Severe COVID-19 is associated with increased immune cell infiltration and diffuse vWF distribution. Representative immunofluorescence images of control and COVID-19 lung tissue (n = 5) stained against endothelial marker vWF (red) and immune cell marker CD45 (green). White arrowheads = immune cells; white asterisks = collagen; scale bar = 50 µm. Reproduced with permission of the ERS 2024: European Respiratory Journal Sep 2021, 58 (3) 2100377; DOI: 10.1183/13993003.00377-2021 (106).

Circulatory levels of vascular and inflammatory factors in COVID-19

Severe COVID-19 is characterized by an excessive release of pro-inflammatory mediators, a so-called "cytokine storm", as reported previously (137-139). The exuberant amounts of pro-inflammatory cytokines support the occurrence of a hyper-activated endothelium. Endothelial hyper-activation is moreover linked to the release and shedding of endothelial-related molecules (140). To determine whether COVID-19 is characterized by increased adhesion molecule shedding, we measured our set of endothelial-cell related markers as well as a set of pro-inflammatory mediators, including IL-6, IL-8, TNF-α and MCP-1 in the plasma of critically ill COVID-19 patients (n = 21) and healthy controls (n = 22). The measurement indeed revealed significantly increased levels of VCAM-1, E-selectin and CD31 in COVID-10 plasma (Figure 9).

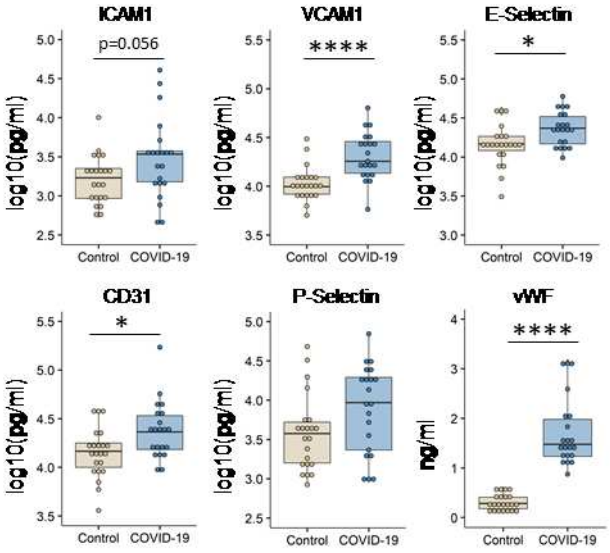

Figure 9: Soluble endothelial markers are increased in COVID-19 plasma. Plasma levels of ICAM-1, VCAM-1, E-selectin, CD31, P-selectin and vWF in the plasma of severely ill COVID-19 patients (n = 21) and healthy controls (n = 22) measured by ELISA. Kruskal-Wallis testing was performed. *: p<0.05; **: p<0.01; ***: p<0.001. Reproduced with permission of the ERS 2024: European Respiratory Journal Sep 2021, 58 (3) 2100377; DOI: 10.1183/13993003.00377-2021 (106).

The increase of soluble endothelial-derived markers was moreover associated with the presence of various inflammatory cytokines IL-6, IL-8, MCP-1 and TNF-α, confirming the aforementioned "cytokine-storm" (Figure 10).

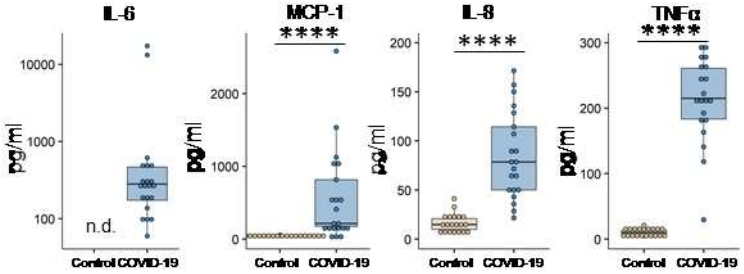

Figure 10: Soluble markers of inflammation are increased in COVID-19 plasma. Plasma levels of interleukin (IL)-6, monocyte chemoattractant protein (MCP)-1, IL-8 and tumor necrosis factor (TNF)-α in the plasma of severely ill COVID-19 patients (n = 21) and healthy controls (n = 22) measured by ELISA. Kruskal-Wallis testing was performed. *: p<0.05; **: p<0.01; ***: p<0.001. Reproduced with permission of the ERS 2024: European Respiratory Journal Sep 2021, 58 (3) 2100377; DOI: 10.1183/13993003.00377-2021 (106).

Importantly, the altered circulatory levels correlated with different clinical parameters. Soluble vWF strongly correlated with D-dimer, a marker of coagulation and poor outcome in COVID-19, and with IL-8 plasma levels, an activator of coagulation (Figure 11A). Elevated P-selectin correlated with increased fibrinogen, another coagulation marker. The shedding of EC surface markers ICAM-1, E-selectin and CD31 was accompanied by an increase of partial thromboplastin time, the time it takes for a clot to

form in a blood sample. In addition, the circulating endothelial-derived markers were also highly correlated with each other (Figure 11B).

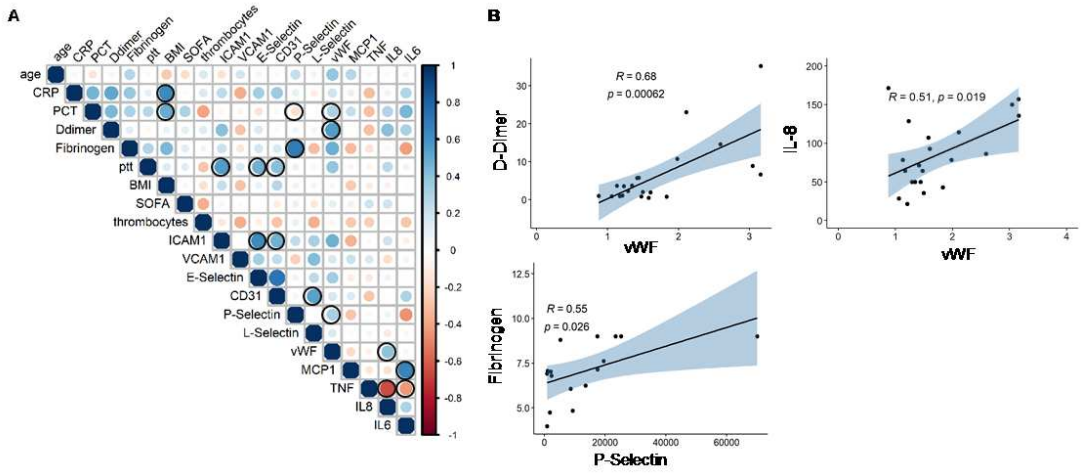

Figure 11: COVID-19 is associated with strong correlations between soluble markers of coagulation. (A) Comprehensive correlation matrix of COVID-19 patients' characteristics (age, BMI), clinical parameters (CRP, PCT, Ddimer, Fibrinogen, ptt; SOFA, thrombocytes) and soluble endotehlial and inflammatory marker. Dot size / color = correlation coefficient. Circled dots = signficant correlation. (B) Pairwise correlation anaylsis between vWF and D-Dimer, vWF and IL-8 and P-selectin and Fibrinogen based on Spearmans rank correlation analysis. *: p<0.05; **: p<0.01; ***: p<0.001; ****: p<0.0001. Reproduced with permission of the ERS 2024: European Respiratory Journal Sep 2021, 58 (3) 2100377; DOI: 10.1183/13993003.00377-2021 (106).

Results 3: Endothelial cells in pulmonary fibrosis

Ultrastructural properties of the pulmonary endothelium

Vascular abnormalities are occurring frequently in the course of PF (129). Whether this also applies to the *structural* properties of individual ECs has not yet been deciphered yet. To uncover potential phenotypic changes and structural deformation of pulmonary ECs in fibrotic lungs, we made use of ultrastructural transmission electron microscopy. While donor lungs were characterized by a flat, organized endothelium, fibrosis lung tissue sections clearly showed disorganized, swollen endothelial cells (Figure 12). The micrographs indicated loss of the healthy, regular shape and marked vascular lumen narrowing.

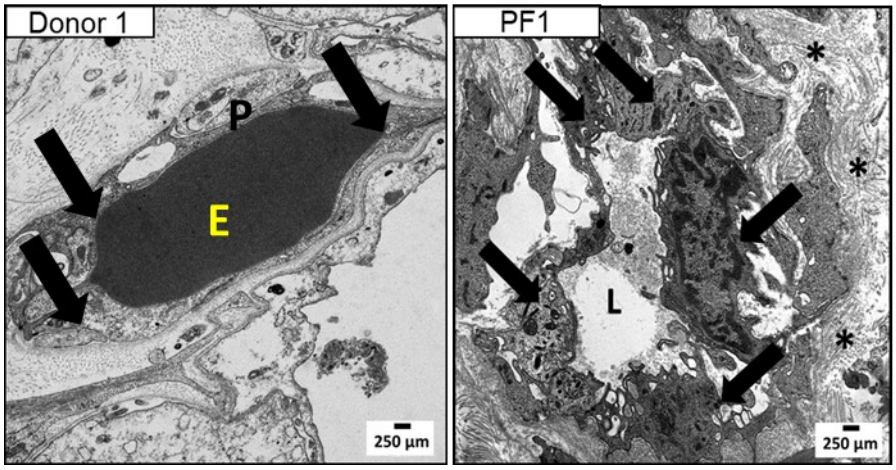

Figure 12: The endothelial ultrastructure is changed in pulmonary fibrosis. Representative ultrastructural micrographs from PF transplant and donor tissue (n = 3). Arrow = EC. P = pericyte. E = erythrocyte. L = lumen. * = collagen. Scale bar = 250 µm. The imaging was done in cooperation with the Core Facility Ultrastructural Analysis, Medical University of Graz, Graz, Austria.

Endothelial integrity and activation in pulmonary fibrosis

The ultrastructural analysis of structural abnormalities of the pulmonary vasculature was complemented by an immunohistochemical staining approach. To better understand structural alterations specifically related to activation and barrier, we stained against vascular activation marker vWF or against the barrier markers VE-Cadherin or CD31. A triple-staining approach together with the immune cell marker CD45 and the tissue fibrosis marker Collagen allowed not only evaluating structural vascular differences between donor and fibrosis lungs, but to also connect vascular changes, tissue remodeling and immune cell infiltration. Indeed, the signal intensity of all three investigated markers was clearly increased in fibrosis lungs as compared to donor tissue. Similar to observations from our ultrastructural analysis (Figure 12), donor lungs showed a flat, well-organized endothelium and only moderate tissue inflammation. On the contrary, fibrotic lungs were marked by heavy inflammation together with a prominent staining of vWF, VE-Cadherin and CD31. This further supports the presence of a heavily activated endothelium with disorganized barrier integrity in PF. More interestingly, vWF is usually located to large vessels and rarely present in the microvasculature (50). However, in fibrotic lungs vWF was located also prominently in the microvasculature/capillaries, which further underpins the heavy inflammatory and coagulative phenotype of fibrotic lungs (Figure 13).

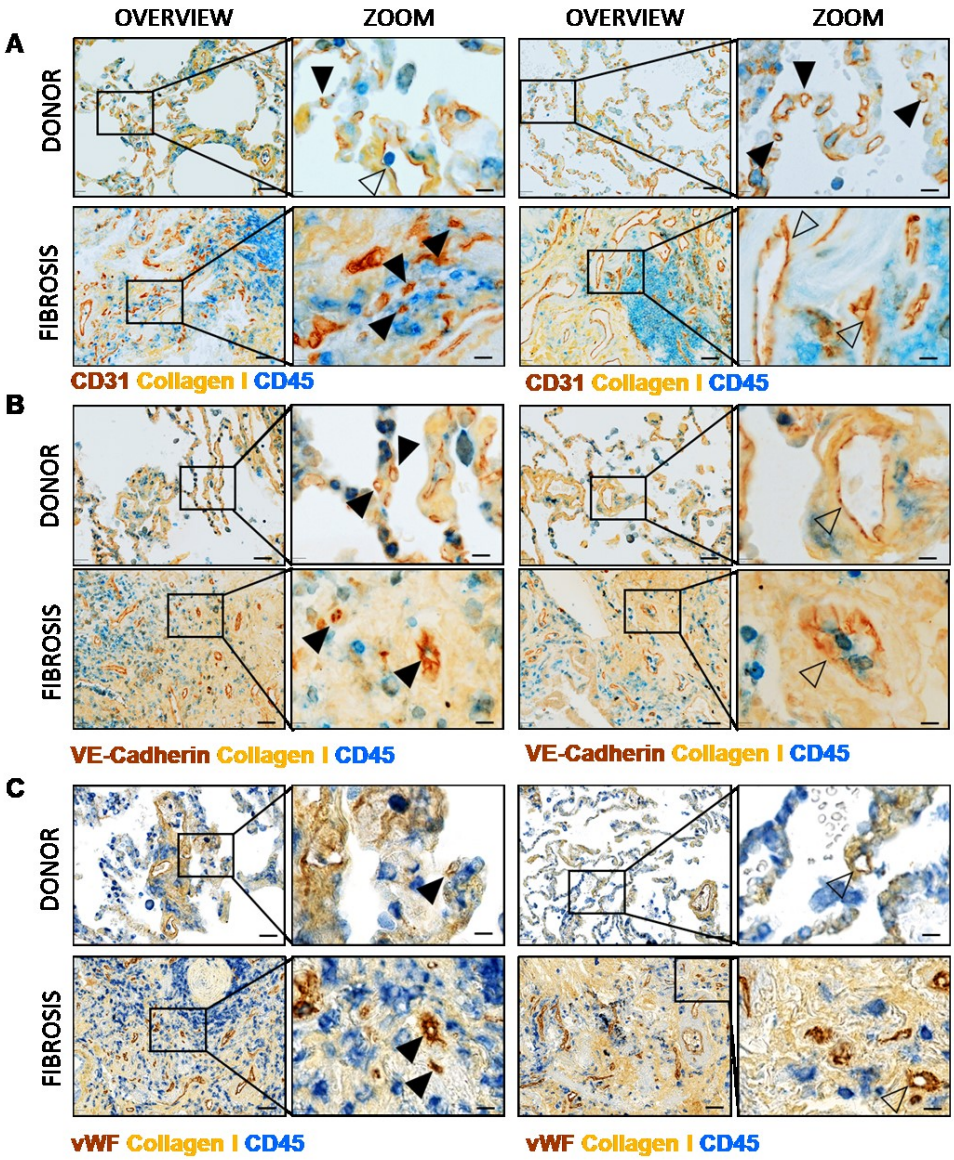

Figure 13: Endothelial cells are structurally distinct compared to donor endothelium. Representative immunohistochemistry images of donor and fibrosis lung sections (n = 5) stained against Collagen I (orange), CD45 (blue) and CD31 (brown, A), VE-Cadherin (brown, B) or vWF (brown, C). Scale bar = 50 µm in Overview, 10 µm in Zoom.

The relationship between endothelial activation, tissue fibrosis and lung inflammation

PF is characterized by chronic inflammation (12, 13, 141) and – as shown above – a hyper-activated vasculature. To better understand the potential relationship between endothelial activation, lung inflammation and tissue fibrosis, we conducted image analysis using the Visiopharm software (Figure 14A). The software enabled us to quantitative assess the area (%) of vWF, collagen I and CD45 within immunohistochemically stained donor and fibrosis lung tissue sections based on colour recognition. As expected, both the collagen-positive area (%) and immune cell infiltration (%) were significantly increased in lung fibrosis as compared to donors (Figure 14B). Moreover, the area covered by vWF (%)

was significantly greater in PF lungs (Figure 14B), confirming our assumption of an augmented activation of the pulmonary vasculature.

Histologically, the UIP pattern is characterized by spatial and temporal heterogeneity (10). Areas with preserved lung architecture and normal lung parenchyma co-exist with heavily remodelled and inflamed areas. Due to this histological heterogeneity, we compared the area of vWF (%) in fibrotic versus non-fibrotic regions. This uncovered a significant increase of vWF-positive areas in the heavily remodelled, fibrotic parts (Figure 14C). The connection between parenchymal remodelling and endothelial activation was moreover supported by a positive correlation between vWF (%) and collagen (%) in fibrotic lungs (Figure 14D).

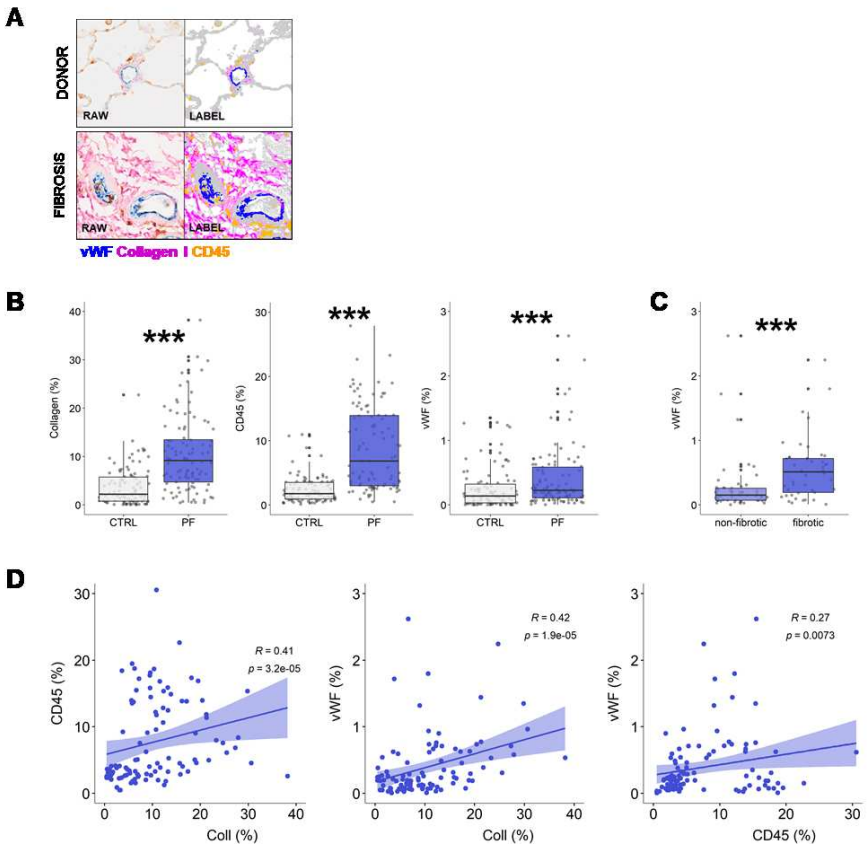

Figure 14: Remodeled and inflamed regions correlate with endothelial alterations. (A) Examples of raw and labeled images for quantification of vWF (blue), collagen (pink) and CD45 (orange) stained on human lung tissue. (B) Determination of the area of collagen (%), CD45 (%) and vWF (%) in twenty randomly chosen donor and fibrosis (n = 5) lung tissue regions based on automated color recognition. (C) Determination of the area of vWF (%) in fibrotic (collagen area > 15%) versus non-fibrotic (collagen area < 15%) randomly chosen areas of fibrosis lung tissue sections (n = 5). (D) Correlation of vWF (%), collagen (%) and CD45 (%) in PF lung tissue sections. Kruskal Wallis test and Spearman's Rank analysis was performed. *: p<0.05; **: p<0.01; ***: p<0.001; ****: p<0.0001.

Alterations of activation and integrity markers in whole lung tissue

To obtain detailed information on the activation, barrier function, cell identity and injury response of EC in PF, we analyzed the respective set of vascular markers in 16 explanted PF and 19 donor lungs by quantitative RT-PCR.

The gene expression analysis revealed a striking decrease of *ICAM2* in PF lung homogenate (LH) compared to control (CTRL) LH ($p = 0.0008$). *PECAM1* and *CDH5* gene expression was downregulated by trend ($p = 0.070$ and $p = 0.053$, respectively). Other investigated markers *THBD, KDR, ICAM1, VCAM1, SELP, VWF* and *CXCL8* did not show significant changes in in this specific lung cohort (Figure 15A). To strengthen our results, we investigated the publicly available microarray dataset GSE47460 (132), which includes RNA samples from 254 PF and 108 CTRL lungs and could observe similar directions as in our cohort (Figure 16B). The differences were even more pronounced in this dataset, with a highly significant downregulation of *PECAM1, THBD, KDR, ICAM1, ICAM2, SELP* and *VWF* gene expression and a strong upregulation of *VCAM1* and *IL8* in PF lung tissue compared to CTRL (Figure 15B).

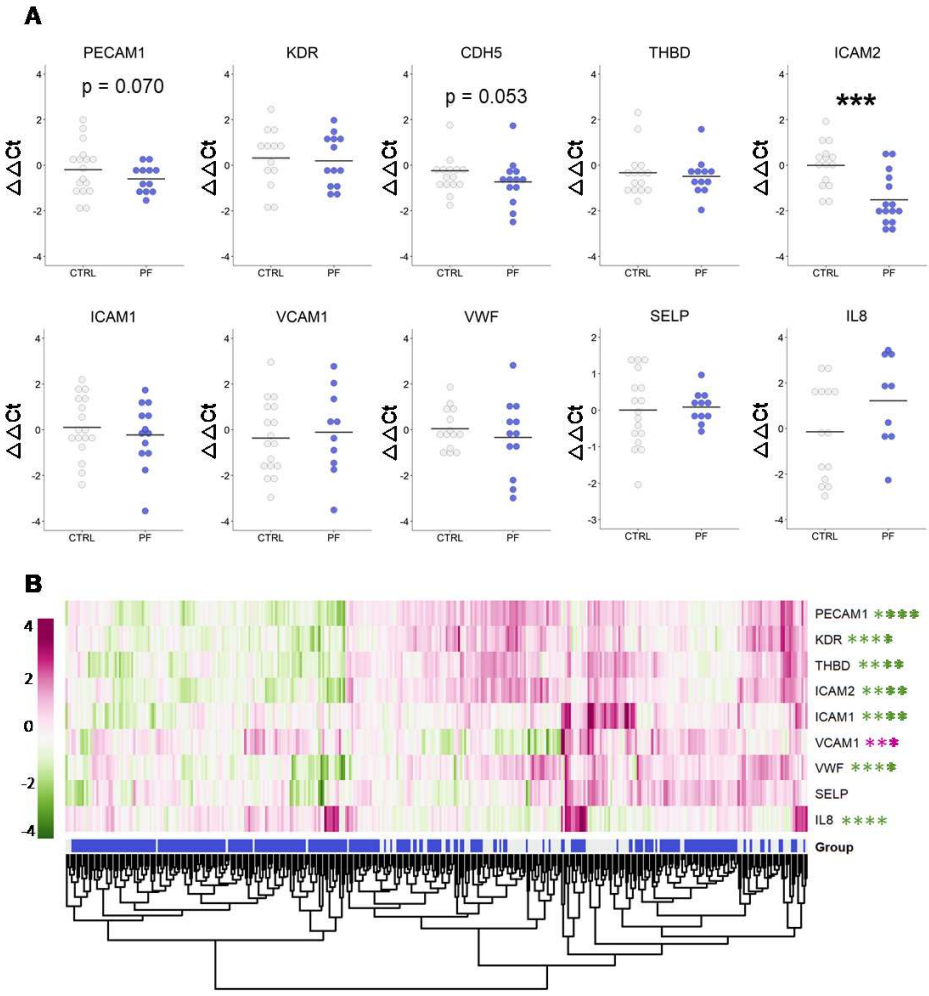

Figure 15: Integrity and activation marker gene expression in donor and fibrosis transplant lungs. (A) RT-qPCR analysis of integrity markers CD31 (PECAM1) vascular endothelial growth factor receptor (VEGFR)-2 (KDR), VE-Cadherin (CDH5), Thrombomodulin (THBD), intercellular adhesion molecule 2 (ICAM2), vascular cell adhesion molecule 1 (VCAM1) von Willebrand Factor (VWF), P-selectin (SELP) and interleukin (IL)-8 measured in whole lung homogenate of PF patients (n = 16) and donors (n = 19). (B) Expression profiling of endothelial cell markers in the publicly available dataset GSE47460, including lung biopsy tissue (CTRL, n = 108, grey) and lung explant tissue (PF, n = 160, blue). Heatmap representation of relative expression changes. Z-scores are shown. Kruskal Wallis test was performed. *: p<0.05; **: p<0.01; ***: p<0.001; ****: p<0.0001.

Loss of vascular endothelial barrier function in pulmonary fibrosis

As we observed a prominent downregulation of integrity markers PECAm1, KDR, THBD and ICAM2 on gene expression level (publicly available microarray dataset) and stronger signal intensity of CD31 and VE-Cadherin on immunohistochemical level in fibrotic lungs, we speculated, that ECs isolated from fibrotic lungs have an altered barrier strength compared to ECs from donor lungs. To investigate this, we conducted electric cell-substrate impedance sensing (ECIS) experiments with HPAECs *in-vitro* and monitored the establishment and maintenance of endothelial barrier over a time of approximately 40h. The measurement revealed that the barrier establishment of HPAECs isolated from fibrotic lungs

was delayed as compared to that of healthy HPAECs (Figure 16A). Moreover, fibrosis HPAECs were not capable to reach a barrier strength as strong as donor HPAECs (Figure 16B). This indicated that, despite an increased gene and protein expression of integrity markers, the vascular barrier was not fully functional in PPF. Our immunofluorescence staining approach further substantiated this. Staining against the junction marker VE-Cadherin in a fully established endothelial monolayer in-vitro showed a disorganization of junctions and loss of the typical cobblestone-like structures, while junctions were uniformly distributed in the donor monolayer (Figure 16C).

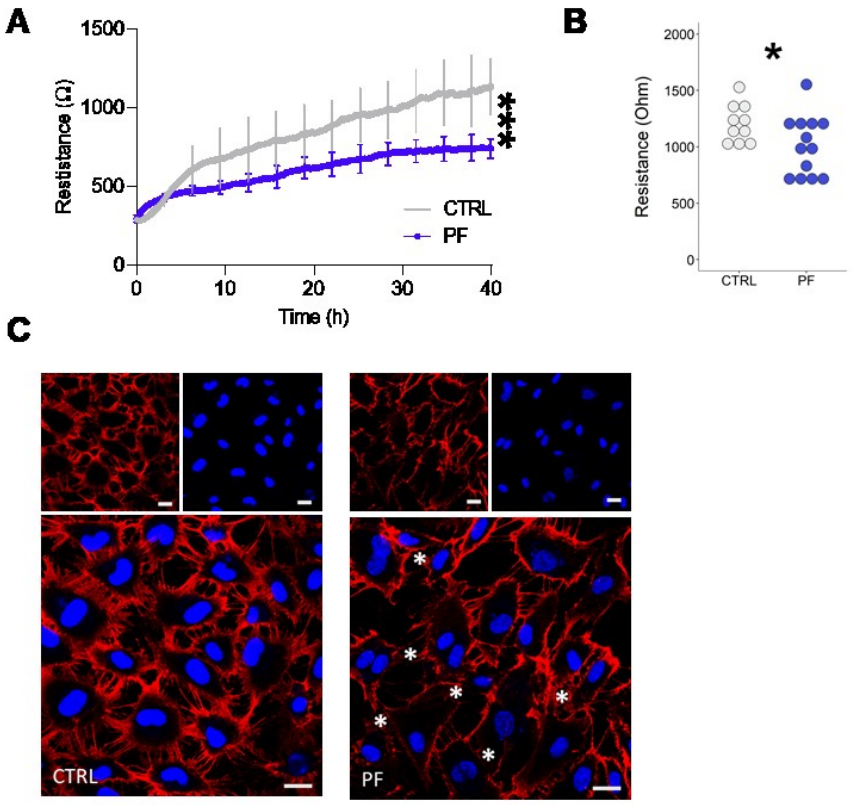

Figure 16: Impairment of endothelial barrier in lung fibrosis. (A) Representation of donor and fibrosis HPAEC barrier establishment and maintenance over a time span of 40 h recorded as resistance (Ohm) by Electrical cell substrate impedance sensing (ECIS). (B) Mean maximum barrier resistance (Ohm) reached by donor (technical replicates of n = 4) and fibrosis (technical replicates of n = 4) HPAECs measured in quadruplicates. (C) Representative images of fully established donor (n = 3) and fibrosis (n = 3) HPAEC monolayers immunofluorescently stained against VE-Cadherin. Nuclear staining was done using DAPI. Arrow heads: disorganized junctions. Scale bar: 20 µm. Kruskal Wallis test was performed. *: p<0.05; **: p<0.01; ***: p<0.001; ****: p<0.0001.

Endothelial response to a pro-inflammatory/anti-fibrotic environment

TNF-α and IL-1β are pro-inflammatory and pro-fibrotic cytokines commonly found in fibrotic lungs (142, 143). On the opposite, the cytokine IFN-γ acts anti-fibrotic and has been shown to increase the effect of Pirfenidone (144). Here, we aimed to test, whether endothelial integrity and/or activation is affected differently in donor and fibrosis ECs in the presence of either TNF-α, IL-1β or IFN-γ. Thus, we measured the gene expression levels of VE-Cadherin (*CDH5*), CD31 (*PECAM1*), Thrombomodulin

(*THBD*), P-Selectin (*SELP*) and vWF (*VWF*) in donor and fibrosis HPAECs after they have been stimulated for one hour. Treatment with the vehicle control revealed a significantly decreased gene expression of *THBD*, while *VWF* gene expression was elevated by trend (p = 0.09, Figure 17). The increase in *vWF* gene expression became significant after TNF-α and IFN-γ. The level of *SELP* was markedly decreased in donor ECs after IFN-γ stimulation as compared to vehicle, TNF-α or IL-1β treated donor ECs, leading to significantly higher P-selectin gene expression in the IFN-γ treated fibrosis HPAECs. A transcriptional regulation of P-selectin after IFN-γ stimulation could account for the drop in the donor HPAECs (145). *PECAM1* was increased by trend in the presence of IFN-γ (p = 0.08, Figure 17).

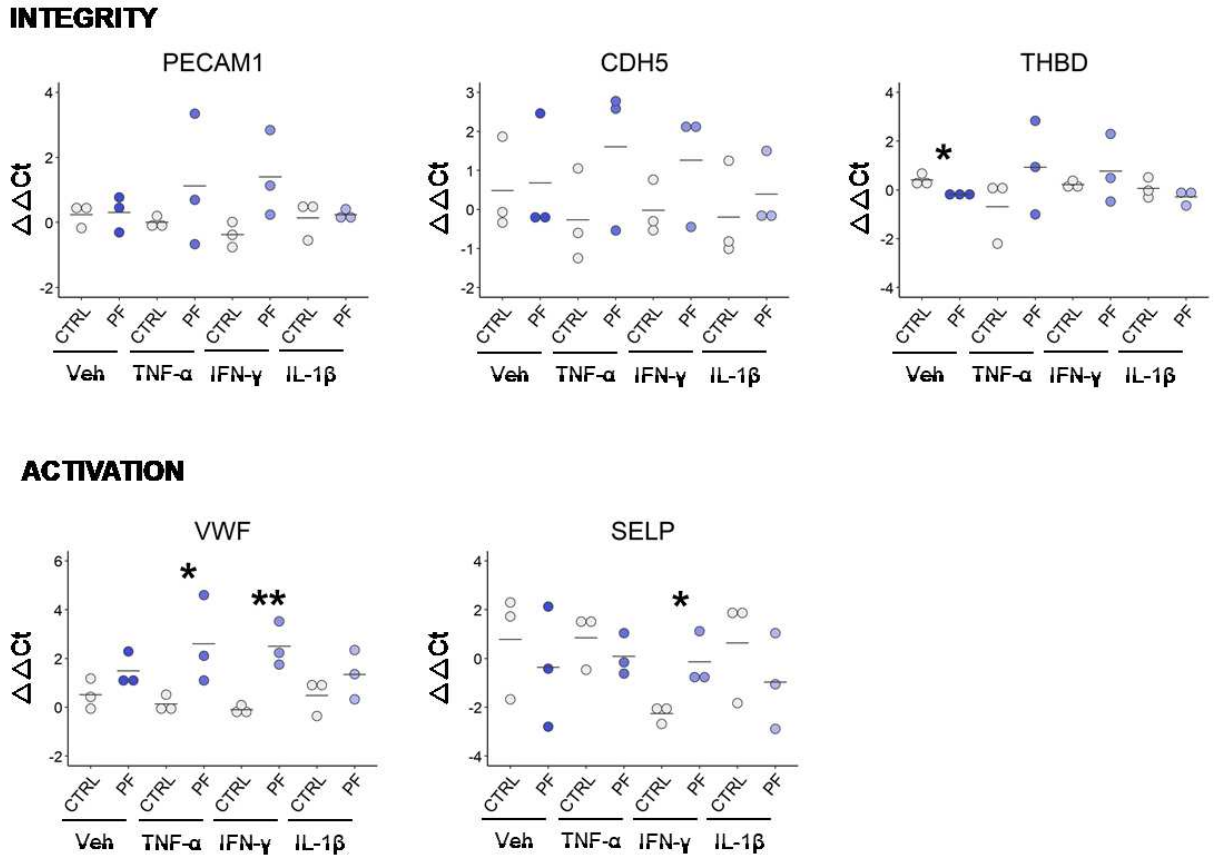

Figure 17: Endothelial cell behavior in a pro-inflammatory milieu. RT-qPCR analysis of CD31 (PECAM1), VE-Cadherin (CDH5), Thrombomodulin (THBD), von Willebrand Factor (VWF) and P-selectin (SELP) in fully established donor (n = 3) or fibrosis (n = 3) HPAEC monolayers after stimulation with either TNF-α, IFN-γ or IL-1β or the corresponding vehicle control. Kruskal Wallis test was performed. *: p<0.05; **: p<0.01; ***: p<0.001; ****: p<0.0001.

Adhesion of immune cells to endothelial monolayers

Neutrophils and eosinophils have been shown to occur in increased numbers in the lung tissue and bronchoalveolar fluid of PF patients (146, 147). This together with our observations, that the endothelium is in its' inflamed/activated state in fibrotic lungs, prompted us to investigate the interaction between ECs and immune cells *in-vitro*. HPAECs isolated from either fibrosis or donor lungs were pre-stimulated with TNF-α, IFN-γ, IL-1β or the corresponding vehicle control for 1 hour and pre-

labeled PMNLs were allowed to adhere to the monolayers for 1.5 h. Generally, pre-treatment of HPAECs led to increased PMNL adhesion (Figure 18A). The count of adhered PMNLs to untreated fibrosis HPAECs was significantly lower as to donor HPAECs (Figure 19B). However, TNF-α pre-treatment led to significantly higher numbers of PMNL adhered to fibrosis HPAECs as to donor ECs (Figure 18B). This indicates that a pro-inflammatory environment induces increased immune – EC interaction in PF.

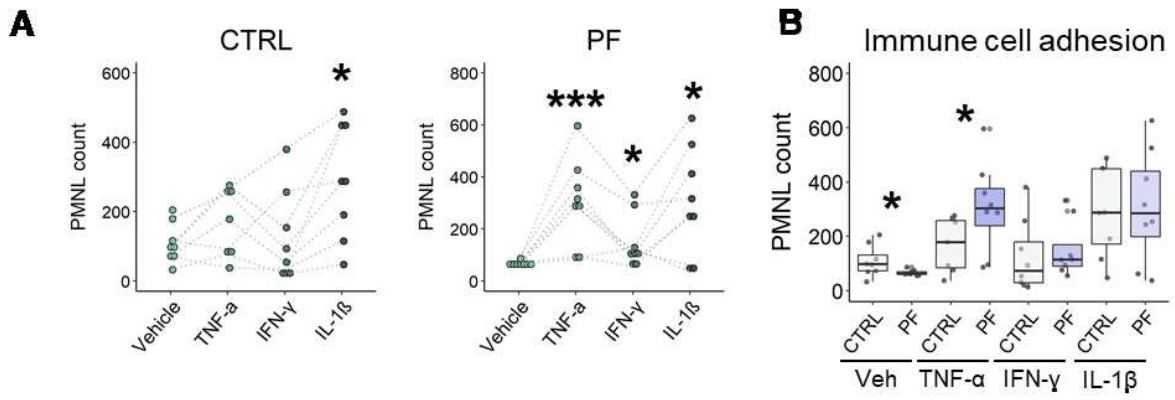

Figure 18: Adhesion of immune cells to endothelial cells. (A) Quantification of adhered polymorphnuclear leucocytes (PMNLs) to an established donor (technical replicates of n = 4) or fibrosis (technical replicates of n = 5) HPAEC monolayer. Pre-stimulation was done using either TNF-α, IFN-γ or IL-1β or the corresponding vehicle control. PMNLs were counted in 5 randomly chosen regions per well and the mean is shown. Kruskal Wallis test was performed. *: p<0.05; **: p<0.01; ***: p<0.001; ****: p<0.0001.

Translocation of immune cells through endothelial monolayers

PF is characterized by chronic inflammation and immune cell accumulation (12, 13, 148). To investigate whether the increased endothelial activation and disturbed integrity was accompanied by an altered immune cell diapedesis, we measured immune cell migration across the EC monolayer. Again, donor and fibrosis HPAEC monolayers were pre-stimulated with TNF-α, IFN-γ or IL-1β for 1 hour and PMNLs were allowed to transmigrate for 3 hours *in-vitro*. The measurement was conducted in a transwell system. The presence of an endothelial monolayer led to a reduced PMNL migration as compared to the control transwell (Figure 19A). The overall count of transmigrated PMNLs was not different between healthy and diseased HPAECs, neither in the unstimulated nor in the stimulated condition (Figure 19B). These data however correspond to disease endstage and might not represent the situation during earlier disease stages.

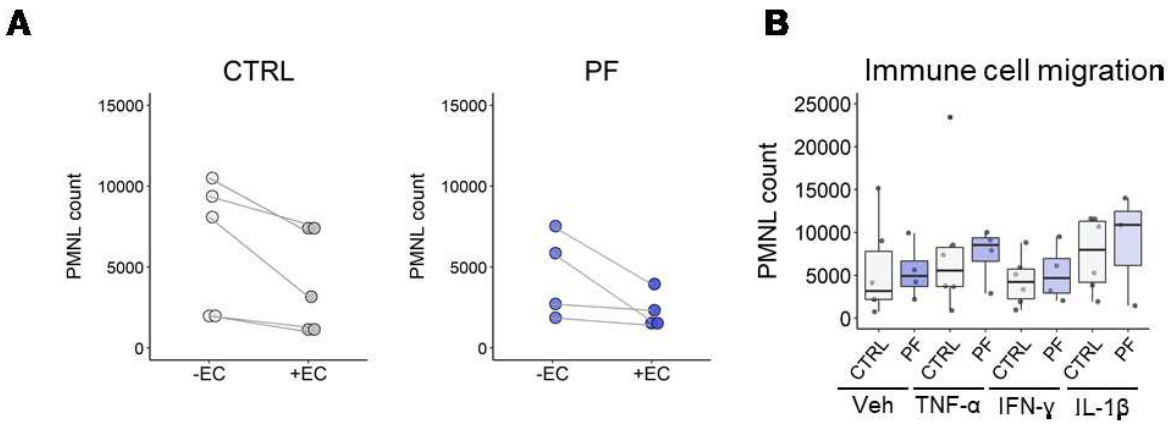

Figure 19: Transmigration of immune cells through endothelial cells. (A) Migration of PMNLs through 3 µm transwell insets with (+EC) and without (-EC) donor (CTRL) or fibrosis (PF) HPAEC monolayers in basal medium with 0% fetal bovine serum. (B) Transendothelial migration of PMNLs to basal media supplemented with 5% fetal bovine serum through established donor (technical replicates of n = 4) and fibrosis (technical replicates of n = 3) HPAEC monolayers after pre-stimulation of HPAECs with TNF-α, IFN-γ, IL-1β or the corresponding vehicle control. Kruskal Wallis test was performed. *: p<0.05; **: p<0.01; ***: p<0.001; ****: p<0.0001.

Endothelial-related molecules can be measured in the systemic circulation

To date diagnostic and predictive peripheral blood biomarkers in PF are still limited (149). Since all markers included in our analysis can be cleaved or secreted from ECs, we determined their levels in EDTA plasma samples from endstage PF patients (n=19) as well as control samples (n=28). Detailed patient and control characteristics are given in Table 3.

We found that the levels of VEGFR-2, VE-Cadherin and Thrombomodulin were significantly lower in plasma samples from PF patients as compared to the control samples, while vWF and IL-8 showed a strong increase. Furthermore, the activity of ICAM-2 was markedly lowered in PF plasma. No changes were observed for CD31, ICAM-1, VCAM-1 and P-selectin (Figure 20). A detailed correlation analysis of altered circulating EC markers and commonly used clinical parameters (e.g. forced vital capacity, total lung capacity, diffusion capacity of carbon monoxide) did not reach any significance (data not shown).

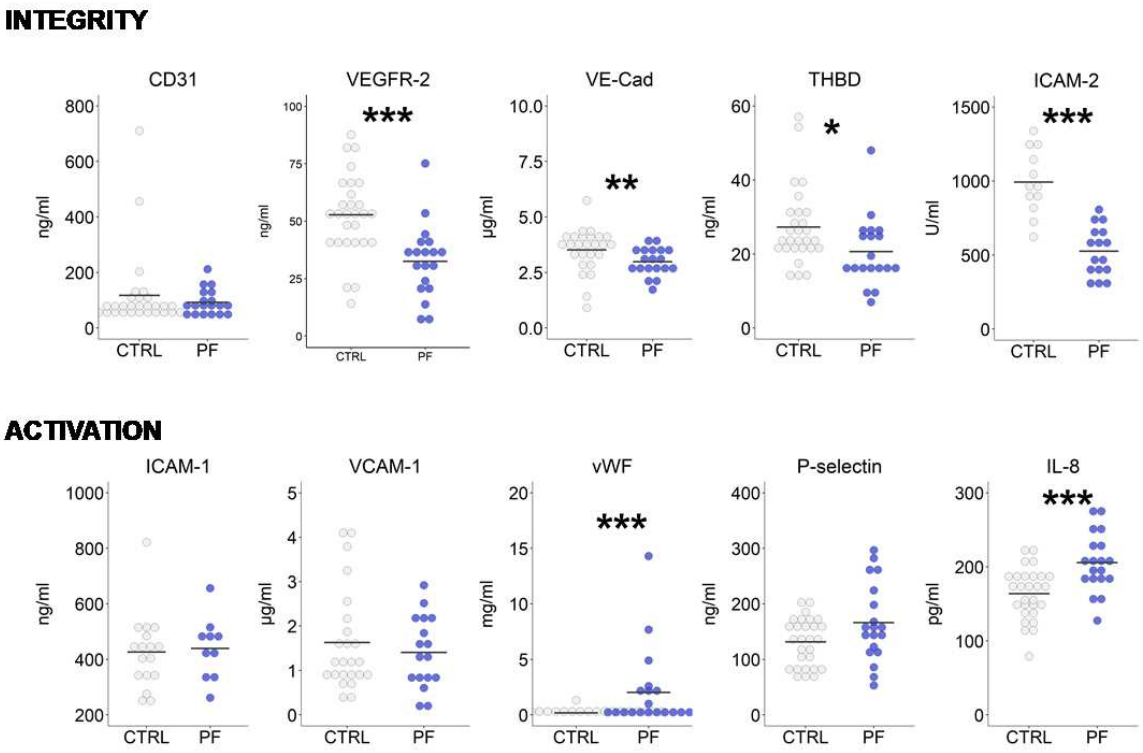

Figure 20: Endothelial cell markers in the systemic blood circulation. Determination of the levels/activity of endothelial integrity markers CD31, VEGFR-2, CDH5, THBD and ICAM-2 and activation markers ICAM-1, VCAM-1, vWF, SELP and IL-8 in EDTA plasma samples of PF patients (n = 19) and healthy controls (n = 28) measured by ELISA. Kruskal Wallis test was performed. *: p<0.05; **: p<0.01; ***: p<0.001; ****: p<0.0001.

Endothelial alterations during disease onset and progression

To investigate, whether the changes of the vascular compartment follow a temporal dependency during disease onset and progression, we employed the mouse model of bleomycin-induced lung fibrosis. After receiving a single dose of either saline or bleomycin, mice were sacrificed 3 days, 14 days or 21 days later. In this way, we were able to analyze vascular changes in the early injury phase (3d), during the strong inflammatory and fibrotic phase (14d) and in the late fibrosis phase (21d) (150). A schematic representation of the experimental setup is given in Figure 21.

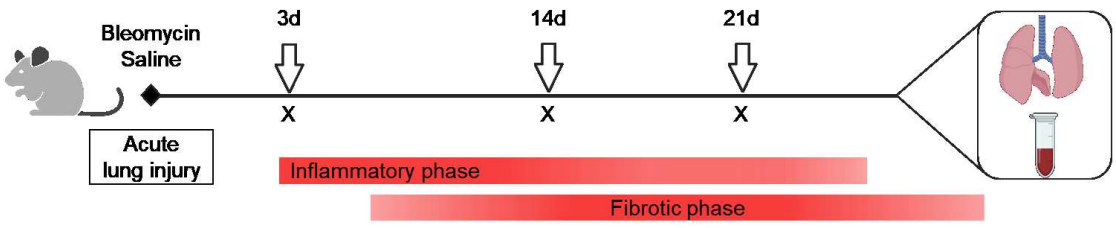

Figure 21: Schematic overview of the experimental strategy for the performance of the bleomycin-induced time course mouse model.

Whole lung gene expression analysis revealed that most changes were apparent in the early injury phase. We observed a significant downregulation of the endothelial integrity genes *Pecam1*, *Cdh5* and

Thbd, while the activation genes *Selp* and *Cxcl1* were significantly upregulated. *Selp* was continuously upregulated also in the strong inflammatory and fibrotic phase (14d), but balanced out again in the late fibrosis phase (21d). *Icam2* gene expression was significantly elevated 3 days after bleomycin administration, but significantly decreased at the later time points. The expression of *Cdh5* and *Kdr* was significantly lowered 21 days after bleomycin application as compared to the saline group. Interestingly, the expression of *Thbd* was significantly decreased 3 and 21 days after bleomycin administration, but increased in the active fibrotic phase (14d) (Figure 22).

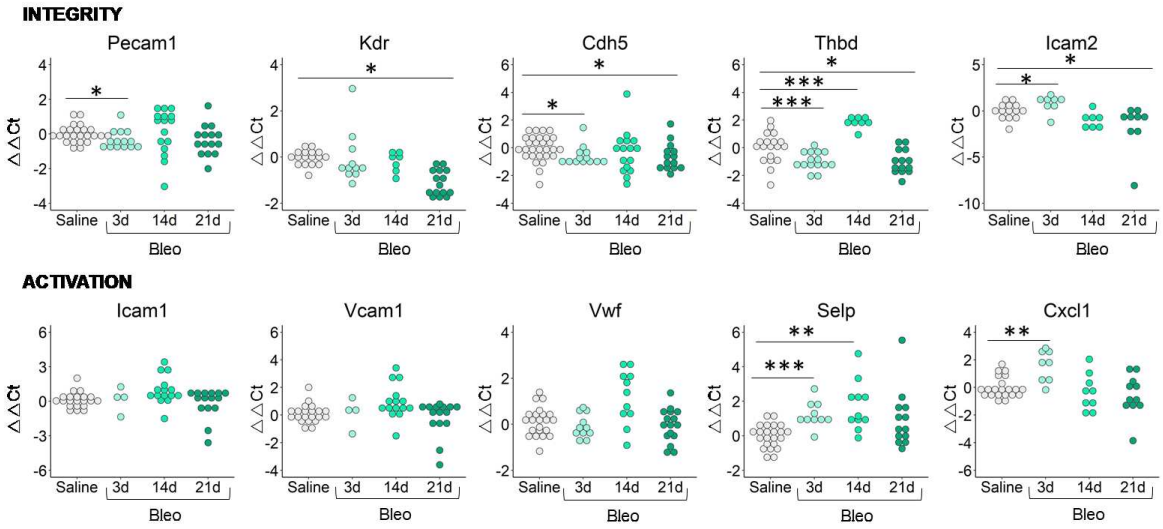

Figure 22: Changes of endothelial marker gene expression over time. RT-PCR analysis of endothelial integrity and activation markers CD31 (Pecam1), vascular endothelial growth factor receptor 2 (VEGFR-2, Kdr), VE-Cadherin (Cdh5), Thrombomodulin (Thbd), intercellular adhesion molecule 2 (Icam2), Icam1, vascular adhesion molecule 1 (Vcam1), von Willebrand Factor (Vwf), P-selectin (Selp) and interleukin-8 (Cxcl1) expression levels in lung homogenates of mice treated with saline (n = 31) or mice three (n = 16), 14 (n = 19) or 21 (n = 17) days post bleomycin administration. Kruskal Wallis test was performed. *: p<0.05; **: p<0.01; ***: p<0.001; ****: p<0.0001.

To investigate the status of EC activation we used immunohistochemical staining of vWF and subsequent quantitative image analysis based on color recognition (Figure 23A). The quantification revealed a significant increase of the relative abundance of vWF-positive regions (%) in mice 14 days after bleomycin administration. There were no differences in vWF-positive regions (%) between the saline group and the 3 day or 21 day bleomycin group (Figure 23B).

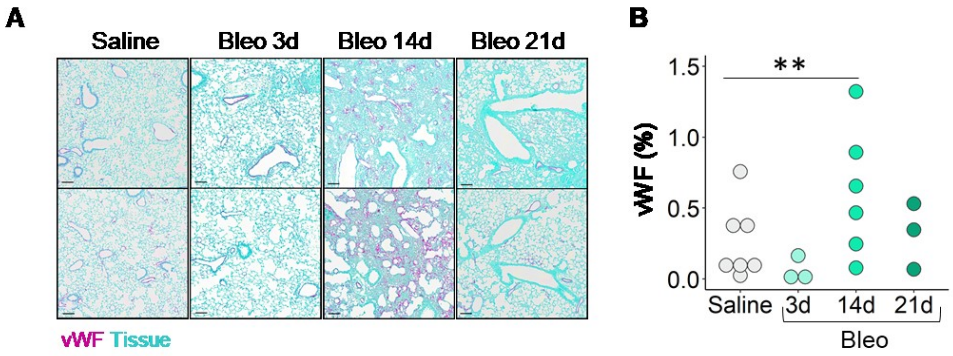

Figure 23: Endothelial activation over time in the lungs of bleomycin-treated mice. Representative images of lung tissue from mice treated with saline or bleomycin immunohistochemically stained against vWF (pink) with Fast Green counterstaining (green). Scale bar = 50 µm. Representative images of n = 7 (saline), n = 3 (3 days bleomycin), n = 6 (14 days bleomycin) and n = 3 (21 days bleomycin). (F) Quantification of vWF (%) in murine lung tissue sections after treatment with saline or bleomycin.

Lastly, we measured the corresponding plasma levels to check whether endothelial alterations are reflected in the animals' circulation. Thrombomodulin was significantly upregulated 14 days after bleomycin treatment, while ICAM-2 was significantly decreased. No changes were measured for other markers (Figure 24).

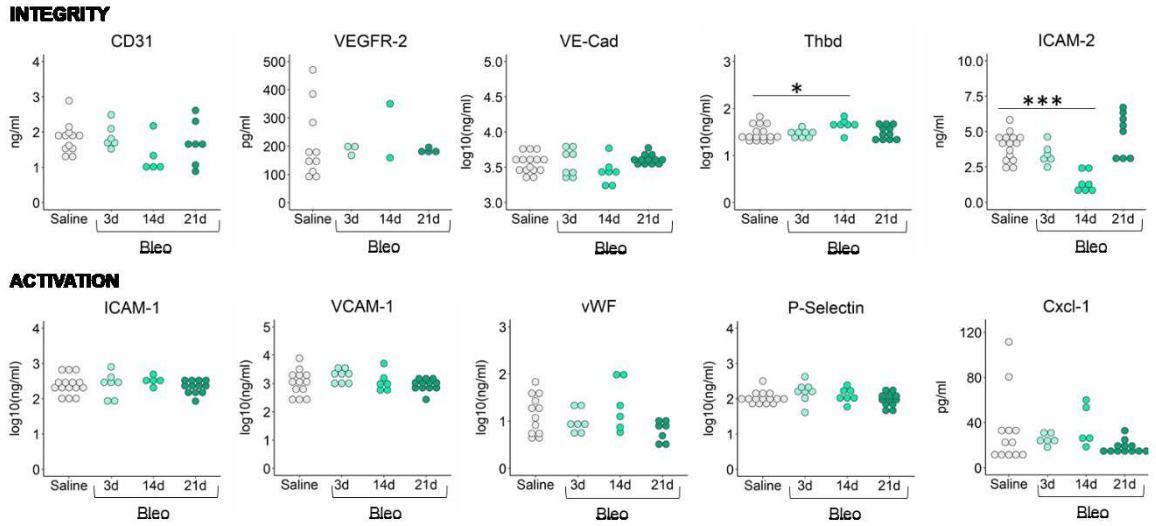

Figure 24: Changes of circulating endothelial cell markers over time in bleomycin-treated mice. Soluble levels of endothelial integrity and activation markers measured by ELISA in plasma samples of mice treated with saline (n = 16) or mice three (n = 8), 14 (n = 7) or 21 (n = 12) days post bleomycin administration measured by ELISA. Kruskal Wallis test was performed. *: p<0.05; **: p<0.01; ***: p<0.001; ****: p<0.0001.

Discussion

The lung is spanned by an extensive vascular network. The thin endothelial lining forms the interface between the blood circulation and the lung tissue, making it a central regulator of lung homeostasis. The maintenance of this homeostasis relies on an optimized gas exchange and nutrient supply, but also on other crucial endothelial functions. These functions include the control of vascular barrier integrity, regulation of vascular tone and inflammation via immune cell recruitment and translocation and finally managing coagulation and wound healing processes (129, 151). Abnormalities of one or several of these functions are central to the pathogenesis of various pulmonary diseases, such as IPAH and COPD and is manifested for example as hyper-permeability, leakage and edema formation, vascular remodeling, chronic endothelial inflammation or hypercoagulability (104, 129, 151, 152).

The current work demonstrates, that the endothelium undergoes significant changes in PPF. This is evident on a structural level in terms of change in shape and distribution as well as functionally in terms of endothelial activation and barrier integrity and strength. Moreover, the vascular changes were already evident during the development of the disease, as investigated in the bleomycin mouse model of lung fibrosis.

COVID-19 and chronic lung diseases

At the onset of the COVID-19 pandemic, it was initially not known, whether patients suffering from CLDs were at higher risk of facing severe infection. However, since it is known from literature, that for example COPD patients are more susceptible to respiratory viruses, which account for approximately 50% of acute exacerbations in COPD patients (153), an association between CLD and critical COVID-19 disease was likely. Also IPF and IPAH were associated with poor outcomes of SARS-CoV2 infection, severe complications during the infection and accelerated progression of CLD after the infection (154-156). These observations however were limited by the fact that they were based only on few case series and surveys back then.

Since then, numerous cohort studies have examined the impact of CLD on the progression of SARS-CoV-2 infection, both prospectively and retrospectively. A Korean retrospective cohort study on 4610 COVID-19 patients revealed increased need for mechanical ventilation and intensive care in COPD patients versus non-COPD controls (157). Moreover, COPD depicted an independent risk factor for all-cause mortality in COVID-19 (157). Two other, even bigger studies, confirmed that COPD increases the severity and mortality of SARS-CoV2 infection (158). The exact underlying molecular mechanisms are poorly understood. Possible explanations suggest that common pathological features occurring in COPD, such as compromised ventilation/hypoxia due to edema, vasoconstriction, and coagulation, may be exacerbated by COVID-19 (135, 159). As mentioned above, bacterial and viral infections are potent triggers of acute exacerbations in COPD-patients, as dampened innate and adaptive immune

responses provoke reoccurrence and persistence of respiratory infections (160). We and others also showed, that the entrance receptor ACE2 and other COVID-19 relevant mediators, such as TMPRSS2 are upregulated in the lungs of COPD patients on both, gene expression and protein level (134, 161-164). Elevated ACE2 gene expression was positively correlated with increased FVC (%), indicating that in non-infected COPD patients ACE2 is important to sustain better lung function. However, in parallel COPD presents several potential mechanisms that may facilitate the easier entry and spread of SARS-CoV-2.

On the other hand, linking IPF with increased susceptibility for and severity of COVID-19 remains inconclusive. Although case reports from COVID-19 patients with pre-existing IPF suggested, that SARS-CoV2 triggers acute exacerbation, a larger cohort could not confirm, that COVID-19 was directly increasing mortality in those patients (165, 166). Another multicenter study suggested increased rate of hospitalization, intensive care and mortality in IPF patients, however it did not include a control group (167). Other smaller studies found increased progression to acute exacerbation and heightened mortality rates in COVID-19 patients with pre-existing IPF (163, 168). Also studies on underlying interaction-mechanisms between SARS-CoV2 and the epithelium in IPF lungs remain contradictory. Our gene expression and immunohistochemical analysis of entrance proteins ACE2 and BSG and SARS-CoV2 modifying proteins TMPRSS2 and Furin did not show any differences between donor or PF transplant lungs. Yet another group reports significantly increased protein levels of the respective molecules in IPF lungs (169).

ACE2 can be cleaved from the cell surface via ADAM17, a disintegrin and metallopeptidase (170). Soluble ACE2 (sACE2) is increased in males and is associated with metabolic maladaptations, higher risk for and severity of SARS-CoV2 infection and comorbidities, such as diabetes mellitus or hypertension (171-173). Whether ACE2-shedding depicts a regulatory mechanism to prevent further SARS-CoV2 spreading or whether it is even accelerating the viral spreading, remains under-investigated. However, the soluble form of ACE2 keeps its' SARS-CoV2 interaction site and can thus form complexes with the virus (174). The administration of sACE2 protein led to increased binding of SARS-CoV2 virus particles in a mouse model of severe COVID-19 and thus alleviated the severity of infection (175). Our measurement of sACE2 revealed significantly lower levels of the mediator in plasma of both COPD and PF patients as compared to donor plasma. However, lowered circulatory ACE2 was neither positively nor negatively correlated with any lung function parameter in COPD or PF. Even today, four years after COVID-19 was declared a pandemic, studies in the field still cannot definitively establish whether CLDs represent a specific risk factor for severe COVID-19 and increased mortality. Larger studies with meticulously chosen patient cohorts would be necessary to address this question.

COVID-19, endotheliopathy and development of COVID-19-PF

Severe cases of acute COVID-19 demonstrated significant functional impairment/dysregulation and partial destruction of the pulmonary endothelium (100, 106, 135). These manifestations might arise both, directly via interaction with the virus and indirectly via the cytokine storm provoked by the virus. The presence of the virus and the cytokine storm initiate vascular hyper-inflammation and inflammasome activation, which in further consequence leads to loss of endothelial barrier structure, damage of endothelial glycocalyx, increased immune cell recruitment and translocation, as well as abnormal angiogenesis and hyper-coagulation (100, 106, 135). This provokes the impairment of central endothelial functions and thus endothelial dysfunction (endotheliopathy), senescence and apoptosis (100, 176). A hallmark of endothelial dysfunction and apoptosis is the release of circulating endothelial cells (CECs) into the bloodstream (177). Clinically, levels of circulating CECs have been considered as a valuable biomarker for assessing the presence and severity of COVID-19 (177). Moreover, the extensive impairment of the endothelium results in a vast array of additional potential biomarkers. The pulmonary endothelium of severely ill COVID-19 individuals exhibits increased gene expression levels of cellular stressors (e.g. NO synthase-2), pro-inflammatory cytokines (e.g. IL-6, TNF-α) and surface adhesion molecules (e.g. ICAM-1, VCAM-1), while genes involved barrier integrity (e.g. VE-Cadherin, CD31, Thrombomodulin) are decreased (100, 178, 179). In line, our findings unveiled a significant dysregulation of several endothelial markers implicated in vascular inflammation, coagulation, integrity and angiogenesis (ICAM-1, vWF, VEGR-2) locally in the lungs of severely ill COVID-19 patients (106). These results confirm the presence of endothelial inflammation and coagulation as well as abnormal angiogenic activities, which have been observed in COVID-19 patients of various disease severity (135). Moreover, activation markers vWF, VCAM-1 and E-selectin as well as integrity molecule CD31 were found to be strongly increased in the patients circulation (106). Shedding of activation markers is associated with a highly activated endothelium, while increased soluble CD31 is reported to originate from apoptotic endothelial cells (15). Therefore, our results reflect significant vascular inflammation as well as endothelial damage in COVID-19. The constant virus-mediated endothelial injury and thus continuous vascular permeability and glycocalyx degradation enhances edema formation in the airspaces as well as inflammatory cell entry into the parenchyma (100).

Concurrently we measured increased soluble levels of various cytokines, such as IL-6, IL-8, MCP-1, and TNF-α (106), which have been implicated in the so-called "cytokine storm" as well as in endothelial activation (96, 100, 179). Furthermore, we observed significant correlations between soluble vWF and D-dimer, soluble P-selectin and fibrinogen, and soluble vWF and IL-8 (106). vWF and IL-8 are stored together in the so-called Weibel-Palade bodies in ECs and get released in case of a "vascular emergency" (180). Moreover, D-dimer, fibrinogen, IL-8, vWF, and P-selectin are crucial components of the coagulation cascade (181).

Coagulopathy is a major complication in severe COVID-19. Coagulopathy involves a complex interaction network between the coagulation cascade and the aberrantly activated immune system, which is summed up as “immune-thrombosis” (96). Under physiological conditions, the endothelium provides an anti-thrombotic surface, which prevents platelet activation via expression of e.g. prostacyclin or NO and inhibits coagulation via thrombomodulin or tissue factor pathway inhibitor (TFPI) amongst others (107). Additionally, the endothelial glycocalyx provides anti-thrombotic heparin sulfate (107). In the case of SARS-CoV2 infection, TFPI loses its’ function and thrombomodulin is shed from the vascular surface, while pro-coagulant mediators, such as TF get upregulated (107). The accompanying endothelial injury and degradation of the glycocalyx attract neutrophils, which are cells of the very early immune response (107). As part of their mechanism of action, neutrophils undergo programmed cell death, so called “NETosis”, which leads to the formation of web-like nets containing DNA, histones, oxidant enzymes, complement factors as well as pro-coagulant mediators (107). Elevated accumulation of active complement factors cause the release of those mediators from NETs and induce platelet activation, P-selectin expression and release of pro-thrombotic factors from platelets (107). Moreover, platelets are being activated by other factors, such as vWF, IL-8 or TF (107). Thus, heightened pro-coagulant activity (TF, vWF, Factor VIII, complement), neutrophil recruitment and NETosis, enhanced fibrinogen to fibrin turn-over via TF and impaired fibrinolysis cause characteristic features of critical COVID-19, such as deep venous thrombosis, pulmonary thromboembolism or arterial embolism (182).

A brief overview of mediators implicated in the COVID-19 – endotheliopathy is given in Figure 25.

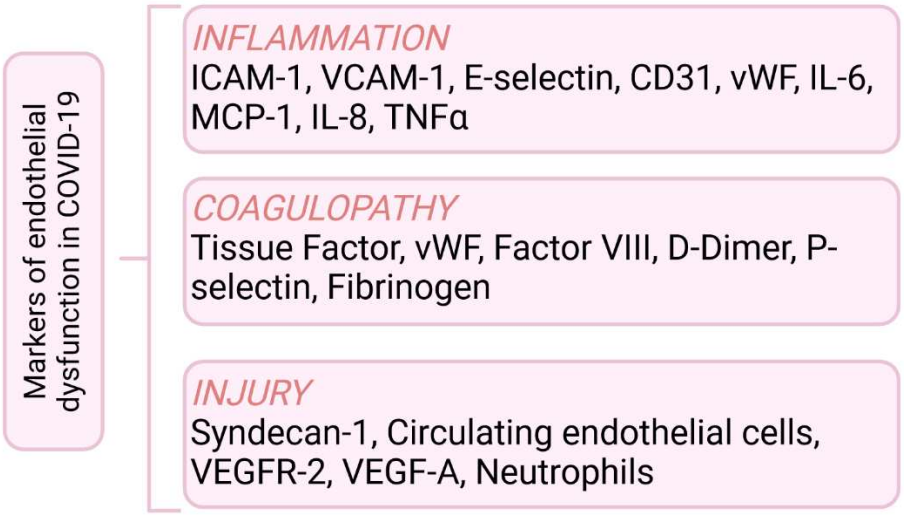

Figure 25: Markers of endothelial dysfunction in COVID-19. Created with BioRender.com (Agreement number: XZ26HLC6EN).

The persistence of endothelial destruction in COVID-19 is further evident from the elevated plasma levels of syndecan-1, a marker of glycocalyx shedding, in convalescent patients as compared to healthy

individuals (100). Moreover, also CEC levels stay continuously elevated in convalescent patients (183). Recently, it is becoming increasingly evident that patients, who experienced prolonged and unresolved endothelial dysfunction after COVID-19 infection are predisposed to develop lung fibrosis (89). A plethora of reports from the COVID-19 research field supports the central role of a dysregulated endothelium in the establishment of a pro-fibrotic environment in the lungs of severe cases. Mediators and pathways, which drive ILD-associated PPF, are also significantly upregulated in COVID-19 associated fibrosis. These include for example TGF-β (113), a central conductor in ILD-PPF, the WNT signaling axis (114), which facilitates cell proliferation or the YAP/TAZ pathway (115, 116), which activates fibroblasts. According to latest observations, COVID-19 associated PF closely resembles the pathological phenotype of end-stage ILD-associated PF (112). COVID-19 associated PF shows a UIP pattern, similar to most ILD-PPFs. Furthermore, parenchymal abnormalities typical for ILD-associated PPF, such as ground glass opacities, septal thickening, traction bronchiectasis and honeycombing, can be observed in 25% of severe COVID-19 cases one year after the infection (112). These observations indeed suggest a role of a disrupted endothelium in the onset and progression of PF.

Endothelial cells in PPF

Observations from COVID-19 suggest a potential association between the loss of endothelial homeostasis, the establishment of a pro-fibrotic milieu, and subsequent transition into parenchymal remodeling. This evidence supports our hypothesis that the endothelium plays a central role in the development and progression of PPF associated with chronic lung diseases, IPF or HP as well.

Vascular remodeling is frequently observed in PPF and follows a disease-specific pattern as compared to vascular remodeling in COPD (22). More interestingly, the vascular remodeling can either go hand in hand with the parenchymal remodeling or even precede PPF, as shown in the bleomycin mouse model and the Fra-2 overexpressing/transgenic mouse model of Systemic Sclerosis associated ILD, respectively (184-186). These observations nicely demonstrate that endothelial dysfunction is not solely a phenomenon of end-stage disease. Moreover, pre-capillary anastomoses between the systemic and pulmonary circulation have been observed in fibrotic lungs (24). These structural changes are consistent with our observations from the ultrastructural transmission electron microscopy of PF lung samples. Abnormally formed capillary endothelial cells in fibrotic lungs suggest, that structural malformations apply not only to arteries and arterioles, but also the capillaries. In addition reports describe a heterogeneous vascularization in the fibrotic lung, with fibrotic foci being completely devoid of any vasculature (50, 187-190). This is accompanied by an imbalance of angiogenic mediators (e.g. VEGF-A, IL-8 or PEDF) between heavy remodeled and normal areas of fibrotic lungs (56, 57). With our staining of progressive PPF lung tissue, we could not confirm the heterogeneous vascularization, but observed higher abundance in stronger remodeled lung areas. This could potentially be explained by

the use of different endothelial markers. Reports so far are based on staining against endothelial CD34 and Thrombomodulin (50). We used the integrity markers CD31 and VE-Cadherin, which gave a markedly stronger signal in PPF lung sections as compared to donors. This is in line with the increased gene expression of both markers in the endothelial compartment, which was extracted from a publicly available scRNA-seq dataset. Additionally, vWF was reported to be localized only to larger vessels with small vessels and capillaries being devoid of vWF (50). We, on the other hand, observed a very strong signal intensity for vWF not only in large vessels, but also capillaries and found a significant association between vWF-positivity and collagen content. Of note, previous reports are based on the analysis of lung fibrosis biopsy tissue, while for our analysis we used endstage transplant tissue. An increase of vWF was also reported in immunohistochemical stained murine lung tissue two weeks and four weeks after bleomycin administration as compared to control lungs, which is in line with our observations in the fibrosis mouse model (191). This could indicate that capillaries undergo a phenotypic switch due to the strong parenchymal distortion, resulting in a highly activated endothelium as the disease progresses.

Dysregulation of endothelial activation in PF

Fibrotic lungs are characterized by immune cell infiltration and chronic inflammation (192). ECs play a crucial role as conductors of immune responses by binding of immune cells and translocating them from the circulation to the lung tissue (15). Different immune cells, including T-cells, B-cells, macrophages and dendritic cells accumulate in fibrotic lungs adjacent to fibrotic foci and secrete both pro-inflammatory (e.g. tumor necrosis factor (TNF)-α, interleukin (IL)-1β, interferon (IFN)-γ) as well as pro-fibrotic (e.g. IL-13, transforming growth factor (TGF)-β) mediators (192). In the bleomycin-induced mouse model of fibrosis, ECs have been shown to facilitate increased macrophage and dendritic cell recruitment throughout the course of the disease, which are subsequently establishing a pro-fibrotic milieu by secreting large amounts of mediators such as TGF-β (191).

ECs isolated from fibrosis lungs showed a marked increase of vWF gene expression in the presence of inflammation mediators TNF-α or IFN-γ, two important mediators in fibrotic lungs (143, 144, 193, 194). Furthermore, those endothelial cells also demonstrated increased interaction with immune cells in the presence of a pro-inflammatory environment. In line, the intensity of vWF in fibrosis lung tissue sections correlated significantly with immune cell infiltrates. Therefore, one can hypothesize that the heightened endothelial activation observed in PF results from their increased sensitivity to a pro-inflammatory environment. Maladapted communication between ECs, immune cells and platelets have been reported in PF (195). Pulmonary injury induced the recruitment and adhesion of platelets in aged mouse lungs, which induce wound healing upon IL-1α secretion and macrophage recruitment (195). However, aged lungs exhibited an abnormally regulated endothelial Neuropilin-1/hypoxia-

inducible-factor2α (Hif2α) pathway, which inhibited anti-thrombotic endothelial protein C receptor (EPCR) (195). PF, induced either by bleomycin or hydrochloric acid, led also to the inhibition of endothelial chemokine receptor CXCR7, which suppressed alveolar regeneration and attracted a pro-fibrotic, VEGFR-1-positive macrophage subpopulation (196). Moreover, reduced levels of natural killer T (NKT) cells caused the attenuation of downstream signal transducer and activator of transcription (STAT) 1-CXC motif chemokine ligand (CXCL) 9 signaling (197). The absent signaling axis between NKT cells and ECs provoked heavy vascular remodeling in both, PF patients and bleomycin-treated mice (197).

This suggests that the abnormally activated pulmonary endothelium can be put in the center of chronic inflammation and fibrogenesis.

Dysregulation of endothelial barrier integrity in PF

It is very likely, that the pro-inflammatory milieu prevailing in fibrotic lungs is not only influencing the activation status of the pulmonary endothelium, but also the vascular barrier integrity (15, 198-203). PF has been postulated to be associated with increased vascular barrier breakdown/leakage (152). This has been determined in human lungs based on the clearance rate of radio-labelled technetium-99m diethylenetriamine pentaacetate (99mTc-DTPA) and of the contrast agent albumin-binding gadolinium (65, 66). Both studies showed, that the alveolar-capillary permeability is already increased in early disease stages and this was observed in both, remodeled and non-remodeled areas of patient's lungs. Moreover, a loss of junction marker VE-Cadherin was recently reported in the Fra2-overexpression mouse model of SSc-ILD (184). In line, we measured a downregulation of several vascular barrier markers in the time-course mouse model of bleomycin-induced lung fibrosis. Other research groups reported alterations of different pathways and mediators involved in the regulation barrier integrity in various animal models and patients. The levels of barrier enhancer sphingosine-1-phosphate (S1P) have been shown to be elevated in the human and murine fibrotic lung tissue and broncho-alveolar lavage fluid as well as in their systemic circulation (69, 204). Interruption of the downstream S1P – S1P receptor (S1PR1) signaling axis attenuated barrier breakdown and parenchymal remodeling in the bleomycin mouse model (68, 70). Similar results have been found in the human disease. Enhanced gene expression levels of S1P kinase were significantly correlated with worse lung function and mortality (70). Also studies dealing with other pathways implicated in vascular integrity (e.g. Ang-1 / Ang-2 / Tie-2 signaling axis or VEGFR-2 / VEGF-A) indicate a significant association between increased vascular permeability and enhanced disease progression and rapid loss of lung function (75-77).

In contrast to the above-mentioned reports on enhanced vascular permeability in lung fibrosis, we observed a strongly elevated signal intensity of integrity markers VE-Cadherin and CD31 in fibrotic lung tissue sections. Simultaneously, the gene expression of those markers as well as other integrity

markers VEGFR-2 and Thrombomodulin was significantly decreased in the LH of fibrotic lungs. In parallel *in-vitro* resistance measurements demonstrated a markedly decreased barrier strength in ECs isolated from fibrosis lungs as compared to control ECs. This suggests that the markers may not be fully functional or may be dysregulated in these contexts. Indeed, staining against VE-Cadherin in a HPAEC monolayer *in-vitro* revealed noticeable differences in the cobblestone pattern and arrangement of junctions between donor and disease. While in donors VE-Cadherin was distributed uniformly between the HPAECs in the monolayer, fibrosis HPAECs exhibited uneven and disrupted junctions. The significantly stronger intensity of vascular barrier markers on immunohistochemically stained lung tissue sections could represent a "rescue" mechanism, where dysfunctional barrier molecules are gathering together to maintain the impaired barrier. A functional impairment is further supported by the results obtained from the *in-vitro* immune cell transmigration assay. Although we measured increased counts of PMNLs adhered to fibrotic as compared to donor HPAEC monolayers, this was not coming along with increased immune cell transmigration through the monolayer. This might indicate that dysfunctional barrier molecules trap immune cells in their adhesion phase and prevent the completion of immune cell diapedesis in the endstage of PF.

Biomarker research

All endothelial markers included in our study exist as either cell-associated or soluble forms. It was shown *in-vitro* that the amount of circulatory activation markers correlated with the level of the respective marker expressed on the EC surface after being exposed to pro-inflammatory TNF-α (82). Thus shedding of activation markers results from increased inflammation and endothelial hyper-activation. The shedding is facilitated by matrix metalloproteinases (MMPs) and disintegrin metalloproteinases (ADAMs), two large protease families, which are central in tissue remodeling, angiogenesis and wound healing. The levels of both proteinase groups are significantly elevated in the lungs and blood of patients with PF and have been postulated as contributors to disease pathogenesis (205-210).

Biomarkers significantly facilitate the diagnosis and prognosis of a disease, but none are available for PPF so far (211). However, some studies have already suggested a role of adhesion molecules as potential biomarkers. Poor progression-free survival, poor transplant-free survival and poor overall survival was predicted in IPF based on soluble VCAM-1, ICAM-1 and IL-8. VCAM-1, ICAM-1 and P-selectin have furthermore been associated with high pulmonary attenuation areas, lowered FVC and increased hospitalization and mortality (86, 87). And an impaired diffusion capacity of the lung for carbon monoxide (DLCO) significantly correlated with increased serum levels of ICAM-1 and ICAM-2 (88, 212). Other smaller studies have also been able to establish links between the elevated levels of

EC markers and disease outcome and suggest blood profiling as a considerable approach in PF diagnosis and prognosis (213).

In line with this, we can also report an imbalance of soluble EC markers in our PF patient cohorts. Plasma analysis revealed a significant downregulation of circulatory VEGFR-2, VE-Cadherin and Thrombomodulin, while vWF and IL-8 were significantly upregulated in endstage PF. It is claimed that imbalances of soluble mediators become even more pronounced as the disease worsens. Thus dysbalances correlate with the presence of acute exacerbations in PF patients. Elevated vWF levels have been associated with ARDS and endothelial injury in general and with emphysema and acute exacerbations specifically in COPD patients (214, 215). In a mouse model of chronic carbon tetrachloride induced liver fibrosis, vWF deficiency led to the attenuation of disease progression (216). Thus, maintaining balanced levels of vWF could also represent a potential treatment option for improving pulmonary fibrosis.

Alterations of the vascular compartment during lung fibrosis onset and progression

To investigate whether there were sequential changes in the EC compartment, we examined the mouse model of bleomycin-induced lung fibrosis. The induction of experimental fibrosis is based on an acute lung injury provoked by the administration of the chemotherapeutic antibiotic “bleomycin” (217). Bleomycin induces an initial pro-inflammatory phase, followed by a strong elevation of pro-fibrotic mediators approximately 7-9 days after the induction. The extent of lung fibrosis peaks around day 14 after the initial bleomycin administration. Contrary to the human disease, in the bleomycin-induced lung fibrosis model, the progression is relatively rapid and begins to resolve approximately 4 weeks after initiation without any intervention (150, 217). In our experimental setup, mice were sacrificed 3, 14 or 21 days after intra-tracheally receiving a single dose of either saline or bleomycin. This approach allowed analyzing vascular changes in the early injury and inflammatory phase (1 – 3d) and during the late inflammatory and early to late fibrotic phase (7 - 21d) (150).

In contrast to our observations in the human disease, the gene expression of investigated barrier markers was significantly downregulated already at disease onset. This was found in both whole murine lungs and in the extracted endothelial cell population. While the gene expression of some markers, like CD31, stabilized again over time, other markers, like Thrombomodulin, ICAM-2, VE-Cadherin or VEGFR-2 were significantly downregulated also in the later time point. Simultaneously, activation molecules P-selectin and CXCL1 (murine IL-8) were strongly elevated in the early phase of disease and again stabilized as the disease progressed into late fibrosis and early resolution. This could be attributed to the fact, that the acute lung injury triggered by bleomycin might have severe impact on the vasculature and thus might not mirror the situation of the slowly and chronically progressing human PF. Currently, various murine models of lung fibrosis are frequently used in the research field

of PF. Although, lung fibrosis development is provoked by different substances, such as bleomycin, asbestos or fluorescein isothiocyanate (FITC) or by adenovirus-mediated overexpression of TFG-β, all models rely on an acute injury to the lung, which is commonly accompanied by vascular remodeling, endothelial inflammation, leakage and coagulopathy (217-221). Thus, a murine model based on acute injury and inflammation might not be the optimal model to study vascular activation and integrity.

Limitations of the study

Our study holds several limitations. First, we investigated our set of markers in a rather small and heterogeneous cohort. Moreover, the presence of a variety of different comorbidities has to be taken into consideration. Their presence as well as the treatment of apparent comorbidities could affect the activation and integrity status of the endothelium and thus influence our findings. However, as all included tissue originated from patients, who underwent lung transplantation, the generalizability of the results is still given.

Furthermore, not all markers included in our investigated panel are specific to endothelium, but can also be expressed by other cell populations, such as fibroblasts, immune cells or epithelium. Therefore, gene expression results obtained from whole lung tissue analysis cannot be solely attributed to the vascular compartment. Ideally, our *in-vitro* analysis would have also included capillary endothelial cells isolated from the patients' lungs. Presently we have not solved the problem of contaminating other (micro- and macrovascular) endothelial cells and we state clearly that our findings obtained with the patients' arteriolar/mixed endothelial cells, may or may not reflect the behaviour of the capillaries.

To get better insights into the time-dependency of vascular alterations during disease onset and progression, we included the mouse model of bleomycin-induced lung fibrosis. This model is well-respected and commonly used by the research community. However, as it remains unclear whether, or to what extent, the bleomycin mouse model represents the human IPF pathology, contradictory findings with regard to endothelial activation and integrity have to be considered with caution.

Conclusion

The significant endothelial dysfunctions observed in COVID-19, along with the increasing number of patients developing long-COVID associated PPF, strongly indicate a central role of the pulmonary endothelium in the transition from a healthy to a fibrotic state. Cumulatively, by taking advantage of the human lung transplant samples, as well as patients' plasma, isolated pulmonary artery ECs and a publicly microarray dataset of PPF, we report that ECs are also altered drastically with regard to structure and function in ILD-associated PPF. We revealed swollen and lumen-obliterating, highly activated ECs in fibrotic lungs. The endothelial hyper-activation was further corroborated by our *in-vitro* analysis, which uncovered increased immune cell adhesion to fibrotic ECs.

The vascular hyper-activation was associated with a pronounced dysfunction of endothelial integrity, which was represented in a reduced barrier strength as well as loss of the typical endothelial cobblestone structure *in-vitro*.

In conclusion, our data show that the pulmonary endothelium is affected in the course of PPF. Moreover, the changes have an essential temporal and spatial dimension during pathogenesis. Whether maladapted endothelial-related functions belong to the main triggers of PPF or rather fuel the fibrogenic process in its later stage, remains unknown. Detailed functional experiments are warranted to elucidate the connection between progressive fibrosis and aberrant EC communication and function. Concentrating on gaining a better understanding of the maladapted endothelial niche could represent a milestone in the development of novel and effective anti-fibrotic therapies.

References

1. Christenson SA, Smith BM, Bafadhel M, Putcha N. Chronic obstructive pulmonary disease. Lancet. 2022;399(10342):2227-42.
2. Polverino F, Sam A, Guerra S. COPD: To Be or Not to Be, That is the Question. Am J Med. 2019;132(11):1271-8.
3. Humbert M, Kovacs G, Hoeper MM, Badagliacca R, Berger RMF, Brida M, et al. 2022 ESC/ERS Guidelines for the diagnosis and treatment of pulmonary hypertension. Eur Heart J. 2022;43(38):3618-731.
4. Humbert M, Kovacs G, Hoeper MM, Badagliacca R, Berger RMF, Brida M, et al. 2022 ESC/ERS Guidelines for the diagnosis and treatment of pulmonary hypertension. Eur Respir J. 2023;61(1).
5. Selman M, Pardo A. When things go wrong: exploring possible mechanisms driving the progressive fibrosis phenotype in interstitial lung diseases. Eur Respir J. 2021;58(3).
6. George PM, Spagnolo P, Kreuter M, Altinisik G, Bonifazi M, Martinez FJ, et al. Progressive fibrosing interstitial lung disease: clinical uncertainties, consensus recommendations, and research priorities. Lancet Respir Med. 2020;8(9):925-34.
7. Wijsenbeek M, Cottin V. Spectrum of Fibrotic Lung Diseases. N Engl J Med. 2020;383(10):958-68.
8. Khor YH, Ng Y, Barnes H, Goh NSL, McDonald CF, Holland AE. Prognosis of idiopathic pulmonary fibrosis without anti-fibrotic therapy: a systematic review. Eur Respir Rev. 2020;29(157).
9. Kondoh Y, Azuma A, Inoue Y, Ogura T, Sakamoto S, Tsushima K, et al. Thrombomodulin Alfa for Acute Exacerbation of Idiopathic Pulmonary Fibrosis. A Randomized, Double-Blind Placebo-controlled Trial. Am J Respir Crit Care Med. 2020;201(9):1110-9.
10. Bosman FT, Damjanov I. Recent Advances in Histopathology - 25: JP Medical; 2022.
11. Sgalla G, Iovene B, Calvello M, Ori M, Varone F, Richeldi L. Idiopathic pulmonary fibrosis: pathogenesis and management. Respir Res. 2018;19(1):32.
12. Balestro E, Calabrese F, Turato G, Lunardi F, Bazzan E, Marulli G, et al. Immune Inflammation and Disease Progression in Idiopathic Pulmonary Fibrosis. PLoS One. 2016;11(5):e0154516.
13. Todd NW, Scheraga RG, Galvin JR, Iacono AT, Britt EJ, Luzina IG, et al. Lymphocyte aggregates persist and accumulate in the lungs of patients with idiopathic pulmonary fibrosis. J Inflamm Res. 2013;6:63-70.
14. Heukels P, Moor CC, von der Thusen JH, Wijsenbeek MS, Kool M. Inflammation and immunity in IPF pathogenesis and treatment. Respir Med. 2019;147:79-91.
15. Pober JS, Sessa WC. Evolving functions of endothelial cells in inflammation. Nat Rev Immunol. 2007;7(10):803-15.
16. Townsley MI. Structure and composition of pulmonary arteries, capillaries, and veins. Compr Physiol. 2012;2(1):675-709.
17. Gillich A, Zhang F, Farmer CG, Travaglini KJ, Tan SY, Gu M, et al. Capillary cell-type specialization in the alveolus. Nature. 2020;586(7831):785-9.
18. Caporarello N, Lee J, Pham TX, Jones DL, Guan J, Link PA, et al. Dysfunctional ERG signaling drives pulmonary vascular aging and persistent fibrosis. Nat Commun. 2022;13(1):4170.
19. Vila Ellis L, Cain MP, Hutchison V, Flodby P, Crandall ED, Borok Z, et al. Epithelial Vegfa Specifies a Distinct Endothelial Population in the Mouse Lung. Dev Cell. 2020;52(5):617-30 e6.
20. Rajagopal K, Bryant AJ, Sahay S, Wareing N, Zhou Y, Pandit LM, et al. Idiopathic pulmonary fibrosis and pulmonary hypertension: Heracles meets the Hydra. Br J Pharmacol. 2021;178(1):172-86.
21. Gaikwad AV, Lu W, Dey S, Bhattarai P, Chia C, Larby J, et al. Vascular remodelling in idiopathic pulmonary fibrosis patients and its detrimental effect on lung physiology: potential role of endothelial-to-mesenchymal transition. ERJ Open Res. 2022;8(1).
22. Hoffmann J, Wilhelm J, Marsh LM, Ghanim B, Klepetko W, Kovacs G, et al. Distinct differences in gene expression patterns in pulmonary arteries of patients with chronic obstructive pulmonary disease and idiopathic pulmonary fibrosis with pulmonary hypertension. Am J Respir Crit Care Med. 2014;190(1):98-111.

23. Ruffenach G, Hong J, Vaillancourt M, Medzikovic L, Eghbali M. Pulmonary hypertension secondary to pulmonary fibrosis: clinical data, histopathology and molecular insights. Respir Res. 2020;21(1):303.
24. Turner-Warwick M. Precapillary Systemic-Pulmonary Anastomoses. Thorax. 1963;18(3):225-37.
25. Babkina AS, Ostrova IV, Yadgarov MY, Kuzovlev AN, Grechko AV, Volkov AV, et al. The Role of Von Willebrand Factor in the Pathogenesis of Pulmonary Vascular Thrombosis in COVID-19. Viruses. 2022;14(2).
26. Mojzisch A, Brehm MA. The Manifold Cellular Functions of von Willebrand Factor. Cells. 2021;10(9).
27. Peyvandi F, Garagiola I, Baronciani L. Role of von Willebrand factor in the haemostasis. Blood Transfus. 2011;9 Suppl 2(Suppl 2):s3-8.
28. Edvardsen MS, Hindberg K, Hansen ES, Morelli VM, Ueland T, Aukrust P, et al. Plasma levels of von Willebrand factor and future risk of incident venous thromboembolism. Blood Adv. 2021;5(1):224-32.
29. Kasper M, Schobl R, Haroske G, Fischer R, Neubert F, Dimmer V, et al. Distribution of von Willebrand factor in capillary endothelial cells of rat lungs with pulmonary fibrosis. Exp Toxicol Pathol. 1996;48(4):283-8.
30. Martin FA, Murphy RP, Cummins PM. Thrombomodulin and the vascular endothelium: insights into functional, regulatory, and therapeutic aspects. Am J Physiol Heart Circ Physiol. 2013;304(12):H1585-97.
31. Kataoka K, Taniguchi H, Kondoh Y, Nishiyama O, Kimura T, Matsuda T, et al. Recombinant Human Thrombomodulin in Acute Exacerbation of Idiopathic Pulmonary Fibrosis. Chest. 2015;148(2):436-43.
32. Sakamoto S, Shimizu H, Isshiki T, Sugino K, Kurosaki A, Homma S. Recombinant human soluble thrombomodulin for acute exacerbation of idiopathic pulmonary fibrosis: A historically controlled study. Respir Investig. 2018;56(2):136-43.
33. Hayakawa S, Matsuzawa Y, Irie T, Rikitake H, Okada N, Suzuki Y. Efficacy of recombinant human soluble thrombomodulin for the treatment of acute exacerbation of idiopathic pulmonary fibrosis: a single arm, non-randomized prospective clinical trial. Multidiscip Respir Med. 2016;11:38.
34. Woodfin A, Voisin MB, Nourshargh S. PECAM-1: a multi-functional molecule in inflammation and vascular biology. Arterioscler Thromb Vasc Biol. 2007;27(12):2514-23.
35. Rho SS, Ando K, Fukuhara S. Dynamic Regulation of Vascular Permeability by Vascular Endothelial Cadherin-Mediated Endothelial Cell-Cell Junctions. J Nippon Med Sch. 2017;84(4):148-59.
36. Harris ES, Nelson WJ. VE-cadherin: at the front, center, and sides of endothelial cell organization and function. Curr Opin Cell Biol. 2010;22(5):651-8.
37. Lyck R, Enzmann G. The physiological roles of ICAM-1 and ICAM-2 in neutrophil migration into tissues. Curr Opin Hematol. 2015;22(1):53-9.
38. Bui TM, Wiesolek HL, Sumagin R. ICAM-1: A master regulator of cellular responses in inflammation, injury resolution, and tumorigenesis. J Leukoc Biol. 2020;108(3):787-99.
39. Ramos TN, Bullard DC, Barnum SR. ICAM-1: isoforms and phenotypes. J Immunol. 2014;192(10):4469-74.
40. Agassandian M, Tedrow JR, Sembrat J, Kass DJ, Zhang Y, Goncharova EA, et al. VCAM-1 is a TGF-beta1 inducible gene upregulated in idiopathic pulmonary fibrosis. Cell Signal. 2015;27(12):2467-73.
41. Filippi MD. Mechanism of Diapedesis: Importance of the Transcellular Route. Adv Immunol. 2016;129:25-53.
42. Kong DH, Kim YK, Kim MR, Jang JH, Lee S. Emerging Roles of Vascular Cell Adhesion Molecule-1 (VCAM-1) in Immunological Disorders and Cancer. Int J Mol Sci. 2018;19(4).
43. Wang X, Bove AM, Simone G, Ma B. Molecular Bases of VEGFR-2-Mediated Physiological Function and Pathological Role. Front Cell Dev Biol. 2020;8:599281.

44. Ou XM, Li WC, Liu DS, Li YP, Wen FQ, Feng YL, et al. VEGFR-2 antagonist SU5416 attenuates bleomycin-induced pulmonary fibrosis in mice. Int Immunopharmacol. 2009;9(1):70-9.
45. She YX, Yu QY, Tang XX. Role of interleukins in the pathogenesis of pulmonary fibrosis. Cell Death Discov. 2021;7(1):52.
46. Qazi BS, Tang K, Qazi A. Recent advances in underlying pathologies provide insight into interleukin-8 expression-mediated inflammation and angiogenesis. Int J Inflam. 2011;2011:908468.
47. Andre P. P-selectin in haemostasis. Br J Haematol. 2004;126(3):298-306.
48. Crooks MG, Fahim A, Naseem KM, Morice AH, Hart SP. Increased platelet reactivity in idiopathic pulmonary fibrosis is mediated by a plasma factor. PLoS One. 2014;9(10):e111347.
49. Horikawa M, Fujimoto M, Hasegawa M, Matsushita T, Hamaguchi Y, Kawasuji A, et al. E- and P-selectins synergistically inhibit bleomycin-induced pulmonary fibrosis. Am J Pathol. 2006;169(3):740-9.
50. Ebina M, Shimizukawa M, Shibata N, Kimura Y, Suzuki T, Endo M, et al. Heterogeneous increase in CD34-positive alveolar capillaries in idiopathic pulmonary fibrosis. Am J Respir Crit Care Med. 2004;169(11):1203-8.
51. Renzoni EA, Walsh DA, Salmon M, Wells AU, Sestini P, Nicholson AG, et al. Interstitial vascularity in fibrosing alveolitis. Am J Respir Crit Care Med. 2003;167(3):438-43.
52. Parra ER, David YR, da Costa LR, Ab'Saber A, Sousa R, Kairalla RA, et al. Heterogeneous remodeling of lung vessels in idiopathic pulmonary fibrosis. Lung. 2005;183(4):291-300.
53. Peao MN, Aguas AP, de Sa CM, Grande NR. Neoformation of blood vessels in association with rat lung fibrosis induced by bleomycin. Anat Rec. 1994;238(1):57-67.
54. Farkas L, Farkas D, Ask K, Moller A, Gauldie J, Margetts P, et al. VEGF ameliorates pulmonary hypertension through inhibition of endothelial apoptosis in experimental lung fibrosis in rats. J Clin Invest. 2009;119(5):1298-311.
55. Caporarello N, Meridew JA, Aravamudhan A, Jones DL, Austin SA, Pham TX, et al. Vascular dysfunction in aged mice contributes to persistent lung fibrosis. Aging Cell. 2020;19(8):e13196.
56. Keane MP, Arenberg DA, Lynch JP, 3rd, Whyte RI, Iannettoni MD, Burdick MD, et al. The CXC chemokines, IL-8 and IP-10, regulate angiogenic activity in idiopathic pulmonary fibrosis. J Immunol. 1997;159(3):1437-43.
57. Cosgrove GP, Brown KK, Schiemann WP, Serls AE, Parr JE, Geraci MW, et al. Pigment epithelium-derived factor in idiopathic pulmonary fibrosis: a role in aberrant angiogenesis. Am J Respir Crit Care Med. 2004;170(3):242-51.
58. Barratt SL, Blythe T, Jarrett C, Ourradi K, Shelley-Fraser G, Day MJ, et al. Differential Expression of VEGF-A(xxx) Isoforms Is Critical for Development of Pulmonary Fibrosis. Am J Respir Crit Care Med. 2017;196(4):479-93.
59. Keane MP, Belperio JA, Moore TA, Moore BB, Arenberg DA, Smith RE, et al. Neutralization of the CXC chemokine, macrophage inflammatory protein-2, attenuates bleomycin-induced pulmonary fibrosis. J Immunol. 1999;162(9):5511-8.
60. Keane MP, Belperio JA, Arenberg DA, Burdick MD, Xu ZJ, Xue YY, et al. IFN-gamma-inducible protein-10 attenuates bleomycin-induced pulmonary fibrosis via inhibition of angiogenesis. J Immunol. 1999;163(10):5686-92.
61. Tager AM, Kradin RL, LaCamera P, Bercury SD, Campanella GS, Leary CP, et al. Inhibition of pulmonary fibrosis by the chemokine IP-10/CXCL10. Am J Respir Cell Mol Biol. 2004;31(4):395-404.
62. Russo RC, Guabiraba R, Garcia CC, Barcelos LS, Roffe E, Souza AL, et al. Role of the chemokine receptor CXCR2 in bleomycin-induced pulmonary inflammation and fibrosis. Am J Respir Cell Mol Biol. 2009;40(4):410-21.
63. Liu X, Qin X, Qin H, Jia C, Yuan Y, Sun T, et al. Characterization of the heterogeneity of endothelial cells in bleomycin-induced lung fibrosis using single-cell RNA sequencing. Angiogenesis. 2021;24(4):809-21.
64. Wallez Y, Huber P. Endothelial adherens and tight junctions in vascular homeostasis, inflammation and angiogenesis. Biochim Biophys Acta. 2008;1778(3):794-809.

65. Montesi SB, Rao R, Liang LL, Goulart HE, Sharma A, Digumarthy SR, et al. Gadofosveset-enhanced lung magnetic resonance imaging to detect ongoing vascular leak in pulmonary fibrosis. Eur Respir J. 2018;51(5).
66. Wells AU, Hansell DM, Harrison NK, Lawrence R, Black CM, du Bois RM. Clearance of inhaled 99mTc-DTPA predicts the clinical course of fibrosing alveolitis. Eur Respir J. 1993;6(6):797-802.
67. Brown LF, Dvorak AM, Dvorak HF. Leaky vessels, fibrin deposition, and fibrosis: a sequence of events common to solid tumors and to many other types of disease. Am Rev Respir Dis. 1989;140(4):1104-7.
68. Shea BS, Brooks SF, Fontaine BA, Chun J, Luster AD, Tager AM. Prolonged exposure to sphingosine 1-phosphate receptor-1 agonists exacerbates vascular leak, fibrosis, and mortality after lung injury. Am J Respir Cell Mol Biol. 2010;43(6):662-73.
69. Huang LS, Sudhadevi T, Fu P, Punathil-Kannan PK, Ebenezer DL, Ramchandran R, et al. Sphingosine Kinase 1/S1P Signaling Contributes to Pulmonary Fibrosis by Activating Hippo/YAP Pathway and Mitochondrial Reactive Oxygen Species in Lung Fibroblasts. Int J Mol Sci. 2020;21(6).
70. Huang LS, Berdyshev E, Mathew B, Fu P, Gorshkova IA, He D, et al. Targeting sphingosine kinase 1 attenuates bleomycin-induced pulmonary fibrosis. FASEB J. 2013;27(4):1749-60.
71. Hamada N, Kuwano K, Yamada M, Hagimoto N, Hiasa K, Egashira K, et al. Anti-vascular endothelial growth factor gene therapy attenuates lung injury and fibrosis in mice. J Immunol. 2005;175(2):1224-31.
72. Chaudhary NI, Roth GJ, Hilberg F, Muller-Quernheim J, Prasse A, Zissel G, et al. Inhibition of PDGF, VEGF and FGF signalling attenuates fibrosis. Eur Respir J. 2007;29(5):976-85.
73. Murray LA, Habiel DM, Hohmann M, Camelo A, Shang H, Zhou Y, et al. Antifibrotic role of vascular endothelial growth factor in pulmonary fibrosis. JCI Insight. 2017;2(16).
74. Stockmann C, Kerdiles Y, Nomaksteinsky M, Weidemann A, Takeda N, Doedens A, et al. Loss of myeloid cell-derived vascular endothelial growth factor accelerates fibrosis. Proc Natl Acad Sci U S A. 2010;107(9):4329-34.
75. Uehara M, Enomoto N, Mikamo M, Oyama Y, Kono M, Fujisawa T, et al. Impact of angiopoietin-1 and -2 on clinical course of idiopathic pulmonary fibrosis. Respir Med. 2016;114:18-26.
76. Ando M, Miyazaki E, Abe T, Ehara C, Goto A, Masuda T, et al. Angiopoietin-2 expression in patients with an acute exacerbation of idiopathic interstitial pneumonias. Respir Med. 2016;117:27-32.
77. Margaritopoulos GA, Antoniou KM, Karagiannis K, Vassalou E, Lasithiotaki I, Lambiri I, et al. Investigation of angiogenetic axis Angiopoietin-1 and -2/Tie-2 in fibrotic lung diseases: a bronchoalveolar lavage study. Int J Mol Med. 2010;26(6):919-23.
78. Jambusaria A, Hong Z, Zhang L, Srivastava S, Jana A, Toth PT, et al. Endothelial heterogeneity across distinct vascular beds during homeostasis and inflammation. Elife. 2020;9.
79. Engelbrecht E, Kooistra T, Knipe RS. The Vasculature in Pulmonary Fibrosis. Curr Tissue Microenviron Rep. 2022;3(4):83-97.
80. Vassiliou AG, Vrettou CS, Keskinidou C, Dimopoulou I, Kotanidou A, Orfanos SE. Endotheliopathy in Acute COVID-19 and Long COVID. Int J Mol Sci. 2023;24(9).
81. Garton KJ, Gough PJ, Philalay J, Wille PT, Blobel CP, Whitehead RH, et al. Stimulated shedding of vascular cell adhesion molecule 1 (VCAM-1) is mediated by tumor necrosis factor-alpha-converting enzyme (ADAM 17). J Biol Chem. 2003;278(39):37459-64.
82. Kjaergaard AG, Dige A, Krog J, Tonnesen E, Wogensen L. Soluble adhesion molecules correlate with surface expression in an in vitro model of endothelial activation. Basic Clin Pharmacol Toxicol. 2013;113(4):273-9.
83. Garton KJ, Gough PJ, Raines EW. Emerging roles for ectodomain shedding in the regulation of inflammatory responses. J Leukoc Biol. 2006;79(6):1105-16.
84. Videm V, Albrigtsen M. Soluble ICAM-1 and VCAM-1 as markers of endothelial activation. Scand J Immunol. 2008;67(5):523-31.
85. Krieglstein CF, Granger DN. Adhesion molecules and their role in vascular disease. Am J Hypertens. 2001;14(6 Pt 2):44S-54S.

86. McGroder CF, Aaron CP, Bielinski SJ, Kawut SM, Tracy RP, Raghu G, et al. Circulating adhesion molecules and subclinical interstitial lung disease: the Multi-Ethnic Study of Atherosclerosis. Eur Respir J. 2019;54(3).
87. Richards TJ, Kaminski N, Baribaud F, Flavin S, Brodmerkel C, Horowitz D, et al. Peripheral blood proteins predict mortality in idiopathic pulmonary fibrosis. Am J Respir Crit Care Med. 2012;185(1):67-76.
88. Okuda R, Matsushima H, Aoshiba K, Oba T, Kawabe R, Honda K, et al. Soluble intercellular adhesion molecule-1 for stable and acute phases of idiopathic pulmonary fibrosis. Springerplus. 2015;4:657.
89. Michalski JE, Kurche JS, Schwartz DA. From ARDS to pulmonary fibrosis: the next phase of the COVID-19 pandemic? Transl Res. 2022;241:13-24.
90. Hirawat R, Jain N, Aslam Saifi M, Rachamalla M, Godugu C. Lung fibrosis: Post-COVID-19 complications and evidences. Int Immunopharmacol. 2023;116:109418.
91. Hama Amin BJ, Kakamad FH, Ahmed GS, Ahmed SF, Abdulla BA, Mohammed SH, et al. Post COVID-19 pulmonary fibrosis; a meta-analysis study. Ann Med Surg (Lond). 2022;77:103590.
92. George PM, Wells AU, Jenkins RG. Pulmonary fibrosis and COVID-19: the potential role for antifibrotic therapy. Lancet Respir Med. 2020;8(8):807-15.
93. Tanni SE, Fabro AT, de Albuquerque A, Ferreira EVM, Verrastro CGY, Sawamura MVY, et al. Pulmonary fibrosis secondary to COVID-19: a narrative review. Expert Rev Respir Med. 2021;15(6):791-803.
94. Bonaventura A, Vecchie A, Dagna L, Martinod K, Dixon DL, Van Tassell BW, et al. Endothelial dysfunction and immunothrombosis as key pathogenic mechanisms in COVID-19. Nat Rev Immunol. 2021;21(5):319-29.
95. Zhang Q, Xiang R, Huo S, Zhou Y, Jiang S, Wang Q, et al. Molecular mechanism of interaction between SARS-CoV-2 and host cells and interventional therapy. Signal Transduct Target Ther. 2021;6(1):233.
96. Bonaventura A, Vecchié A, Dagna L, Martinod K, Dixon DL, Van Tassell BW, et al. Endothelial dysfunction and immunothrombosis as key pathogenic mechanisms in COVID-19. Nature Reviews Immunology. 2021.
97. Jackson CB, Farzan M, Chen B, Choe H. Mechanisms of SARS-CoV-2 entry into cells. Nat Rev Mol Cell Biol. 2022;23(1):3-20.
98. Kuba K, Imai Y, Penninger JM. Angiotensin-converting enzyme 2 in lung diseases. Curr Opin Pharmacol. 2006;6(3):271-6.
99. Pelle MC, Zaffina I, Luca S, Forte V, Trapanese V, Melina M, et al. Endothelial Dysfunction in COVID-19: Potential Mechanisms and Possible Therapeutic Options. Life (Basel). 2022;12(10).
100. Xu SW, Ilyas I, Weng JP. Endothelial dysfunction in COVID-19: an overview of evidence, biomarkers, mechanisms and potential therapies. Acta Pharmacol Sin. 2023;44(4):695-709.
101. Sturrock BR, Milne KM, Chevassut TJ. The renin-angiotensin system - a therapeutic target in COVID-19? Clin Med (Lond). 2020;20(4):e72-e5.
102. Avdonin PP, Rybakova EY, Trufanov SK, Avdonin PV. SARS-CoV-2 Receptors and Their Involvement in Cell Infection. Biochem (Mosc) Suppl Ser A Membr Cell Biol. 2023;17(1):1-11.
103. Selickman J, Vrettou CS, Mentzelopoulos SD, Marini JJ. COVID-19-Related ARDS: Key Mechanistic Features and Treatments. J Clin Med. 2022;11(16).
104. Borek I, Birnhuber A, Voelkel NF, Marsh LM, Kwapiszewska G. The vascular perspective on acute and chronic lung disease. J Clin Invest. 2023;133(16).
105. Montazersaheb S, Hosseiniyan Khatibi SM, Hejazi MS, Tarhriz V, Farjami A, Ghasemian Sorbeni F, et al. COVID-19 infection: an overview on cytokine storm and related interventions. Virol J. 2022;19(1):92.
106. Birnhuber A, Fliesser E, Gorkiewicz G, Zacharias M, Seeliger B, David S, et al. Between inflammation and thrombosis: endothelial cells in COVID-19. Eur Respir J. 2021;58(3).
107. Conway EM, Mackman N, Warren RQ, Wolberg AS, Mosnier LO, Campbell RA, et al. Understanding COVID-19-associated coagulopathy. Nat Rev Immunol. 2022;22(10):639-49.

108. Chowdary P. COVID-19 coagulopathy - what should we treat? Exp Physiol. 2022;107(7):749-58.
109. Lasry A, Ben-Neriah Y. Senescence-associated inflammatory responses: aging and cancer perspectives. Trends Immunol. 2015;36(4):217-28.
110. The L. Long COVID: 3 years in. Lancet. 2023;401(10379):795.
111. Proal AD, VanElzakker MB. Long COVID or Post-acute Sequelae of COVID-19 (PASC): An Overview of Biological Factors That May Contribute to Persistent Symptoms. Front Microbiol. 2021;12:698169.
112. Cirjaliu RE, Deacu M, Gherghisan I, Marghescu AS, Enciu M, Baltatescu GI, et al. Clinicopathological Outlines of Post-COVID-19 Pulmonary Fibrosis Compared with Idiopathic Pulmonary Fibrosis. Biomedicines. 2023;11(6).
113. Ferreira-Gomes M, Kruglov A, Durek P, Heinrich F, Tizian C, Heinz GA, et al. SARS-CoV-2 in severe COVID-19 induces a TGF-beta-dominated chronic immune response that does not target itself. Nat Commun. 2021;12(1):1961.
114. Choi EY, Park HH, Kim H, Kim HN, Kim I, Jeon S, et al. Wnt5a and Wnt11 as acute respiratory distress syndrome biomarkers for severe acute respiratory syndrome coronavirus 2 patients. Eur Respir J. 2020;56(5).
115. Gokey JJ, Patel SD, Kropski JA. The Role of Hippo/YAP Signaling in Alveolar Repair and Pulmonary Fibrosis. Front Med (Lausanne). 2021;8:752316.
116. Garcia G, Jr., Jeyachandran AV, Wang Y, Irudayam JI, Cario SC, Sen C, et al. Hippo signaling pathway activation during SARS-CoV-2 infection contributes to host antiviral response. PLoS Biol. 2022;20(11):e3001851.
117. Gujski M, Jankowski M, Rabczenko D, Gorynski P, Juszczyk G. The Prevalence of Acute Respiratory Distress Syndrome (ARDS) and Outcomes in Hospitalized Patients with COVID-19-A Study Based on Data from the Polish National Hospital Register. Viruses. 2022;14(1).
118. Glass DS, Grossfeld D, Renna HA, Agarwala P, Spiegler P, DeLeon J, et al. Idiopathic pulmonary fibrosis: Current and future treatment. Clin Respir J. 2022;16(2):84-96.
119. Ruwanpura SM, Thomas BJ, Bardin PG. Pirfenidone: Molecular Mechanisms and Potential Clinical Applications in Lung Disease. Am J Respir Cell Mol Biol. 2020;62(4):413-22.
120. Wollin L, Distler JHW, Redente EF, Riches DWH, Stowasser S, Schlenker-Herceg R, et al. Potential of nintedanib in treatment of progressive fibrosing interstitial lung diseases. Eur Respir J. 2019;54(3).
121. Flaherty KR, Wells AU, Cottin V, Devaraj A, Walsh SLF, Inoue Y, et al. Nintedanib in Progressive Fibrosing Interstitial Lung Diseases. N Engl J Med. 2019;381(18):1718-27.
122. Behr J, Prasse A, Kreuter M, Johow J, Rabe KF, Bonella F, et al. Pirfenidone in patients with progressive fibrotic interstitial lung diseases other than idiopathic pulmonary fibrosis (RELIEF): a double-blind, randomised, placebo-controlled, phase 2b trial. Lancet Respir Med. 2021;9(5):476-86.
123. Gan D, Cheng W, Ke L, Sun AR, Jia Q, Chen J, et al. Biphasic Effect of Pirfenidone on Angiogenesis. Front Pharmacol. 2021;12:804327.
124. Kolb M, Raghu G, Wells AU, Behr J, Richeldi L, Schinzel B, et al. Nintedanib plus Sildenafil in Patients with Idiopathic Pulmonary Fibrosis. N Engl J Med. 2018;379(18):1722-31.
125. Waxman A, Restrepo-Jaramillo R, Thenappan T, Ravichandran A, Engel P, Bajwa A, et al. Inhaled Treprostinil in Pulmonary Hypertension Due to Interstitial Lung Disease. N Engl J Med. 2021;384(4):325-34.
126. Nathan SD, Waxman A, Rajagopal S, Case A, Johri S, DuBrock H, et al. Inhaled treprostinil and forced vital capacity in patients with interstitial lung disease and associated pulmonary hypertension: a post-hoc analysis of the INCREASE study. Lancet Respir Med. 2021;9(11):1266-74.
127. Strieter RM, Mehrad B. New mechanisms of pulmonary fibrosis. Chest. 2009;136(5):1364-70.
128. Bagnato G, Harari S. Cellular interactions in the pathogenesis of interstitial lung diseases. Eur Respir Rev. 2015;24(135):102-14.
129. Fliesser E, Lins T, Berg JL, Kolb M, Kwapiszewska G. The endothelium in lung fibrosis: a core signaling hub in disease pathogenesis? Am J Physiol Cell Physiol. 2023;325(1):C2-C16.

130. Lambers C, Roth M, Jaksch P, Murakozy G, Tamm M, Klepetko W, et al. Treprostinil inhibits proliferation and extracellular matrix deposition by fibroblasts through cAMP activation. Sci Rep. 2018;8(1):1087.
131. Nikitopoulou I, Manitsopoulos N, Kotanidou A, Tian X, Petrovic A, Magkou C, et al. Orotracheal treprostinil administration attenuates bleomycin-induced lung injury, vascular remodeling, and fibrosis in mice. Pulm Circ. 2019;9(4):2045894019881954.
132. Kim S, Herazo-Maya JD, Kang DD, Juan-Guardela BM, Tedrow J, Martinez FJ, et al. Integrative phenotyping framework (iPF): integrative clustering of multiple omics data identifies novel lung disease subphenotypes. BMC Genomics. 2015;16:924.
133. Wang J, Zhao H, An Y. ACE2 Shedding and the Role in COVID-19. Front Cell Infect Microbiol. 2021;11:789180.
134. Fliesser E, Birnhuber A, Marsh LM, Gschwandtner E, Klepetko W, Olschewski H, et al. Dysbalance of ACE2 levels - a possible cause for severe COVID-19 outcome in COPD. J Pathol Clin Res. 2021;7(5):446-58.
135. Ackermann M, Verleden SE, Kuehnel M, Haverich A, Welte T, Laenger F, et al. Pulmonary Vascular Endothelialitis, Thrombosis, and Angiogenesis in Covid-19. N Engl J Med. 2020;383(2):120-8.
136. Klok FA, Kruip M, van der Meer NJM, Arbous MS, Gommers D, Kant KM, et al. Confirmation of the high cumulative incidence of thrombotic complications in critically ill ICU patients with COVID-19: An updated analysis. Thromb Res. 2020;191:148-50.
137. Moore JB, June CH. Cytokine release syndrome in severe COVID-19. Science. 2020;368(6490):473-4.
138. Libby P, Luscher T. COVID-19 is, in the end, an endothelial disease. Eur Heart J. 2020;41(32):3038-44.
139. Chen L, Wang G, Tan J, Cao Y, Long X, Luo H, et al. Scoring cytokine storm by the levels of MCP-3 and IL-8 accurately distinguished COVID-19 patients with high mortality. Signal Transduct Target Ther. 2020;5(1):292.
140. Yung S, Chan TM. Endothelial cell activation and glycocalyx shedding - potential as biomarkers in patients with lupus nephritis. Front Immunol. 2023;14:1251876.
141. Amersfoort J, Eelen G, Carmeliet P. Immunomodulation by endothelial cells - partnering up with the immune system? Nat Rev Immunol. 2022;22(9):576-88.
142. Kolb M, Margetts PJ, Anthony DC, Pitossi F, Gauldie J. Transient expression of IL-1beta induces acute lung injury and chronic repair leading to pulmonary fibrosis. J Clin Invest. 2001;107(12):1529-36.
143. Lundblad LK, Thompson-Figueroa J, Leclair T, Sullivan MJ, Poynter ME, Irvin CG, et al. Tumor necrosis factor-alpha overexpression in lung disease: a single cause behind a complex phenotype. Am J Respir Crit Care Med. 2005;171(12):1363-70.
144. Vu TN, Chen X, Foda HD, Smaldone GC, Hasaneen NA. Interferon-gamma enhances the antifibrotic effects of pirfenidone by attenuating IPF lung fibroblast activation and differentiation. Respir Res. 2019;20(1):206.
145. Melrose J, Tsurushita N, Liu G, Berg EL. IFN-gamma inhibits activation-induced expression of E- and P-selectin on endothelial cells. J Immunol. 1998;161(5):2457-64.
146. Peterson MW, Monick M, Hunninghake GW. Prognostic role of eosinophils in pulmonary fibrosis. Chest. 1987;92(1):51-6.
147. Hunninghake GW, Gadek JE, Lawley TJ, Crystal RG. Mechanisms of neutrophil accumulation in the lungs of patients with idiopathic pulmonary fibrosis. J Clin Invest. 1981;68(1):259-69.
148. Desai O, Winkler J, Minasyan M, Herzog EL. The Role of Immune and Inflammatory Cells in Idiopathic Pulmonary Fibrosis. Front Med (Lausanne). 2018;5:43.
149. Zhang Y, Kaminski N. Biomarkers in idiopathic pulmonary fibrosis. Curr Opin Pulm Med. 2012;18(5):441-6.
150. Bordag N, Biasin V, Schnoegl D, Valzano F, Jandl K, Nagy BM, et al. Machine Learning Analysis of the Bleomycin Mouse Model Reveals the Compartmental and Temporal Inflammatory Pulmonary Fingerprint. iScience. 2020;23(12):101819.

151. Huertas A, Guignabert C, Barbera JA, Bartsch P, Bhattacharya J, Bhattacharya S, et al. Pulmonary vascular endothelium: the orchestra conductor in respiratory diseases: Highlights from basic research to therapy. Eur Respir J. 2018;51(4).
152. Probst CK, Montesi SB, Medoff BD, Shea BS, Knipe RS. Vascular permeability in the fibrotic lung. Eur Respir J. 2020;56(1).
153. Linden D, Guo-Parke H, Coyle PV, Fairley D, McAuley DF, Taggart CC, et al. Respiratory viral infection: a potential "missing link" in the pathogenesis of COPD. Eur Respir Rev. 2019;28(151).
154. Earl N, Schoeneberg D, Davidson PD. Severe progression of idiopathic pulmonary fibrosis post-COVID-19 infection. BMJ Case Rep. 2021;14(10).
155. Naqvi SF, Lakhani DA, Sohail AH, Maurer J, Sofka S, Sarwari A, et al. Patients with idiopathic pulmonary fibrosis have poor clinical outcomes with COVID-19 disease: a propensity matched multicentre research network analysis. BMJ Open Respir Res. 2021;8(1).
156. Sulica R, Cefali F, Motschwiller C, Fenton R, Barroso A, Sterman D. COVID-19 in Pulmonary Artery Hypertension (PAH) Patients: Observations from a Large PAH Center in New York City. Diagnostics (Basel). 2021;11(1).
157. Lee SC, Son KJ, Han CH, Park SC, Jung JY. Impact of COPD on COVID-19 prognosis: A nationwide population-based study in South Korea. Sci Rep. 2021;11(1):3735.
158. Meza D, Khuder B, Bailey JI, Rosenberg SR, Kalhan R, Reyfman PA. Mortality from COVID-19 in Patients with COPD: A US Study in the N3C Data Enclave. Int J Chron Obstruct Pulmon Dis. 2021;16:2323-6.
159. Kotwica A, Knights H, Mayor N, Russell-Jones E, Dassios T, Russell-Jones D. Intrapulmonary shunt measured by bedside pulse oximetry predicts worse outcomes in severe COVID-19. Eur Respir J. 2021;57(4).
160. Bhat TA, Panzica L, Kalathil SG, Thanavala Y. Immune Dysfunction in Patients with Chronic Obstructive Pulmonary Disease. Ann Am Thorac Soc. 2015;12 Suppl 2(Suppl 2):S169-75.
161. Brake SJ, Eapen MS, McAlinden KD, Markos J, Haug G, Larby J, et al. SARS-CoV-2 (COVID-19) Adhesion Site Protein Upregulation in Small Airways, Type 2 Pneumocytes, and Alveolar Macrophages of Smokers and COPD - Possible Implications for Interstitial Fibrosis. Int J Chron Obstruct Pulmon Dis. 2022;17:101-15.
162. Eapen MS, Lu W, Hackett TL, Singhera GK, Thompson IE, McAlinden KD, et al. Dysregulation of endocytic machinery and ACE2 in small airways of smokers and COPD patients can augment their susceptibility to SARS-CoV-2 (COVID-19) infections. Am J Physiol Lung Cell Mol Physiol. 2021;320(1):L158-L63.
163. Drake TM, Docherty AB, Harrison EM, Quint JK, Adamali H, Agnew S, et al. Outcome of Hospitalization for COVID-19 in Patients with Interstitial Lung Disease. An International Multicenter Study. Am J Respir Crit Care Med. 2020;202(12):1656-65.
164. Leung JM, Yang CX, Tam A, Shaipanich T, Hackett TL, Singhera GK, et al. ACE-2 expression in the small airway epithelia of smokers and COPD patients: implications for COVID-19. Eur Respir J. 2020;55(5).
165. Goto Y, Sakamoto K, Fukihara J, Suzuki A, Omote N, Ando A, et al. COVID-19-Triggered Acute Exacerbation of IPF, an Underdiagnosed Clinical Entity With Two-Peaked Respiratory Failure: A Case Report and Literature Review. Front Med (Lausanne). 2022;9:815924.
166. Ghincea A, Ryu C, Herzog EL. An Acute Exacerbation of Idiopathic Pulmonary Fibrosis After BNT162b2 mRNA COVID-19 Vaccination: A Case Report. Chest. 2022;161(2):e71-e3.
167. Cilli A, Hanta I, Uzer F, Coskun F, Sevinc C, Deniz PP, et al. Characteristics and outcomes of COVID-19 patients with IPF: A multi-center retrospective study. Respir Med Res. 2022;81:100900.
168. Gallay L, Uzunhan Y, Borie R, Lazor R, Rigaud P, Marchand-Adam S, et al. Risk Factors for Mortality after COVID-19 in Patients with Preexisting Interstitial Lung Disease. Am J Respir Crit Care Med. 2021;203(2):245-9.
169. Lu W, Eapen MS, Singhera GK, Markos J, Haug G, Chia C, et al. Angiotensin-Converting Enzyme 2 (ACE2), Transmembrane Peptidase Serine 2 (TMPRSS2), and Furin Expression Increases in the Lungs

of Patients with Idiopathic Pulmonary Fibrosis (IPF) and Lymphangioleiomyomatosis (LAM): Implications for SARS-CoV-2 (COVID-19) Infections. J Clin Med. 2022;11(3).
170. Lambert DW, Yarski M, Warner FJ, Thornhill P, Parkin ET, Smith AI, et al. Tumor necrosis factor-alpha convertase (ADAM17) mediates regulated ectodomain shedding of the severe-acute respiratory syndrome-coronavirus (SARS-CoV) receptor, angiotensin-converting enzyme-2 (ACE2). J Biol Chem. 2005;280(34):30113-9.
171. Mariappan V, Ranganadin P, Shanmugam L, Rao SR, Balakrishna Pillai A. Early shedding of membrane-bounded ACE2 could be an indicator for disease severity in SARS-CoV-2. Biochimie. 2022;201:139-47.
172. Kornilov SA, Lucas I, Jade K, Dai CL, Lovejoy JC, Magis AT. Plasma levels of soluble ACE2are associated with sex, Metabolic Syndrome, and its biomarkers in a large cohort, pointing to a possible mechanism for increased severity in COVID-19. Crit Care. 2020;24(1):452.
173. Maza MDC, Ubeda M, Delgado P, Horndler L, Llamas MA, van Santen HM, et al. ACE2 Serum Levels as Predictor of Infectability and Outcome in COVID-19. Front Immunol. 2022;13:836516.
174. Yeung ML, Teng JLL, Jia L, Zhang C, Huang C, Cai JP, et al. Soluble ACE2-mediated cell entry of SARS-CoV-2 via interaction with proteins related to the renin-angiotensin system. Cell. 2021;184(8):2212-28 e12.
175. Hassler L, Wysocki J, Gelarden I, Sharma I, Tomatsidou A, Ye M, et al. A Novel Soluble ACE2 Protein Provides Lung and Kidney Protection in Mice Susceptible to Lethal SARS-CoV-2 Infection. J Am Soc Nephrol. 2022;33(7):1293-307.
176. Six I, Guillaume N, Jacob V, Mentaverri R, Kamel S, Boullier A, et al. The Endothelium and COVID-19: An Increasingly Clear Link Brief Title: Endotheliopathy in COVID-19. Int J Mol Sci. 2022;23(11).
177. Zhang X, Jiang M, Yang J. Potential value of circulating endothelial cells for the diagnosis and treatment of COVID-19. Int J Infect Dis. 2021;107:232-3.
178. Passi R, Brittan M, Baker AH. The role of the endothelium in severe acute respiratory syndrome coronavirus 2 infection and pathogenesis. Curr Opin Physiol. 2023;34:100670.
179. Ma Z, Yang KY, Huang Y, Lui KO. Endothelial contribution to COVID-19: an update on mechanisms and therapeutic implications. J Mol Cell Cardiol. 2022;164:69-82.
180. Valentijn KM, Sadler JE, Valentijn JA, Voorberg J, Eikenboom J. Functional architecture of Weibel-Palade bodies. Blood. 2011;117(19):5033-43.
181. Jandial A, Gupta A, Malviya A, Agastam S, Kumar D. Coagulation abnormalities & thromboprophylaxis in COVID-19. Indian J Med Res. 2021;153(5&6):606-18.
182. Teimury A, Khameneh MT, Khaledi EM. Major coagulation disorders and parameters in COVID-19 patients. Eur J Med Res. 2022;27(1):25.
183. Chioh FW, Fong SW, Young BE, Wu KX, Siau A, Krishnan S, et al. Convalescent COVID-19 patients are susceptible to endothelial dysfunction due to persistent immune activation. Elife. 2021;10.
184. Birnhuber A, Jandl K, Biasin V, Fliesser E, Valzano F, Marsh LM, et al. Pirfenidone exacerbates Th2-driven vasculopathy in a mouse model of systemic sclerosis-associated interstitial lung disease. Eur Respir J. 2022;60(4).
185. Biasin V, Crnkovic S, Sahu-Osen A, Birnhuber A, El Agha E, Sinn K, et al. PDGFRalpha and alphaSMA mark two distinct mesenchymal cell populations involved in parenchymal and vascular remodeling in pulmonary fibrosis. Am J Physiol Lung Cell Mol Physiol. 2020;318(4):L684-L97.
186. Birnhuber A, Crnkovic S, Biasin V, Marsh LM, Odler B, Sahu-Osen A, et al. IL-1 receptor blockade skews inflammation towards Th2 in a mouse model of systemic sclerosis. Eur Respir J. 2019;54(3).
187. Parra ER, Silverio da Costa LR, Ab'Saber A, Ribeiro de Carvalho CR, Kairalla RA, Fernezlian SM, et al. Nonhomogeneous density of CD34 and VCAM-1 alveolar capillaries in major types of idiopathic interstitial pneumonia. Lung. 2005;183(5):363-73.
188. Cossu M, Andracco R, Santaniello A, Marchini M, Severino A, Caronni M, et al. Serum levels of vascular dysfunction markers reflect disease severity and stage in systemic sclerosis patients. Rheumatology (Oxford). 2016;55(6):1112-6.

189. Kawamoto M, Fukuda Y. Cell proliferation during the process of bleomycin-induced pulmonary fibrosis in rats. Acta Pathol Jpn. 1990;40(4):227-38.
190. Tzouvelekis A, Anevlavis S, Bouros D. Angiogenesis in interstitial lung diseases: a pathogenetic hallmark or a bystander? Respir Res. 2006;7:82.
191. Leach HG, Chrobak I, Han R, Trojanowska M. Endothelial cells recruit macrophages and contribute to a fibrotic milieu in bleomycin lung injury. Am J Respir Cell Mol Biol. 2013;49(6):1093-101.
192. Mutsaers SE, Miles T, Prele CM, Hoyne GF. Emerging role of immune cells as drivers of pulmonary fibrosis. Pharmacol Ther. 2023;252:108562.
193. Fusiak T, Smaldone GC, Condos R. Pulmonary Fibrosis Treated with Inhaled Interferon-gamma (IFN-gamma). J Aerosol Med Pulm Drug Deliv. 2015;28(5):406-10.
194. Azuma A, Li YJ, Abe S, Usuki J, Matsuda K, Henmi S, et al. Interferon-beta inhibits bleomycin-induced lung fibrosis by decreasing transforming growth factor-beta and thrombospondin. Am J Respir Cell Mol Biol. 2005;32(2):93-8.
195. Chen Y, Pu Q, Ma Y, Zhang H, Ye T, Zhao C, et al. Aging Reprograms the Hematopoietic-Vascular Niche to Impede Regeneration and Promote Fibrosis. Cell Metab. 2021;33(2):395-410 e4.
196. Cao Z, Lis R, Ginsberg M, Chavez D, Shido K, Rabbany SY, et al. Targeting of the pulmonary capillary vascular niche promotes lung alveolar repair and ameliorates fibrosis. Nat Med. 2016;22(2):154-62.
197. Jandl K, Marsh LM, Mutgan AC, Crnkovic S, Valzano F, Zabini D, et al. Impairment of the NKT-STAT1-CXCL9 Axis Contributes to Vessel Fibrosis in Pulmonary Hypertension Caused by Lung Fibrosis. Am J Respir Crit Care Med. 2022;206(8):981-98.
198. Fahey E, Doyle SL. IL-1 Family Cytokine Regulation of Vascular Permeability and Angiogenesis. Front Immunol. 2019;10:1426.
199. Ganter MT, Roux J, Miyazawa B, Howard M, Frank JA, Su G, et al. Interleukin-1beta causes acute lung injury via alphavbeta5 and alphavbeta6 integrin-dependent mechanisms. Circ Res. 2008;102(7):804-12.
200. Gong T, Liu L, Jiang W, Zhou R. DAMP-sensing receptors in sterile inflammation and inflammatory diseases. Nat Rev Immunol. 2020;20(2):95-112.
201. Hofmann S, Grasberger H, Jung P, Bidlingmaier M, Vlotides J, Janssen OE, et al. The tumour necrosis factor-alpha induced vascular permeability is associated with a reduction of VE-cadherin expression. Eur J Med Res. 2002;7(4):171-6.
202. Madge LA, Pober JS. TNF signaling in vascular endothelial cells. Exp Mol Pathol. 2001;70(3):317-25.
203. Mako V, Czucz J, Weiszhar Z, Herczenik E, Matko J, Prohaszka Z, et al. Proinflammatory activation pattern of human umbilical vein endothelial cells induced by IL-1beta, TNF-alpha, and LPS. Cytometry A. 2010;77(10):962-70.
204. Milara J, Navarro R, Juan G, Peiro T, Serrano A, Ramon M, et al. Sphingosine-1-phosphate is increased in patients with idiopathic pulmonary fibrosis and mediates epithelial to mesenchymal transition. Thorax. 2012;67(2):147-56.
205. Peng Z, Konai MM, Avila-Cobian LF, Wang M, Mobashery S, Chang M. MMP-1 and ADAM10 as Targets for Therapeutic Intervention in Idiopathic Pulmonary Fibrosis. ACS Pharmacol Transl Sci. 2022;5(8):548-54.
206. McKeown S, Richter AG, O'Kane C, McAuley DF, Thickett DR. MMP expression and abnormal lung permeability are important determinants of outcome in IPF. Eur Respir J. 2009;33(1):77-84.
207. Chulia-Peris L, Carreres-Rey C, Gabasa M, Alcaraz J, Carretero J, Pereda J. Matrix Metalloproteinases and Their Inhibitors in Pulmonary Fibrosis: EMMPRIN/CD147 Comes into Play. Int J Mol Sci. 2022;23(13).
208. Todd JL, Vinisko R, Liu Y, Neely ML, Overton R, Flaherty KR, et al. Circulating matrix metalloproteinases and tissue metalloproteinase inhibitors in patients with idiopathic pulmonary fibrosis in the multicenter IPF-PRO Registry cohort. BMC Pulm Med. 2020;20(1):64.
209. Bormann T, Maus R, Stolper J, Tort Tarres M, Brandenberger C, Wedekind D, et al. Role of matrix metalloprotease-2 and MMP-9 in experimental lung fibrosis in mice. Respir Res. 2022;23(1):180.

210. Corbel M, Caulet-Maugendre S, Germain N, Molet S, Lagente V, Boichot E. Inhibition of bleomycin-induced pulmonary fibrosis in mice by the matrix metalloproteinase inhibitor batimastat. J Pathol. 2001;193(4):538-45.
211. Stainer A, Faverio P, Busnelli S, Catalano M, Della Zoppa M, Marruchella A, et al. Molecular Biomarkers in Idiopathic Pulmonary Fibrosis: State of the Art and Future Directions. Int J Mol Sci. 2021;22(12).
212. Tsoutsou PG, Gourgoulianis KI, Petinaki E, Mpaka M, Efremidou S, Maniatis A, et al. ICAM-1, ICAM-2 and ICAM-3 in the sera of patients with idiopathic pulmonary fibrosis. Inflammation. 2004;28(6):359-64.
213. Hayashi S, Abe K, Matsuoka H, Goya S, Morishita H, Mori M, et al. Increased level of soluble E-selectin in the serum from patients with idiopathic pulmonary fibrosis. Inflammation. 2004;28(1):1-5.
214. Collard HR, Calfee CS, Wolters PJ, Song JW, Hong SB, Brady S, et al. Plasma biomarker profiles in acute exacerbation of idiopathic pulmonary fibrosis. Am J Physiol Lung Cell Mol Physiol. 2010;299(1):L3-7.
215. Langholm LL, Ronnow SR, Sand JMB, Leeming DJ, Tal-Singer R, Miller BE, et al. Increased von Willebrand Factor Processing in COPD, Reflecting Lung Epithelium Damage, Is Associated with Emphysema, Exacerbations and Elevated Mortality Risk. Int J Chron Obstruct Pulmon Dis. 2020;15:543-52.
216. Joshi N, Kopec AK, Ray JL, Cline-Fedewa H, Groeneveld DJ, Lisman T, et al. Von Willebrand factor deficiency reduces liver fibrosis in mice. Toxicol Appl Pharmacol. 2017;328:54-9.
217. Moeller A, Ask K, Warburton D, Gauldie J, Kolb M. The bleomycin animal model: a useful tool to investigate treatment options for idiopathic pulmonary fibrosis? Int J Biochem Cell Biol. 2008;40(3):362-82.
218. Moore BB, Hogaboam CM. Murine models of pulmonary fibrosis. Am J Physiol Lung Cell Mol Physiol. 2008;294(2):L152-60.
219. B BM, Lawson WE, Oury TD, Sisson TH, Raghavendran K, Hogaboam CM. Animal models of fibrotic lung disease. Am J Respir Cell Mol Biol. 2013;49(2):167-79.
220. Garcia JG, Gray LD, Dodson RF, Callahan KS. Asbestos-induced endothelial cell activation and injury. Demonstration of fiber phagocytosis and oxidant-dependent toxicity. Am Rev Respir Dis. 1988;138(4):958-64.
221. Christensen PJ, Goodman RE, Pastoriza L, Moore B, Toews GB. Induction of lung fibrosis in the mouse by intratracheal instillation of fluorescein isothiocyanate is not T-cell-dependent. Am J Pathol. 1999;155(5):1773-9.